REVIEW ARTICLE

Check for updates

Bioinspired photonic materials for advanced thermal management

Kan Yao, †*[a] Gaoyang Kong,†[bc] Chengyu Xiao, [bc] Shaowen Chen,[bc] Yifan Zhang,[bc] Xing Lou, [bc] Jing Li, [bc] Di Zhang,*[b] Han Zhou *[bc] and Yuebing Zheng *[a]

Maintenance of temperature within a suitable range is essential for human activity, and thermal management is the science dedicated to this goal. From an optical point of view, thermal management requires engineered photonic materials with versatile responses over the broad solar and thermal spectra to perform complex functions, including cooling, heating, energy conversion, camouflage, and dynamic control of heat flow, many of which are highly desirable in renewable energy research. The sophisticated spectral requirements of these applications pose fundamental challenges in materials design. While advances in computational methods have led to many technological breakthroughs, a parallel route—drawing inspiration from biological systems—has also yielded impressive progress. Guided by the unmatched power of natural selection, biomimetic approaches facilitate the development of high-performance bioinspired materials with intricate hierarchical architectures. In this review, we present the concepts and recent advances in biomimetic photonic materials and strategies for thermal management, along with our perspectives on the current challenges and future directions. The engineering principles evolved in nature to meet complex spectral demands are also broadly applicable to other applications involving ultra-broadband and band-selective optical responses.

[a] *Walker Department of Mechanical Engineering and Texas Materials Institute, The University of Texas at Austin, Austin, TX 78712, USA. E-mail: ustcykk@gmail.com, zheng@austin.utexas.edu*

[b] *State Key Laboratory of Metal Matrix Composites, School of Materials Science and Engineering, Shanghai Jiao Tong University, Shanghai 200240, China. E-mail: hanzhou_81@sjtu.edu.cn, zhangdi@sjtu.edu.cn*

[c] *Future Materials Innovation Center, Zhangjiang Institute for Advanced Study, Shanghai Jiao Tong University, Shanghai 201203, China*

† These authors contributed equally to this work.

Kan Yao is currently a research fellow in the University of Texas at Austin. He received his PhD in Electrical Engineering from Northeastern University (Boston, USA) in 2017. Prior to that, he received his bachelor's and master's degrees from the University of Science and Technology of China and Chinese Academy of Sciences (CAS) in 2006 and 2009, respectively, and then worked as a research assistant in CAS and as a visiting scholar in Soochow University (Suzhou, China). His research interests span various topics in photonics, such as nanoplasmonics, metamaterials and metasurfaces, light-matter interactions, chiroptics, quantum photonics, and inverse design.

Kan Yao

Gaoyang Kong is currently a master's student at Shanghai Jiao Tong University. She received her bachelor's degree from the School of Materials Science and Engineering, Tianjin University in 2022. Her research is focused on radiative thermal management materials.

Gaoyang Kong

1. Introduction

Maintenance of temperature within an appropriate range is critical to human activity. On the lowest level, keeping the body temperature at $\sim$37 °C ensures human survival.[1] On upper levels, methods that can improve thermal comfort and the reliability of equipment have been pursued throughout the history of human civilization,[2–5] resulting in technologies and strategies that can now be generally referred to as thermal management or thermoregulation. In the contemporary era, the crises of global warming and sustainable development further highlight some previously overlooked aspects of thermal management, such as energy consumption. Tremendous efforts from different disciplines have been made to address the emerging grand challenges in thermal management.
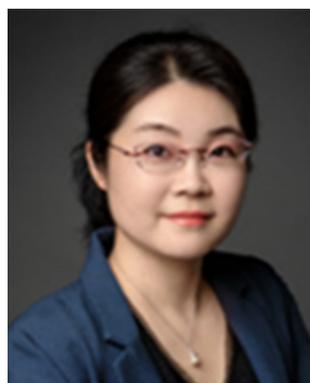
Particularly, photonic solutions based on rationally engineered photonic materials are considered a promising avenue.[6] This is primarily because sunlight is a major energy source and thermal radiation serves as an important channel of heat transfer. In optics, the favored conditions for different scenarios of thermal management can be cast into corresponding spectral requirements. However, fulfilling such requirements over the broad range of wavelengths from ultraviolet (UV) through visible and near-infrared (NIR) to mid-infrared (MIR) with the responses of structured materials is a computationally very costly task of inverse design, which is usually dealt with by using upgraded hardware (*e.g.*, computer clusters, graphics processing units) and/or software (*e.g.*, advanced algorithms for optimization or machine learning).

An effective approach to overcoming this difficulty is biomimicry.[7] Many living organisms on Earth are recipients of solar energy. And in spite of the inhabiting environments, they need to manage the heat load with certain organs to maintain the body temperature within some ranges, solving the thermal management problem of their own version. Since the structures in biological systems are shaped during the course of evolution taking place continuously over millions of years, identifying them and understanding the mechanisms can be very inspiring for the design of optical materials targeting functions similar to those of biological systems.[8] Compared with traditional design methods that start the search from scratch, imitation of natural materials offers a shortcut to complex designs, especially those with intricate hierarchical structures,[9] for the optimization to begin with, remarkably facilitating the search of high-performance devices. In extreme circumstances, direct modification of natural materials can provide practical solutions to selective applications as well. Moreover, devices for thermal management do not always operate in a fixed mode or in environments at a constant temperature. To cope with the

Di Zhang is an academician of Chinese Academy of Sciences and a Chair Professor of Materials Science at Shanghai Jiao Tong University, China. He is the director of the State Key Laboratory of Metal Matrix Composites at Shanghai Jiao Tong University and the founder and leader of the Morphology Genetic Materials group. He received his PhD in Materials Science (1988) from Osaka University, Japan. His research interests include the design, synthesis, and characterization of bioinspired materials and metal matrix composites.

Di Zhang

Han Zhou is a Professor at the State Key Laboratory of Metal Matrix Composites, Shanghai Jiao Tong University. She has long been dedicated to cutting-edge interdisciplinary research and applied translation in AI-designed thermal radiation meta-materials, bioinspired thermal metamaterials, and intelligent metamaterials. As a corresponding author, she has published SCI papers in prestigious journals such as Nature, Proceedings of the National Academy of Sciences (PNAS), and Advanced Materials. She has received honors, including the National Young Talent Program, being listed in the World's Top 2% Scientists (2023/2024), the WILEY Young Researcher Award, the Humboldt Research Fellowship (Germany), and the Second Prize of the National Natural Science Award.

Han Zhou

Yuebing Zheng is a Professor of Mechanical Engineering and Materials Science and Engineering at The University of Texas at Austin, where he holds the Cullen Trust for Higher Education Endowed Professorship in Engineering. His research drives the virtuous cycle of light and matter—where light reveals and refines matter, and matter decodes and directs light—to illuminate new frontiers in science, engineering, and medicine. He is a Fellow of Optica, SPIE, the Institute of Physics, and the Royal Society of Chemistry, and a recipient of the NIH Director's New Innovator, Beckman Young Investigator Award, NASA Early Faculty Award, and ONR Young Investigator Award.

Yuebing Zheng

This journal is © The Royal Society of Chemistry 2025

Chem. Soc. Rev., 2025, **54**, 10690–10723 | 10691

changing conditions, introducing dynamic materials with responses adaptable to external stimuli will add great value to the devices, and the design process could also benefit from biomimicry.[10]

In this review, we discuss the recent advances in thermal management enabled by biophotonics and bioinspired photonic materials. Here, photonic materials are defined as composites of micro-/nanostructured materials that interact with photons in the optical regime. Although the rapid progress in biophotonics and thermal management, particularly in photovoltaics and passive cooling, has separately led to innovative concepts and practical technologies,[11,12] these developments have so far been reviewed mainly from the respective viewpoints of, for instance, biomimicry of structural coloration,[13–15] bioinspired materials,[10,16–19] energy conversion,[20–23] radiative cooling (RC),[6,24–26] smart windows,[27–29] *etc.* In pursuit of better photonic solutions to thermal management, which are critical for fighting against global warming and searching for renewable energy sources, the inspiring role of biological systems has not been examined from an integrative perspective. Therefore, we believe a comprehensive survey on this topic is timely and will provide new insights into thermal photonics.

The manuscript is organized as follows. In Section 2, we first introduce the concepts of several representative scenarios of thermal management, including passive RC, heating, smart windows, and infrared (IR) stealth, establishing discrete connections between each of these applications and their requirements on optical responses. Subsequently, a quick overview is presented to outline how inspirations of designing new materials can be obtained by studying biological models that have naturally evolved to meet certain parts of such spectral requirements, namely broadband reflection, antireflection, and selective reflection. Section 3 breaks down the subject of static thermal management and discusses in detail biological structures and materials featuring the above three types of characteristic optical responses, along with the respective mechanism. Natural examples of thermoregulation employing multiple mechanisms are also discussed. Section 4 is analogous to Section 3 but focuses on dynamic thermal management. After walking through the essentials, Section 5 switches gears and reviews the applications of bioinspired photonic materials for thermoregulation. In line with the structure of Sections 2–4, the discussion starts with static cases, such as RC, solar energy harvesting and photothermal conversion, and then goes to dynamic materials for smart thermal control and adaptive IR camouflage. Finally, Section 6 concludes the survey with an outlook on the future directions of bioinspired photonic solutions to thermal management.

2. Background and concepts

Thermal management refers to the strategies and techniques used to maintain the temperature of a system so that it can function with desirable performance. Governed by the principles of thermodynamics, the concept generally applies to many scenarios spanning a broad range of length scales, from the cooling of electronics and batteries, the design and engineering of solar cells, to the temperature control of the human body, vehicles, and buildings. Because this review focuses on bioinspired solutions, of which the sources of inspiration mainly deal with solar irradiation and dissipation of heat *via* thermal radiation, the context of the following discussion is tailored accordingly. More specifically, we consider the problems of RC, solar energy harvesting, thermochromic smart windows, and IR stealth (Fig. 1).

Finding solutions to the named applications can be formulated as tasks of designing photonic materials with suitable optical properties over a unified wavelength range of 0.3–25 μm, covering the entire solar irradiation spectrum and the MIR region overlapping the blackbody radiation spectrum of objects near the ambient temperatures of about 300 K (shaded areas in Fig. 1(a)–(e)). For the most emerging and practically significant concept in modern thermal management, the spectral requirements of daytime RC are illustrated in Fig. 1(a). Without employing any formalism, which is widely available elsewhere and useful for performance evaluation,[24] here we describe them in a qualitative manner to keep the explanation concise and more consistent with the background of biomimicry. Briefly, an ideal daytime radiative cooler minimizes its thermal load by reflecting all the sunlight and environmental thermal radiation impinging on it, except over the atmospheric transparency window at 8–13 μm wavelength, where the cooler has unit emissivity or absorptivity and thus can send heat to the cold outer space most efficiently. In other situations of RC, for instance, where the device operates above the ambient temperature, a much broader range of MIR wavelengths can be utilized for emitting the excessive heat (solid curve in Fig. 1(b)).[30] Further adjustments may be applied to optimizing solar cells based on the bandgaps.[31,32] Similarly, in extending the RC concept to meet additional functional or aesthetic requirements, it is possible to introduce colors by carefully engineering the reflection behavior of the coolers in the visible region (dashed curve in Fig. 1(b)).[33] For heating and solar energy harvesting purposes, the spectral requirements are reversed with respect to RC. In this case, total absorption of the incident solar power is desirable, while heat loss *via* thermal radiation should be avoided at all MIR wavelengths (Fig. 1(c)).

A more sophisticated case of thermal management is the thermochromic smart windows.[34] Fig. 1(d) and (e) illustrates the concept when such devices operate at high and low temperatures, respectively. The two states share the same response of high transparency to visible light to perform the basic function of windows but have opposite requirements in the IR region. In summer, the smart window should block the invisible part of sunlight to reduce the heating of the indoor environment and meanwhile, possess high emissivity in the MIR region to promote RC (Fig. 1(d)); the reversal of both functions is favored in winter (Fig. 1(e)).

Besides the above scenarios involving sunlight, another compelling application requiring engineered thermal responses is IR stealth or camouflage. Although traditionally more efforts
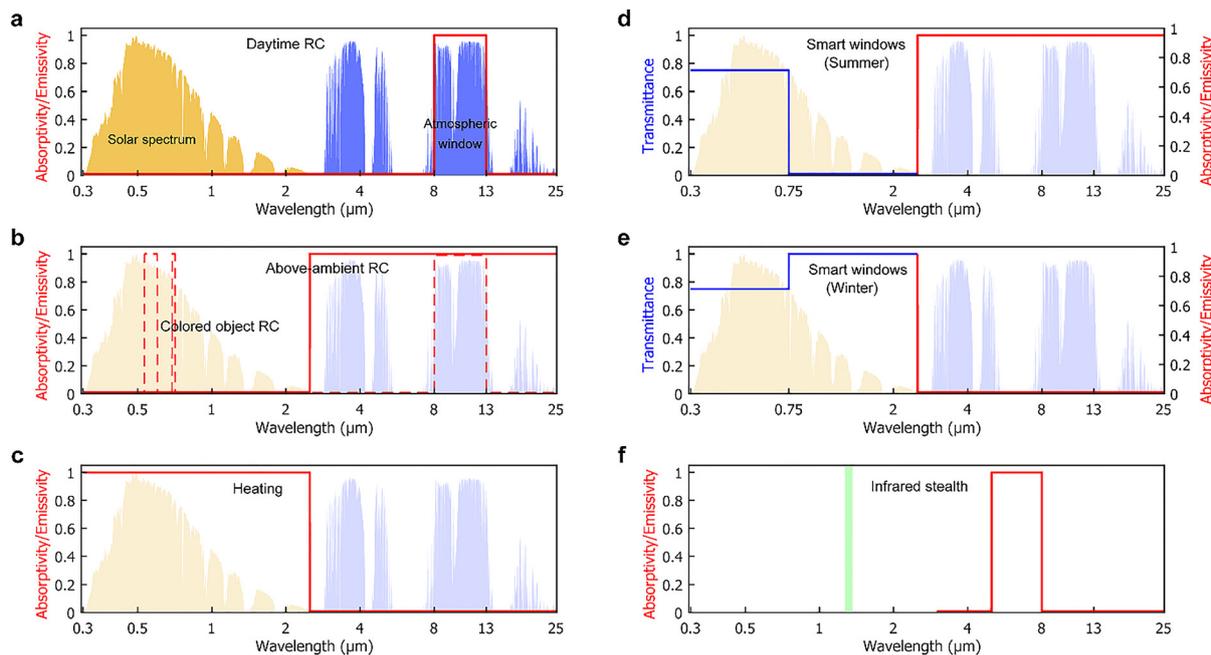
Fig. 1 Spectral requirements for different scenarios of thermal management. (a) Solar irradiance spectrum at the sea level (yellow shaded area) and the atmospheric transmission spectrum (blue shaded area) including the atmospheric transparency window at the wavelength range of 8–13 μm. The same spectra are displayed in the background of (b)–(e) as a reference. The red curve outlines the ideal spectrum for daytime RC, which eliminates absorption of light at all wavelengths but within the atmospheric window. (b) The spectral requirements for RC that operates above the ambient air temperature (solid curve) or needs to exhibit a certain color in the daytime (dashes curve). (c) Opposite to passive cooling, heating favors total absorption of the solar irradiation or in other words, solar energy harvesting, with the heat dissipation *via* thermal radiation being completely avoided. (d), (e) A good thermochromic smart window should retain transparency in the visible region and have opposite infrared optical properties at high (d) and low (e) temperatures. (f) For infrared stealth, the desired spectral responses vary in specific application scenarios. In one exemplary case, retroreflection is minimized by engineering the MIR spectral response (*e.g.*, selective absorption outside atmospheric windows) and angular scattering behavior at the wavelength of the incident NIR laser from a light detection and ranging device (green strip).

were put in optimizing the reflection directions of the incident NIR laser,[35] recent research has suggested taking thermal effects into account as well.[36] By overlapping the high emissivity band with the non-atmospheric window at 5–8 μm wavelength, the device could improve in thermal stability without sacrificing low IR detectability (Fig. 1(f)).

The representative spectral profiles summarized in Fig. 1 exhibit two features, both of which could pose substantial challenges for the design of photonic materials for thermal management. First, the wavelength span from UV to MIR is very broad. Over such an interval, not only will the dielectric properties of most materials vary significantly, but also the micro- and nanostructures can lose the desired functions once the operating wavelengths shift to another band. Second, when comparing across applications, it is noticed that in managing the heat load from solar absorption and thermal radiation, the ideal spectra are essentially combinations of three types of characteristic responses: broadband reflection, antireflection, and selective reflection. The two features therefore render the design a process of searching and optimizing ultra-broadband photonic materials with band-selective functions. Typically, design tasks of this kind are extremely challenging and need to be solved through trial and error, requiring iterative optimizations or training large-scale machine learning models based on computationally costly simulations. In this regard, finding alternative

shortcuts to high-performance materials can potentially reshape the landscape of materials design as well as the fields where the materials are used.

Interestingly, one possible solution may be just hidden in plain sight. Most if not all organisms can only live if their body temperature is within a relatively narrow range of temperatures. In other words, the need for thermal management is universal. Given the diversity of living organisms on Earth, numerous strategies, structures, and materials have been developed by nature through evolution, the ultimate and everlasting "optimization", to perform various functions that help the organisms to better survive in the dynamically changing environment. Natural selection results in a comprehensive library of exceptional examples for human to explore, learn and imitate in engineering. When coming to thermal management, the process of biomimicry can be adapted in accord with the aforementioned features, inspecting primarily organisms inhabiting in hot or cold environments. And even with simultaneous requirements for ultrabroad bandwidths and critical band selectivity, instructive natural prototypes fulfilling both aspects have still been discovered. A well-known example is the Saharan silver ants capable of performing RC.[37] More generally, as illustrated in Fig. 2, the search for inspiring prototypes can target one of the three characteristic responses to address the individual band-selective function. This approach is particularly
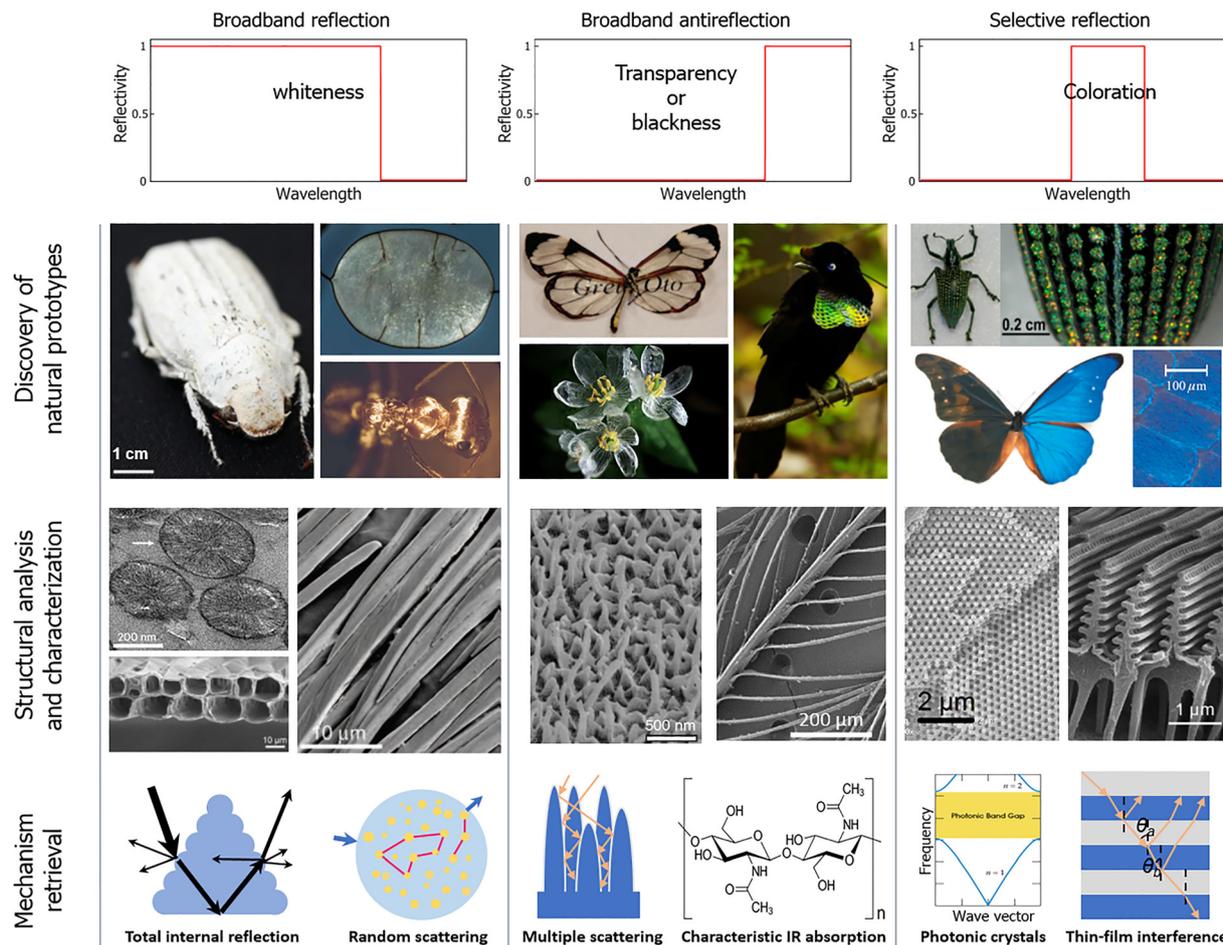
This journal is © The Royal Society of Chemistry 2025

Chem. Soc. Rev., 2025, **54**, 10690–10723 | **10693**

Fig. 2 Retrieval of structures and mechanisms from biological models. Typical spectral profiles needed for static thermal management (first row) and their possible origins from natural creatures (second row) containing diverse hierarchical micro- and nanostructures (third row), based on which various mechanisms (fourth row) are retrieved through modeling and analysis. Whiteness, blackness, and coloration on the spectra are broadly defined, referring to not only visual appearance in the visible region but also infrared responses featuring similar characteristic spectral profiles of broadband reflection (whiteness), broadband absorption (blackness), and selective reflection (coloration), respectively. Examples in the second, third, and fourth rows are selected to be representative in each step and do not necessarily have correspondence between the groups. Photographs of natural models in the second row (from left to right, top to bottom): a white *Cyphochilus* beetle. Reproduced with permission from ref. 61, Copyright (2018) The Royal Society. The highly reflective septum of the *Lunaria annua* plant. Reproduced with permission from ref. 49, Copyright (2020) CC BY-NC. A Saharan silver ant. Credit: Norman Nan Shi and Nanfang Yu. The ''glasswing butterfly'' *Greta oto*. Reproduced with permission from ref. 100, Copyright (2009) The Royal Society of Chemistry. Petals of *Diphylleia grayi* in the rain. Reproduced with permission from ref. 187, Copyright (2015) The Royal Society of Chemistry. A super black bird Wahnes' Parotia *Parotia wahnesi*. Reproduced with permission from ref. 106. Copyright (2018) CC BY. The Brazilian weevil *Entimus imperialis*. Reproduced with permission from ref. 127. Copyright (2010) Elsevier. A male *Morpho rhetenor* butterfly. Reproduced with permission from ref. 198. Copyright (2009) AIP Publishing. Electron microscopy images of analysed micro-/nanostructures in the third row: three nanospheres in the white chromatophore cells of a Pacific cleaner shrimp *Lysmata amboinensis* showing spoke-like structures. Reproduced with permission from ref. 56. Copyright (2023) Springer Nature. Hollow cell bilayer arrays in the septum of *L. annua*. Reproduced with permission from ref. 49, Copyright (2020) CC BY-NC. Hairs of the Saharan silver ants. Reproduced with permission from ref. 37, Copyright (2015) AAAS. Quasi-randomly positioned pillars in the transparent regions of *G. oto* butterfly wing. Reproduced with permission from ref. 101. Copyright (2015) Springer Nature. Normal black feather of *Lycocorax pyrrhopterus*. Reproduced with permission from ref. 106. Copyright (2018) CC BY. The scale of *E. imperialis*. Reproduced with permission from ref. 127. Copyright (2010) Elsevier. Wing scale of *Morpho sulkowskyi* butterfly. Reproduced with permission from ref. 203. Copyright (2020) Wiley-VCH. Although not included in the diagram, active thermal control can be achieved by switching between different static states, for which some strategies are adapted from those of natural creatures such as chameleons and cephalopods.

effective in the visible region, where broadband reflection, anti-reflection, and selective reflection are manifested as whiteness, blackness, and coloration, respectively. On the other hand, the IR optical properties of biological structures are usually not visually perceivable with the naked eye. However, the physical mechanisms and design principles retrieved from analyzing colored

functional organs are broadly applicable to the thermal wavelength range, still providing valuable guidance for engineering the IR part of the spectrum. Besides static spectral engineering, another important function that has inspiring solutions from nature is the active tuning of optical responses. Typical paradigms are species with the ability to change color, such as chameleons

10694 | *Chem. Soc. Rev.*, 2025, **54**, 10690–10723

This journal is © The Royal Society of Chemistry 2025

and cephalopods. To lay the basis for understanding bioinspired materials for thermal management, we discuss in the two succeeding sections illustrative examples of biological structures with static and dynamic optical properties, respectively.

3. Biological structures and mechanisms for static thermal management

In the complex tapestry of nature, organisms have evolved a diverse array of biological structures and mechanisms to maintain thermal stability in various environments. This section focuses on the subfield of static thermal management, delving into the intrinsic mechanisms by which organisms regulate temperature. Common strategies include broadband reflection to scatter incident light and minimize heating, antireflection for optimizing light absorption, and band-selective reflection that fine-tunes thermal properties. Biological structures with functions featuring these mechanisms exemplify the power of natural selection and adaptive evolution. Moreover, some organisms integrate multiple mechanisms into hybrid structures, enabling synergistic interactions towards optimal thermal management.

3.1 Broadband reflective structures

Color is essentially a visual perception and can be produced in many ways by mixing different spectral components of visible light properly. Structural whiteness, although commonly observed in insects, aquatic organisms, mammals and avifaunae, along with other colors and patterns, has garnered growing attention across multiple research domains. This phenomenon, arising from intricately evolved structures, presents tangible concepts for a wide spectrum of applications, spanning from displays to energy-saving thermal control materials and devices.[7,18,38]

Unlike structural colors, which are caused by the selective absorption or reflection of light at specific wavelengths, structural whiteness is heavily dependent on intricate surface microstructures that lead to the broadband reflection of light. Achieving a white appearance is challenging, as it requires reflection with uniform efficiency over the whole visible range,[39] resulting in a step-like reflectance spectrum. Natural structural whiteness could arise through diverse mechanisms of broadband light reflection, stemming from various physical origins including multilayer interference, total internal reflection, multiple scattering in disordered structures, and the color-mixing effect.[38,39] This section discusses representative biological structures that exhibit these mechanisms, aiming to lay the foundation for understanding structural whiteness and, more generally, broadband reflection. And as previously noted, the mechanisms also hold in the IR region.

3.1.1 Multilayer reflector and total internal reflection.
Certain organisms exhibit a silver or gold-like appearance due to broadband reflection resulting from multilayer interference. Bragg stacks, which are multilayered structures composed of alternating layers of two materials with different refractive indices, represent a widely utilized system for generating structural colors.[40–42] When two materials, denoted as A and B, each possessing refractive indices n_A and n_B, are stacked as alternating layers with thicknesses d_A and d_B, constructive interference of the reflected light from the interfaces occurs only when the wavelength meets the following condition:[43]

$$\lambda = \frac{2}{m}[n_A d_A \cos(\theta_A) + n_B d_B \cos(\theta_B)]. \qquad (1)$$

Here, θ_A and θ_B are the angles at which light is refracted in the respective materials, while m is an integer.

An illustrative instance is an "optimal" stack where each layer with high and low refractive indices has a thickness equivalent to a quarter-wavelength (Fig. 3(a)). Parker *et al.* introduced three multilayer designs to generate broadband reflectance: multi-stacked, chirped, and chaotic.[44] Consequently, the general approach to achieving broadband reflection in a multilayer stack involves creating diverse layer spacings to satisfy the conditions for constructive interference across multiple wavelengths within the visible spectrum.[45]

The classical example of multilayer reflectors is found in some fish species.[45] The phenomenon of diffuse whiteness is commonly associated with Mie scatterers. Nevertheless, an atypical configuration of multilayer reflectors results in diffuse whiteness across a broad range of observation angles in pyjama squid, offering a novel mechanism for generating angle-independent diffuse whiteness using multilayer structures (Fig. 3(b) and (c)). It effectively achieves a broadband reflectance of about 40% in the 200–1000 nm wave segment (Fig. 3(d)).[46] The white or silvery appearance observed in fish originates from alternating layers of guanine crystals and cytoplasm, functioning as a broadband, wavelength-independent reflector. Gur and colleagues discovered that the shiny surface of Gin-Rin is caused by multilayered reflectors comprising intertwined guanine crystals and cytoplasmic layers. Accumulations of guanine platelets with random yaw angles in the fish skin generate broadband reflectance through color blending.[47] Brady's study revealed that open-ocean fish species display camouflage that surpassed that of both nearshore fish and mirror-like surfaces, demonstrating significantly greater concealment at angles linked to predator detection and pursuit.[48]

Similarly, one-dimensional (1D) photonic nanostructures could be found in some plants. For example, Guidetti described and characterized that the septum of the *Lunaria annua* plant produced sizable, multi-centimeter, self-supporting iridescent sheets, exhibiting a unique silvery-white reflective appearance (see Fig. 2, row two, column one, top-right panel). This arises from the arrangement of cellulose fibers in the cells of the septum, which elicited colors resembling thin-film interference at the microscale (Fig. 3(e) and (f)). Hence, the vibrant, iridescent hues seen in the natural world frequently result from light interference within nanoscale periodic structures.[49]

We then move on to total internal reflection, which occurs when a beam of light propagates from a high refractive index medium to a low index one and impinges the interface at an angle exceeding the critical angle. Early research discovered that some plant leaves, due to their micro–nano surface
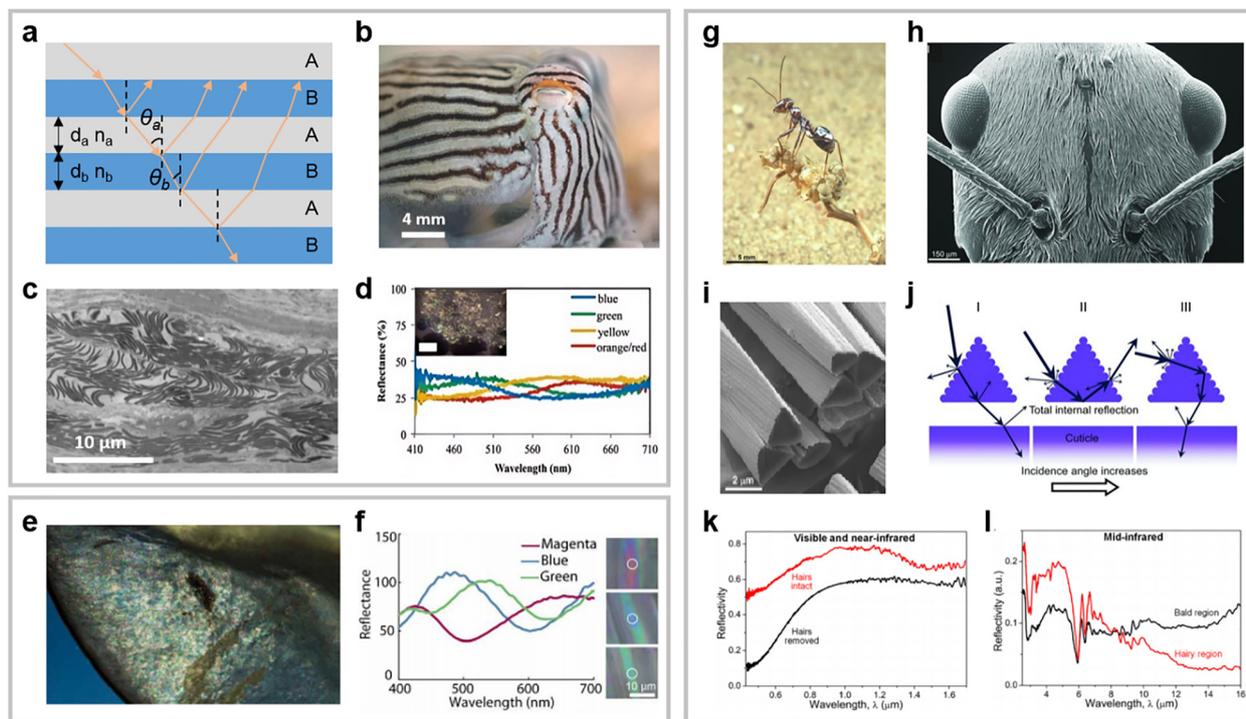
This journal is © The Royal Society of Chemistry 2025

Chem. Soc. Rev., 2025, **54**, 10690–10723 | **10695**

Fig. 3 Multilayer structures and total internal reflection mechanism of biological static systems. (a) Schematic diagram of the multilayer model. (b)–(d) Diffuse white of *Sepioloidea lineolata* white stripe. (b) The white and dark stripes produced by iridophores and superficial brown chromatophores. (c) Transmission electron microscopy (TEM) composite image displaying the contents of iridophores and the morphology of Bragg stacks. (d) Changes in spectral reflectance within the visible wavelength range. Reproduced with permission from ref. 46. Copyright (2014) Wiley-VCH. (e), (f) Reflective appearance of the septum of *Lunaria annua* plant. (e) A close-up photograph of *L. annua* septum showing interference colors with a high degree of reflectivity over an area sized about a few square millimeters. (f) Spectra taken from single-colored regions reflecting magenta, blue, and green light, along with corresponding optical micrographs. Reproduced with permission from ref. 49. Copyright (2020) CC BY-NC. (g)–(l) Thermoregulatory mechanisms of the triangular hair of the Saharan silver ant. (g) The silver ants emitting a dazzling radiance in the African desert. (h) Scanning electron microscopy (SEM) image of the head covered with a uniform and dense layer of hairs. (i) Cross-sectional view of a silver ant's hairs milled by focused ion beams. (j) Schematic diagram illustrating the optical interaction between visible and NIR light and a hair at different angles of incidence. The two surfaces on the ripple could enhance diffuse reflection in the UV-visible range. (k) Hemispherical reflectance measured within the visible-NIR range. The hair-covered region (red curve) shows evidently higher reflectivity than regions with hairs removed (black curve). (l) Reflectance in the MIR range under normal incidence. Reproduced with permission from ref. 37. Copyright (2015) AAAS.

structures, exhibit superhydrophobicity, and the air within their nanostructures can cause total internal reflection when immersed in water. Subsequently, this mechanism has also been found in other organisms.[50] A well renowned example of a natural creature exhibiting functions enabled by total internal reflection is the silver ant (*Cataglyphis bombycina*) (Fig. 3(g)).[37,51] Shi *et al.* were the first to discover that the heads of Saharan silver ants are adorned with densely packed triangular hairs (Fig. 3(h) and (i)) with two thermoregulatory effects: (1) improvement of broadband reflectivity across the visible and NIR spectrum (Fig. 3(j) and (k)). The hairs with a triangular cross-section interact with the incident light differently as the incidence angle varies. This property makes the reflectivity enhancement particularly strong for incidence angles beyond 30° and up to about 75°, as a result of total internal reflection at the hairs' bottom facets (Fig. 3(j), middle panel). Outside this angular range, Mie scattering by the hairs and total internal reflection at their top facets have increasing impacts (Fig. 3(j), left and right panels), directing more light into the ant's body. (2) Enhancement of emissivity in the MIR region that dissipates heat efficiently *via* thermal radiation. This effect at long wavelengths is caused

primarily by the effective gradient refractive index of the thin layer of hair structure, which reduces MIR reflectivity (Fig. 3(l)) and helps to keep body temperature much lower than the surroundings. Further discussions on the mechanisms of anti-reflection will be presented in Section 3.2, and it is worth mentioning that in bioluminescent systems such as the lantern of fireflies, total internal reflection needs to be suppressed with fine structures.[52] The biological remedy for a thermoregulatory issue may greatly influence technology by stimulating the advancement of biomimetic coatings for the passive cooling of objects.[37]

On this basis, Zhang and coworkers found another example of total internal reflection.[53] They paid attention to *Neocerambyx gigas'* outstanding temperature regulation with its dual-scale fluffs. The longicorn beetle's forewings display a radiant golden sheen. Upon closer examination, it is observed that the fluffs create upward triangular patterns from the base to the tip, forming a dual-scale structure comprising two smooth surfaces and a rippled surface with fringes. The intense reflectiveness of the forewings is a result of the combined impact of Mie scattering near the edges of the fluffs and total internal

10696 | *Chem. Soc. Rev.*, 2025, **54**, 10690–10723

This journal is © The Royal Society of Chemistry 2025

reflection within the triangular structure, where light is captured and then emitted in all directions. This example will be discussed again in Section 5.1.

3.1.2 Multiple scattering in disordered structures. At the crossing of biomimicry and thermal management, where Sun is a major thermodynamic source, the creation of a white appearance requires the capability to diffuse light of all visible wavelengths in the continuous spectrum of solar radiation through, *e.g.*, scattering. The diffusion minimizes the coherent interference of light that leads to coloration and therefore, provides a possible route to wide-angle, broadband high reflectance.

Light diffusion is a common effect in materials with random scattering inclusions or disordered structures.[54,55] Indeed, by investigating the biological organisms of animals and plants exhibiting a white appearance, plenty of inspiring disordered photonic materials have been discovered.[39] At the individual scatterer level, a particularly interesting example based on birefringent nanospheres was recently identified in shrimp by Lemcoff and coworkers.[56] As shown in Fig. 4(a), a Pacific cleaner shrimp (*Lysmata amboinensis*) features a bright white color over several regions of its body, such as the carapace, tail

(Fig. 4(b)), and antennae, arising from a thin layer of white chromatophore cells. Using cryo-SEM, it is revealed that assemblies of very densely packed nanospheres ($\sim$50–65% in filling fraction, Fig. 4(c)) are most likely responsible for the whiteness, whereas the dense packings noticeably deviate from the typical optimal condition of $\sim$30% that suppresses undesired optical crowding. This puzzle is resolved by further analyzing the chemical identity and structural properties of the nanospheres, which turn out to be isoxanthopterin molecules stacked in a spherulitic arrangement (Fig. 4(d)). The oriented stacking results in birefringence of the particles, with the radial and tangential refractive indices being 1.4 and 1.96, respectively. The influence of this anisotropy on the optical properties of particle assemblies is significant.[57] Within a modest degree of polydispersity, the birefringent nanospheres consistently produce higher and more uniform reflectance than isotropic particles of comparable refractive indices do in the visible regime for a wide range of filling fractions (Fig. 4(e)). The mechanism behind the drastic improvement is that birefringence in the present configuration helps to reduce the near-field coupling between the particles, especially when they are densely packed. Consequently, scattering is enhanced, allowing
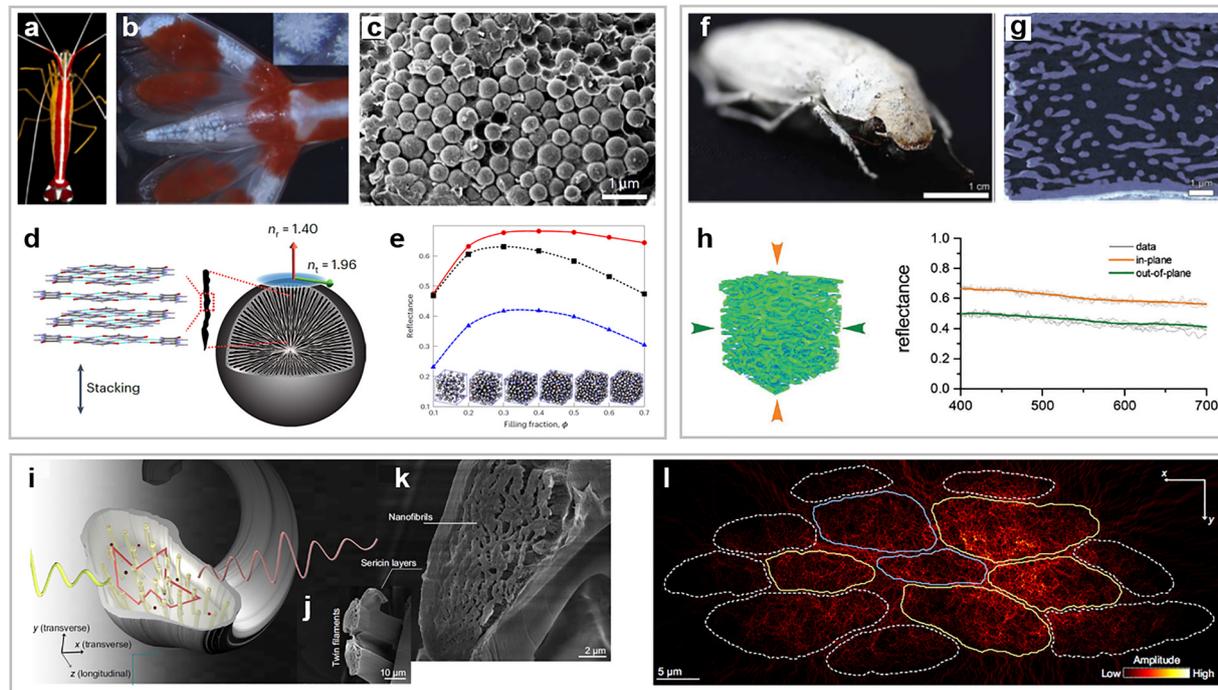

Fig. 4 Whiteness arising from multiple scattering. (a)–(e) Thin layers of birefringent nanospheres in shrimp. (a) Image of the Pacific cleaner shrimp. (b) Optical micrograph of white chromatophore cells in the tail. (c) Densely packed nanospheres in the white region from an antenna. (d) Schematic of a birefringent nanosphere showing oriented stacking of isoxanthopterin molecules. (e) Comparison of simulated total reflectance for disordered assemblies of 305-nm birefringent (red curve) and isotropic (black and blue curves) nanospheres at different filling fractions. Reproduced with permission from ref. 56. Copyright (2023) Springer Nature. (f)–(h) 3D chitinous networks in a white beetle wing scale. (f) Image of a white beetle Cyphochilus. (g) High-resolution tomographic slice of a beetle wing scale. (h) Left: 3D reconstructed morphology of the inner structure of a beetle wing scale; right: simulated reflectance for different orientations of the network volume. Reproduced with permission from ref. 64. Copyright (2018) Wiley-VCH. (i)–(l) Nanofibrils in native silk. (i) Schematic of biogenic light localization in a silk filament through multiple scattering by the interior nanofibrillar structures. (j,k) SEM micrographs showing the edge of twin fibroin filaments (i) and nanofibrils in a filament (k). (l) Light localization as indicated by simulated electric field distribution in 14 cohesively bonded silk filaments at $\sim$600 nm wavelength. Reproduced with permission from ref. 66. Copyright (2018) CC BY.

This journal is © The Royal Society of Chemistry 2025

Chem. Soc. Rev., 2025, **54**, 10690–10723 | **10697**

whiteness to arise from ultra-thin layers of materials. Another appealing aspect of this strategy is its effectiveness in an aqueous environment, which is more challenging than in air due to the reduced refractive-index contrast.

One of the best-known examples effective in air is the white beetles (Fig. 4(f)), *e.g.*, *Cyphochilus* and *Lepidiota stigma*. In ref. 58, Vukusic *et al.* first reported the brilliant whiteness resulting from a three-dimensional (3D) photonic medium in the *Cyphochilus* beetles' scales, which have an elongated flat shape and are only about 5 μm thick, substantially thinner than many synthetic systems. The interior fine structure of the scales is identified to be a network of randomly interconnected chitin filaments with a diameter of around 250 nm. To fully understand how this 3D photonic network can result in efficient light scattering to generate white reflection, tremendous research efforts have been devoted to modelling its optical properties.[59–61] However, given the random orientations of the chitin filaments and distributions of their junctions, analytical treatments would suffer various limitations. If possible, a better approach is otherwise to import the reconstructed 3D replica into a Maxwell's equations solver for numerical solutions.[62,63] An important advancement in this regard is demonstrated in ref. 64. By employing a powerful technique that allows ptychographic X-ray computed tomography under cryogenic conditions, the 3D network morphology of the interior of white beetle wing scale is obtained at a high resolution (Fig. 4(g) and (h)). Based on this model, full-wave simulations reveal several interesting properties of the photonic network structure, including the dependence of reflectance on its orientation (Fig. 4(h)) and that the scattering power is achieved with minima of scale thickness and material use, showing the power of evolutionary optimization. Besides beetles, certain types of pierid butterflies, *e.g.*, *Pieris rapae*,[65] have also been identified to have whiteness generated from thin layers of photonic materials.

Some biological photonic materials can host physics that is conceptually more complicated. In native silk, numerous nanofibrils follow a parallel arrangement along the axis of the silk fiber (Fig. 4(i)–(k)), making it possible for light to undergo scattering in a quasi-two-dimensional (quasi-2D) structure on the transverse plane and get Anderson-localized, an exotic physical phenomenon rarely found in 3D or in nature.[66–68] As single silk filaments are bundled, the degree of localization increases; see Fig. 4(l). The biogenic localization strongly suppresses light transmission and hence, enhances reflectance in the visible and NIR bands, giving rise to the white appearance of silk under sunlight illumination. Moreover, thanks to its protein composition, native silk exhibits strong MIR emissivity, through which more heat is radiated than generated by solar absorption, providing another natural solution to passive cooling.[66,69,70] The observation of Anderson localization also implies the possibility to discover more exceptional optical properties in natural systems.

3.1.3 Color mixing. Complex effects can also be achieved through color blending, a phenomenon observed in certain organisms. As such, a structural coloration may be linked to pigment-based hues (for example, cephalopods[71]), luminescence

(as seen in the *Troides magellanus* butterfly[72]), or another form of structural coloration (such as in the *Entimus imperialis* weevil[73] or the *Papilio* butterfly[74]).

The production mechanism of white may also be the color mixing effect, such as red, green, blue superposition to produce white. Arising from the relationship between the intensity of reflected light and the angles of observation or incidence, structural whiteness can be categorized into two forms: diffuse whiteness (independent of angle) and metallic silver (angle-dependent).[75,76] In the case of the former, light scattered by random media like particles, micropores, chitinous networks, and multidirectional plates retains its inherent colors regardless of the viewing angle. This diffuse whiteness can serve as a backdrop for colored patches, enhancing contrast and visual distinction, as seen in the white scales adorned with scattering beads of the pierid butterfly.[76] However, there are very few documented instances of angle-dependent whiteness in butterflies. One prime example is the Costa Rican hesperiid butterfly, *Carystoides escalantei*, which showcases diverse manifestations of whiteness, encompassing both angle-dependent and angle-independent characteristics, evident on its wings and antennae (Fig. 5(a)).[77] Ge and colleagues focused on the scales of angle-dependent spots, which are oriented vertically and exhibit variable tilting. These scales display undulating patterns resembling ripples and are composed of periodic ridges and ribs that run perpendicular to the ridges on both sides of the scale (Fig. 5(b) and (c)). The white coloration seems to result from the combination of diffracted colors originating from the hierarchical structure and the tilting of the scales. The angle-dependent scales amplify retro-reflection (Fig. 5(d)).[77] This examination can potentially accelerate the advancement of materials that imitate structural whiteness, suitable for applications in sensing and low-energy consumption displays. The wing scales of the butterfly *Argyrophorus argenteus*,[76] not just *Carystoides escalantei*, demonstrate exceptional broadband reflectivity with an extremely thin structure (thickness smaller than 1 μm). They feature a distinct variation in periodicity aligned parallel to the reflective surface rather than perpendicular to it. The unique coloration is due to a sub-micron scale design that generates broadband diffuse silver reflectivity through the addition of multiple colors. The combination of structural colors reflected from the membrane scale results in a transition from metallic to silvery white on certain butterfly wings. Liu *et al.* found that the ventral side of the butterfly *Curetis acuta* features highly improved broadband reflection from bright silver scales (Fig. 5(e)). This is due to the color mixing effect resulting from the irregular spacing and thickness of the laminated scales (Fig. 5(f) and (g)). In air, the maximum temperature difference is 2.4 °C, whereas in a vacuum (Fig. 5(d)), it reaches up to 5.8 °C as a result of the elimination of convective heat transfer (Fig. 5(h)).[75] Seashells have bright whiteness that are considered to be ideally designed for display devices. Various species of giant clams employ two mechanisms to create white coloration, which are directly comparable to the RGB pixel strategy used in modern electro-optical technology. Both mechanisms are distinctive
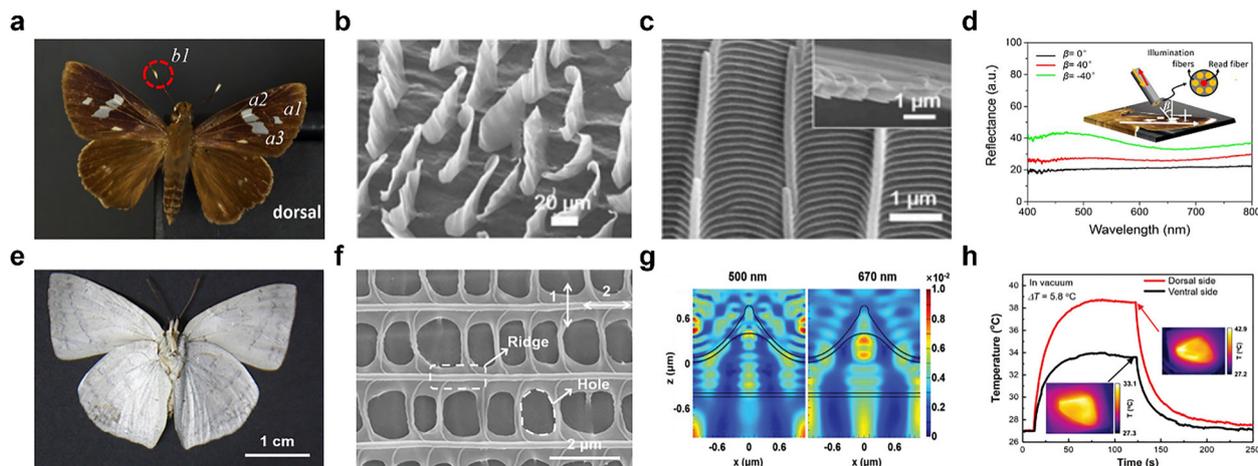
Fig. 5 Colour mixing structures in biological static systems. (a)–(d) Angle-dependent white of *Carystoides escalantei*. (a) A photograph of a male specimen of *Carystoides escalantei*. (b), (c) The SEM images of angle-dependent spot a1 (male, dorsal) and, in the inset, a cross-sectional image illustrating the scale thickness. (d) The reflectance spectra of spot a1 (male, dorsal) obtained from the vertical, wingtip, and wing surfaces. Reproduced with permission from ref. 77. Copyright (2017) National Academy of Sciences. (e)–(h) Bright silver brilliancy from irregular microstructures in butterfly *Curetis acuta*. (e) Image of the ventral side of the male *C. acuta*. (f) SEM image of the middle section of a silver scale. (g) The arrangement of Poynting vectors on cross sections of full-scale models at 500 and 670 nm. (h) The temporal variation curves of the temperature on the dorsal and ventral sides of the wings measured under both air and vacuum conditions. Reproduced with permission from ref. 75. Copyright (2019) Wiley-VCH.

systems of structural color that achieve white through color mixing.[78,79]

3.2 Antireflective structures

In addition to regulating thermal energy to sustain a stable body temperature, organisms can also harness thermal energy from the surroundings for additional use. Solar radiation serves as the primary energy source for both Earth's surface and organisms. The efficient utilization of this resource is crucial for the survival of the majority of living organisms, particularly those that are small in size.[80,81] Under these circumstances, diverse micro- and nanostructures have emerged across various organisms to mitigate unwanted reflection for specific purposes. For example, the compound eyes of nocturnal insects, such as moths, feature subwavelength-sized nanoarray structures, which give rise to highly efficient anti-reflective (AR) properties.[82] These properties significantly enhance light transmission under low-light conditions, thereby substantially improving the visual sensitivity in the visible and NIR spectra.[83] Following this, comparable structures have been found on the compound eyes and translucent wings of various arthropods.[84,85] In this discussion, we present the designs and functions of these biological antireflective structures.

The moth eye structure consists of a regular arrangement of sub-wavelength cones or cylinders, which function to progressively align the optical impedance of the object with its environment. AR properties can be attributed to the interaction of light with objects and the surrounding medium, which have different refractive indices.[80,84,86,87] As depicted in Fig. 6(a), when the dimensions of the AR structures are smaller than the wavelength and are situated at the sub-wavelength or nanoscale, an alternative approach is utilized. The AR structures do not significantly affect the behavior of light and instead cause it

to gradually bend, as if the AR surface possesses a gradient of effective refractive index.[83,88] Even though the angle of incidence is changed, the coating still demonstrates a relatively uniform change in the refractive index towards the direction of incident light, thereby reducing the reflection of light across a wide range of wavelengths.[82,88–91]

The ommatidium of the nocturnal moth is equipped with AR nanostructures, comprising an array of pillars measuring 200 to 300 nm in size.[86,90,92] These structures serve the dual purpose of diminishing light reflection and improving the moth's ability to see in low-light conditions (Fig. 6(b)). As depicted in Fig. 6(c), the sub-wavelength structures are meticulously organized in a precise array on the surface of the moth ommatidia. The anti-reflective capabilities of the moth eye structure were initially validated through scaled-up microwave experiments involving dielectric lens models adjusted to the microwave frequency. This was subsequently corroborated through comparative spectrophotometric assessments conducted on corneal fragments from insects with both nippled and non-nippled facets.[92] The moth possesses a compound eye consisting of a hexagonal arrangement of ommatidia. Stavenga and coworkers identified that the corneal surface of the ommatidium was additionally adorned with a hexagonal array of cone-shaped nanostructures, approximately 200 nm in height, which they referred to as "nipples". Furthermore, a scalable biomimetic antireflective film was developed, featuring a multiscale hierarchical architecture inspired by the ommateum.[90] Ding *et al.* examined the red dragonfly (*Crocothemis servilia*), which has two eyes with a substantial surface area. Their findings demonstrated the remarkable anti-reflective properties of the compound eyes of the dragonfly *C. servilia*.[93]

Following this, extensive electron microscopy investigations revealed comparable organized nipple arrays in numerous

This journal is © The Royal Society of Chemistry 2025

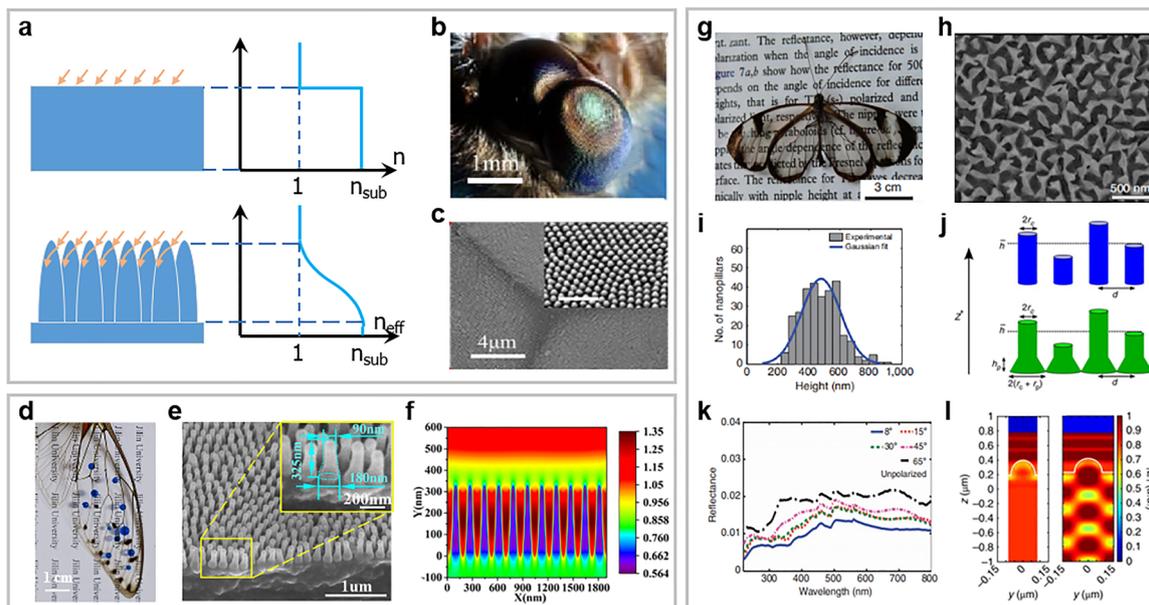*Chem. Soc. Rev.*, 2025, **54**, 10690–10723 | **10699**

Fig. 6 Gradient index mechanism and disordered structures of biological static system: (a) Diagrams of the mechanism for antireflection of the moth eye and cicada wing. (b)−(f) Anti-reflection mechanism of periodic arrays in moth eyes and cicada wings. (b) Complete compound eyes of a moth and (c) SEM image of the details of ommatidia showing the top view of the surface. Inset is a close-up SEM image to show the sub-wavelength structure array in one ommatidium; scale bar: 1 μm. Reproduced with permission from ref. 92. Copyright (2018) CC BY. (d) Digital photograph of a cicada *M. intermedia* wing, with droplets on it to show hydrophobicity, placed on a sheet of paper. (e) Magnified image of a cicada wing. (f) Simulated electric field profile for the cicada wing. Reproduced with permission from ref. 95. Copyright (2019) American Chemical Society. (g)−(l) Random nanostructures for the omnidirectional anti-reflection properties of the glasswing butterfly. (g) The wings of the glasswing butterfly (*Greta oto*) are comprised of three distinct regions, including transparent, deep brown, and white sections. (h) The top perspective reveals the seemingly haphazard arrangement of the columns, a pattern supported by the 2D Fourier power spectrum of the nanostructure positions derived from this SEM image. (i) A statistical analysis of the nanostructure height in the transparent region on the dorsal side of the butterfly wing. (j) The established model diagram of the anti-reflection structure. The glass wing structure is modeled using nanorods with fixed radius but randomly distributed heights. (k) The omnidirectional and broadband reflection in the visible light range. Reproduced with permission from ref. 101. Copyright (2015) Springer Nature. (l) Finite-difference time-domain simulations were utilized to examine the near-field scattering profile in the postdiscal and basal regions at the wavelength of 420 nm. Reproduced with permission from ref. 102. Copyright (2018) Springer Nature.

Lepidoptera species, encompassing both moths and butterflies.[94] Over 30 years following the initial identification of the moth eye structure, a nearly indistinguishable nanostructure was found in the translucent wing areas of the hawkmoth.[95–98] The cicada wing depicted in Fig. 6(d) appeared thin and transparent, with a fibrous support network distributed on it, and the distributed nanostructures on the cicada wing (Fig. 6(e)) are clearly visible. The effective refractive index of the mixed media underwent a smooth change along the height of the nanocones, presenting a significant contrast to the interface lacking nanostructures. Consequently, the nanocones facilitate a seamless transition from air to the substrate, leading to reduced Fresnel reflection and exceptional antireflection performance (Fig. 6(f)).[95] Additionally, a unique antireflection structure was identified on the black scales of the West African Gaboon viper (*Bitis rhinoceros*). The leaf-like microstructures on the black scales comprise densely packed crests. The angle-independent low reflectance of the black scales is attributed to the synergistic effect of the microstructures and dark pigments.[99]

The *Greta oto* butterfly wings (Fig. 6(g)) exhibit omnidirectional broadband antireflection[100] due to the disordered arrangement and varied size distribution of nanopillars (Fig. 6(h)).[101]

The angular independence of the broadband antireflection is experimentally characterized through angular resolved specular reflection measurements (Fig. 6(k) and (l)). The omnidirectional antireflection properties stem from the random distribution of nanopillar height and width (Fig. 6(i) and (j)) rather than their random arrangement. *Chorinea faunus*, a member of the Riodinidae family native to South America, exhibits a noteworthy feature: the basal transparent area is comprised of nanostructures of similar shapes but at a lower density. The findings indicated minimal alterations with changes in the incident angle, indicating its potentially valuable angle-independent scattering characteristic.[102] This scattering attribute can alleviate the challenge of detecting optical signals at wide angles, a common issue encountered in numerous light-based devices, including implantable intraocular pressure sensors. Another instance of utilizing disordered surfaces for transparency in nature can be seen in the wing membrane of the dragonfly *Aeshna cyanea*, where a rough surface consisting of wax structures has been observed.[103]

When the depth scale and spacing between individual structures are comparable to the wavelength of incident light, light may become trapped between these structures, resulting in multiple internal reflections.[104] As a result, incident light can

10700 | *Chem. Soc. Rev.*, 2025, **54**, 10690–10723

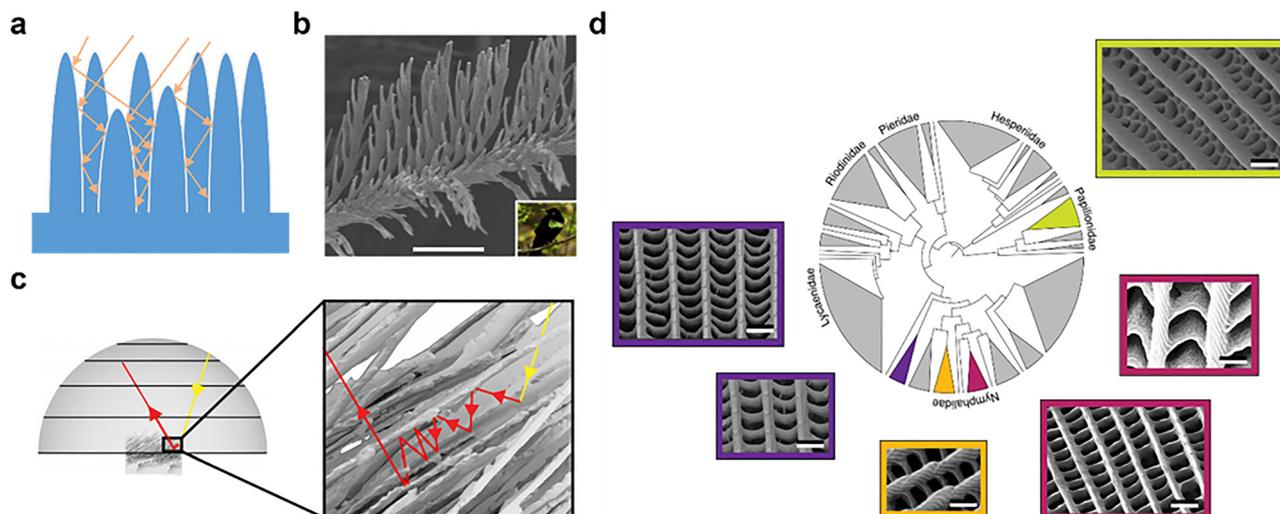This journal is © The Royal Society of Chemistry 2025

Fig. 7 Multi-scattering mechanism of biological static systems. (a) The multiple reflections of incident light within the microstructure. (b), (c) Multi-scattering in super black bird of paradise feathers. (b) SEM image of a spherical tubular array of super black feathers. Scale bar: 50 μm. (c) Simulation from software package FRED demonstrates multiple scattering of a ray of light between the spherical tubular structures of the super black feathers. Reproduced with permission from ref. 106. Copyright (2018) CC BY. (d) The widely distributed and morphologically diverse super black butterfly scales. Scale bar: 1 μm. Reproduced with permission from ref. 110. Copyright (2020) CC BY.

be effectively absorbed, significantly minimizing reflection at the specific wavelength (Fig. 7(a)). McCoy *et al.* documented the super black effect associated with microstructures on the peacock spiders. The birds of paradise (Paradiseidae), which are ecological counterparts of peacock spiders, have also developed super black areas near bright color patches.[105] McCoy and colleagues established the connection between super black plumage in five species of birds of paradise and their microstructures. They identified highly altered barbules with microscale spikes along the edges on the super black feathers (Fig. 7(b)). The intricate arrangement of deep, curved indentations between the tiniest branches of the feather vane ensnared incoming light and absorbed it through multiple instances of scattering and reflection. The most minimal reflectance (0.05–0.3%) is attained when observed from the distal direction (Fig. 7(c)).[106] Due to an intricate hierarchical microarchitecture, butterfly wing antireflection function has received particular interest. In 2004, Vukusic and colleagues initially demonstrated that the nanostructures found in the wing scales of *Papilio ulysses* butterflies played a substantial role in their black appearance.[107] The microstructure of the black area on butterfly wings differs from the other colored regions, resulting in a high level of light absorption.[108,109] Several black butterfly wings with angle-resolved scattering were documented.[110] While the specific morphologies vary in these accounts, four types of characteristic structures can be identified. The initial category consists of an upper lamina layer perforated with a nanohole array, also known as a quasi-honeycomb-like configuration.[111] The second and third categories, referred to as longitudinal ridges or an inverse V-type structure and trabeculae, are both distinct and beneficial for the enhancement of absorption.[110,112] In addition, there is a basal lamina layer at the bottom. Unlike the regular arrangement of the

moth eye structure, the majority of the quasi-honeycomb-like structures on butterfly wings lack order to prevent reflection with a dependence on incidence or azimuthal angles. The lower lamina layer is smooth and unstructured, capable of reflecting light that escapes from the upper structures, resulting in the reabsorption of light.[85,108,113,114] Zhang's group conducted a study on a nano-scale antireflection pattern found in the black scales of the *Troides aeacus* butterfly wing, which can be considered a natural solar energy absorber.[115] They also described a disordered nanohole structure with ridges, inspired by *Papilio ulysses*, which exhibits omnidirectional light absorption in contrast to the typical ordered structure.[116] In 2017, Siddique and colleagues conducted a study on the scales of *Pachliopta aristolochiae*, which harbor complex micro and nanostructures.[117] These nanoholes are supported by the ridges and cross-ribs, extending approximately 800 ± 35 nm into the interior of the scales. Davis initially analyzed the scale structure of 11 butterflies, consisting of seven ultra-black specimens and four control specimens. Each of the butterflies exhibit scales with a top layer penetrated by quasi-periodic apertures (Fig. 7(d)).[110] Their findings illustrate that butterflies achieve ultra-black appearance by fabricating a sparse material with a large surface area to enhance absorption and reduce surface reflection. The primary absorption takes place within the nanohole arrays rather than the ridges. These discoveries carry significant implications for the development of optical devices, solar cells, and, if enlarged, radar-absorbing materials. Although the surface microstructures of butterfly wings have been thoroughly examined for their structural coloration or optical characteristics in the visible spectrum, their attributes in the IR wavelengths, which may be linked to thermoregulation, remain largely unexplored. Krishna and colleagues discovered that the MIR emissivity of butterfly wings from warmer

This journal is © The Royal Society of Chemistry 2025

Chem. Soc. Rev., 2025, **54**, 10690–10723 | **10701**

regions, such as *Archaeoprepona demophoon* and *Heliconius sara*, is as much as twice that of butterfly wings from cooler regions, such as *Celastrina echo* and *Limenitis arthemis*. Additionally, they elucidate the pivotal role of periodic microstructures in the MIR.[118]

3.3 Structures for selective reflection

The third class of spectral profiles correspond to band-selective reflection. This type of optical responses is easily perceivable at visible wavelengths and has thus been studied most extensively in that spectral range.[13–15] In the IR region critical for thermal management, the discovery of band-selective reflective structures is not as straightforward as in the visible region, but the mechanisms retrieved from the latter can be readily referenced to guide the design, and in certain applications such as RC, the visual appearance of the devices can be a secondary consideration.[33] In this sense, we introduce biophotonic structures that possess static or dynamic band-selective reflection properties through discussing examples of color production.

3.3.1 Photonic crystals. Of all the possible origins of structural coloration, a particularly interesting category is photonic crystals (PhCs).[119] While as seen in the preceding sections, whiteness often results from scattering by random structures or mixing color components generated by different sources (*e.g.* pigments, luminescence, and optical resonances), producing

a particular color intuitively requires optical effects from much ordered structures. PhCs represent a wide range of such media. Analogous to crystals in solid state physics, PhCs are periodic arrangements of dielectric materials, with the periodicity typically on the order of the wavelengths concerned. The multilayer film discussed earlier is an example of the simplest PhCs in 1D, where interference is responsible for the optical properties including coloration. More sophisticated optical phenomena can be expected with 2D and 3D PhCs, both widely existing in nature,[120–122] when diffraction is brought into play by the lattices. Here, we focus on representative 3D biological PhC structures found or derived from insects and shrimps. For 2D PhCs and other mechanisms of structural coloration, the interested reader may refer to ref. 123, among excellent references discussing relevant topics in a broader context.[14,43,124]

The first 3D architecture identified in nature displaying organismal structural colors and terminologically associated with PhCs is probably in a weevil, *Pachyrhynchus argus*.[125] Since then, many examples of natural PhCs have been discovered not only in beetles (*e.g.*, weevils and longhorns) but also in butterflies. Fig. 8(a) presents the dorsal-view optical images of a neotropical weevil *Entimus imperialis*, along with the SEM micrographs of its rainbow-colored wing scales, showing domains of single-network diamond (D-surface) structures formed by stacks of chitinous slabs with air cavities.[122,123,126–128] Different colors
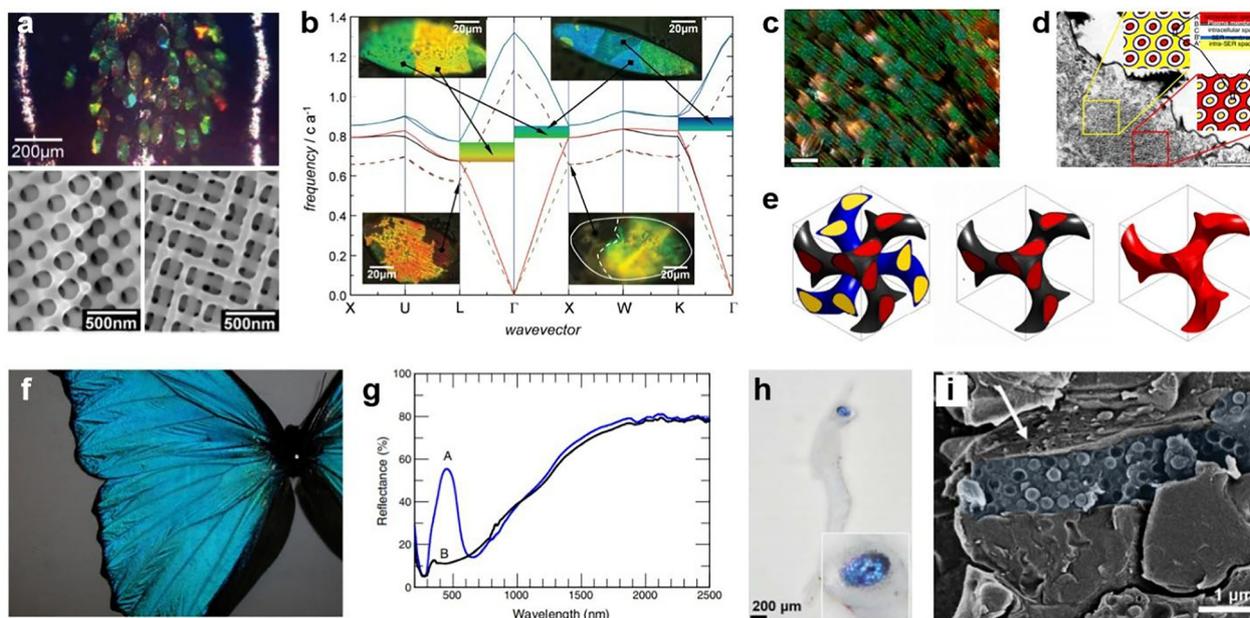

Fig. 8 Natural photonic crystals in beetles (a), (b) and butterflies (c)–(g) and biological glasses in shrimps (h), (i). (a) Microscopy image (top panel) of the scales covering the elytra of neotropical weevil, *Entimus imperialis* and SEM images showing the 3D PhCs in the green/yellow domain (lower left/right panel). (b) Calculated photonic band structure for the colored (solid lines) and colorless (dashed lines) regions in the scales of *E. imperialis* in (a). Reproduced with permission from ref. 128. Copyright (2013) Wiley-VCH. (c)–(e) 3D gyroid PhCs in butterfly wing scales. (c) Optical micrograph of the ventral wing scales of the butterfly *Callophrys gryneus* (scale bar: 100 μm). (d) TEM image of a wing scale cell from a developing pupa of *Callophrys gryneus* (scale bar: 1 μm) showing concentric rings arranged in a triangular lattice. (e) Unite cell model showing the development of the wing scale cell. From left to right: core–shell double gyroid structure, core–shell single gyroid, and single gyroid network of chitin. Reproduced with permission from ref. 129. Copyright (2010) National Academy of Sciences. (f) Image of the top surface of a butterfly *Morpho didius* wing and (g) its total reflectance (curve A) in comparison to that of the bottom surface (curve B). Reproduced with permission from ref. 130. Copyright (2011) Elsevier. (h) Polarized optical micrograph of a zoea of caridean shrimp (inset: zoom-in image of the eyes), and (i) Cryo-SEM image of the reflector cells for the color blue. Average particle size: ∼247 nm. Reproduced with permission from ref. 132. Copyright (2023) AAAS.

10702 | *Chem. Soc. Rev.*, 2025, **54**, 10690–10723

This journal is © The Royal Society of Chemistry 2025

are originated from different orientations of the same PhC structure in each domain. Great efforts have been devoted to understanding the optical function based on the results of structural analysis. For example, ref. 128 reported a comprehensive investigation of the correlation between the structure/composition and the optical properties of these PhCs. The computed photonic band diagram in Fig. 8(b) clearly shows the different band-gap widths in different directions (solid curves), in accordance with the iridescent visual appearance. It is also revealed that for the colorless domains of the scales, the vanishing band gaps (dashed curves) are a consequence of reduced refractive index contrast, as air is replaced by SiO_2 in these regions.[128] The physiological mechanism of the substitution is nonetheless still not clear.

Another simple yet important class of triply periodic cubic structures found in insects is gyroid. For many butterflies, vivid colors are produced by a chitinous matrix with ordered air holes or networks of cuticular chitin and air in the wing scales (Fig. 8(c)).[129] Particularly, with the help of synchrotron small angle X-ray scattering technique, the complex color-generating nanostructures in papilionid and lycaenid butterfly scales have been identified to be single network gyroid PhCs. The optical function can be predicted fairly well based on the structural data. More interesting is how the model helps to understand the development of these biological PhCs. By referencing the TEM images of the structures in a developing pupa of *Callophrys gryneus* (Fig. 8(d)), it is deduced that these butterfly PhCs in scale cells initially develop as a thermodynamically favored, core–shell double gyroid (Fig. 8(e), left panel). The precursor motifs then transform through chitin deposition and cell degeneration into a single gyroid network (Fig. 8(e), middle and right panels), which is more efficient in performing optical functions. This study exemplifies a possible route to engineering and fabricating complex gyroid structures at the micro/nanoscale. With other PhC structures found in certain butterflies such as *Morpho didus*,[130] very bright colors are produced in the blue region of the visible spectrum (Fig. 8(f)), which is rare with natural pigments. When the structures' long-range order is removed, a stark difference in color is observed on the bottom side of the same wing (Fig. 8(g)). Moreover, chitin as the most common constituent material of the shell of insects exhibits modest thermo-optic effects.[130] This property leads to traceable lowering of its refractive index and in turn blue-shifting of the photonic band when the temperature increases within a moderate range, offering a new way to control the optical properties of chitin-based photonic structures, in addition to heat- and stress-induced expansion.

3.3.2 Photonic glasses. Inspiring coloration strategies have also been discovered in sea creatures. To lower the risk of being detected in aquatic habitats, many oceanic prey animals need to possess transparent bodies while trying to make their conspicuous eye pigments unseen by the predators from any directions.[131] Besides reducing the size of the eyes/retinas, certain larval decapods develop a reflector overlying the eye pigments and showing a color matched to the background, usually varying from deep blue to yellow-green. One such

example of a zoea of caridean shrimp is shown in Fig. 8(h). Shavit et al. unveiled the mechanism of the eyeshine phenomenon with systematic structural analyses and optical modelling.[132] The results suggest that a compact photonic glass comprising an assembly of wavelength-sized, high-index ($n = 1.96$) isoxanthopterin nanospheres lacking long-range ordering is key to achieve the desired crypsis. The color of the eyes can be tuned by changing the sizes of the nanospheres (across different shrimp species) and/or the particle ordering. Because of the relatively lower particle filling fraction and lack of long-range periodicity, this photonic glass does not produce iridescence as many biological PhCs do but exhibits colors insensitive to the viewing angle. If limiting the context strictly to PhCs, similar non-iridescent coloration has been reported for certain parrots (e.g., the scarlet macaw[133] and Steller's jay[134]), where the spongy keratin structures in the feather barbs only have short-term order, and many other animals and plants.[135] These photonic structures possessing only short-range order are sometimes termed amorphous PhCs.[136]

3.4 Thermoregulation with multiple mechanisms

As can be seen from the above discussion, diverse nanostructures and mechanisms of light manipulation have been identified in biological models showing exotic responses to certain electromagnetic radiations. In realizing effective thermal management, nonetheless, individual nanostructures and associated mechanisms are usually inadequate to give optimal performance over all the involving frequency bands. Instead, complementary functions need to be achieved properly in each band. Before concluding this section, we highlight two cases of thermoregulation where multiple mechanisms are combined to fulfill the electromagnetic requirements in different wavelength regimes and environments. Note that some examples discussed earlier with a different focus, such as the Saharan silver ants, also fall into this category.

Insects inhabiting in hot environments has proved a bountiful pool for searching inspirations for biomimetic coatings in pursuit of passive cooling. Provided their small thermal capacities, insects must employ very efficient strategies to maintain a constrained range of body temperatures. While the silver ants are representative species found in extreme temperature environments, there are plenty of thermophilic insects in the urban habitat as well. Many of them are reported to have expanded in population during urbanization, likely a consequence of the increasing urban heat island effect.[137] Two such examples are the cicadas *Cryptotympana atrata* and *Hyalessa fuscata*. For the *C. atrata*, which exhibits a bright golden color on the dorsal side of the abdomen (Fig. 9(a)), Liu et al. revealed that it is the porous structure of the golden microspikes (Fig. 9(b)) responsible for the desired thermoregulation function.[138] Specifically, in the visible and NIR region, the unique cross-sectional shape of the microspikes helps to bend the path of light hitting the edges along the surface (see black arrows in Fig. 9(c)), an effect similar to total internal reflection. Meanwhile, the bundle of porous structures of various sizes scatters light impinging on the central area (see red arrows in Fig. 9(c)), considerably increasing reflectivity in a broadband fashion in contrast to a

This journal is © The Royal Society of Chemistry 2025

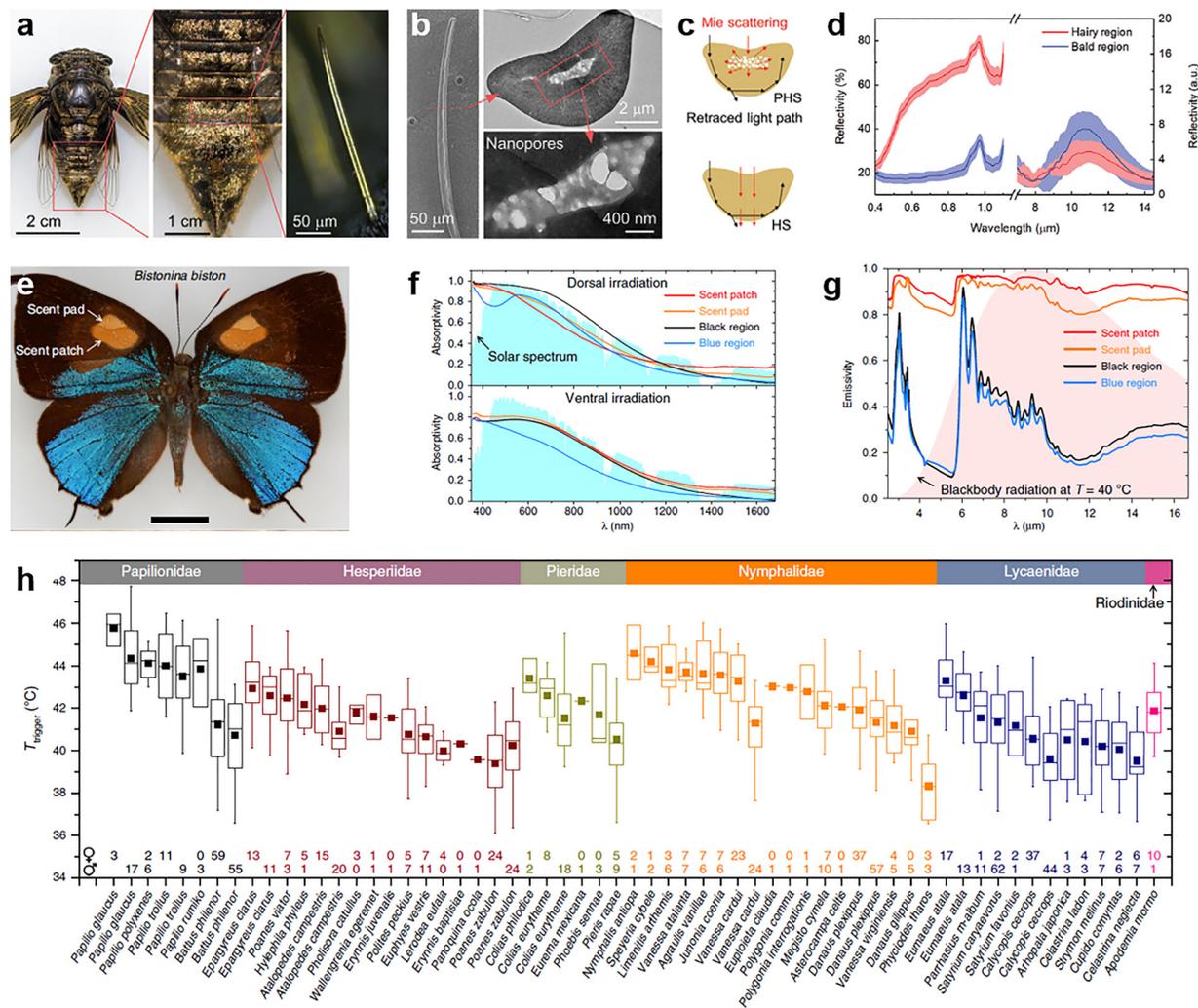*Chem. Soc. Rev.*, 2025, **54**, 10690–10723 | **10703**

Fig. 9 Biological examples of radiative cooling in cicadas (a)–(d) and butterflies (e)–(h). (a) Photographs of a female *Cryptotympana atrata* (left and center) and of a single golden microspike of it (right). (b) SEM (left) and TEM (right) images of the microspike in (a). (c) Schematic illustrating a microspike with porous heart-shaped inner structures on its cross-sectional plane and how Mie scattering of visible light by such pores helps to enhance the backscattering efficiency of microspikes. (d) Comparisons of measured reflectivity spectra in the vis-NIR and MIR regions for hairy (in red) and bald (in blue) areas. Reproduced with permission from ref. 138. Copyright (2021) Wiley-VCH. (e) Photograph of a male *Bistonina biston*, showing four colors on the dorsal forewing surface corresponding to four types of wing scales. Scale bar: 5 mm. (f), (g) Solar absorption (f) and thermal emissivity spectra (g) measured from different regions of the *Bistonina biston* forewing. Data are overlaid on a normalized solar spectrum and the normalized thermal radiation spectrum of a blackbody at 40 °C, respectively. (h) A box plot of the temperatures that start to trigger displacement responses of butterflies. The comparison is made across 50 species in 6 families (see legends on the upper boundary). Reproduced with permission from ref. 140. Copyright (2020) CC BY.

solid spike. If taking a macroscopic view of the specimen, the hairy area is essentially covered by densely distributed and spatially overlapped microspikes. This stacking further enhances the reflection of vis-NIR light, as shown in Fig. 9(d). In the MIR region, especially over the atmospheric window, the hairy area also displays favorable lower reflectivity (*i.e.* higher emissivity) than the bald area. The mechanism is somewhat close to the previously discussed case of moth-eye: the rounded shape of the microspikes' cross section results in a smoothened transition of effective refractive index profile across the inter-face, leading to improved broadband and wide-angle antire-flection. With all the above properties combined, structured

microspikes enable effective thermoregulation that protects cicadas' body from overheating in hot environments.

Likewise, many butterflies develop structural and behavioral strategies to manage the heating of their wings when exposed to sunlight.[139] In a comprehensive study of the wings of Lepidoptera across 50 species, Tsai *et al.* examined the thermo-dynamic and thermoregulatory properties of the wings covered by diverse scales and studied the response of wings to local heating.[140] Fig. 9(e) shows an example of an adult male *Bistonina biston*. On the dorsal side of the forewings, four types of nanostructured scales are identified through structural analysis, corresponding to the black region, blue region, as

10704 | *Chem. Soc. Rev.*, 2025, **54**, 10690–10723

This journal is © The Royal Society of Chemistry 2025

well as the "scent patch" and "scent pad" of the androconial organs, respectively. Despite not having a white appearance but bright coloration, different regions of the *B. biston* wings consistently have a modest solar absorption under dorsal and ventral irradiation, mainly contributed by the substantially higher absorptivity in the visible than in the NIR (Fig. 9(f)). This effectively helps to reduce the wings' temperature in the sun. In the MIR regime, however, the four types of scales exhibit drastically different abilities to dissipate heat through thermal radiation. As compared in Fig. 9(g), only the scent patch and pad have emissivities as high as near unity. Further study resolves two different mechanisms for these seemingly similar spectral responses. In the scent patch, specialized nanostructures of the scales are key to realize high emissivity, which also exist with minor structural variations in other species of Eumaeini tribe. In the scent pad, it is the thickness of the unfused membranes resulting in its high emissivity. Temperature mapping reveals the power of combined low solar absorption and high thermal emissivity: under simulated environmental conditions, the regions featuring both properties are ~10 °C cooler than the hottest part of the wings. Besides the static characterization, a particularly interesting finding of this study is that wings as living structures also function as a distributed network of sensors to modulate the dynamic behaviors of butterflies under thermal stimuli. Various displacement responses are observed when the wings are locally heated by a laser beam to certain temperatures (Fig. 9(h)).

4. Biological models and mechanisms for dynamic thermal management

In addition to examples of static thermal management, some organisms in nature have evolved the remarkable capability to adjust their appearance in real time. For instance, chameleons and squids have developed adaptive camouflage abilities for self-protection and hunting. Such adaptable and dynamic camouflage allows organisms to conceal themselves in intricate and fluctuating surroundings. While the biological camouflage effect is primarily observed in the visible light spectrum, it has sparked interest in developing adaptive infrared camouflage for thermal engineering systems as well.[141–143] The ever-changing coloration of these animals' skin serves as a rich source of inspiration for infrared regulation systems.

4.1 Cephalopods

For millions of years, cephalopods have utilized their adjustable iridescence for concealment and signaling, highlighting the enduring nature of this evolutionary trait.[144–148] The cephalopod skin, in its broadest sense, dynamically and reversibly regulates the passage, uptake, and emission of light through an intricate hierarchical structure, within which various strata house specialized organs referred to as chromatophores, as well as cells known as iridocytes and leucophores.[149–154] Iridocyte cells generate iridescence by causing constructive interference of light with intracellular Bragg reflectors (Fig. 10(a)). The leucophores function as

dispersed reflectors that disperse light, the iridophores function as active Bragg stacks that mirror light, and the chromatophores function as adjustable spectral filters that absorb/transmit light. The cell membrane periodically folds inward within the iridocyte to create a potential Bragg reflector composed of a series of narrow, parallel channels that separate the resulting high refractive index, protein-rich layers within the cytoplasm from the low index channels that connect with the extracellular space. Upon stimulation by a neurotransmitter, the iridocytes selectively absorb or release water in accordance with variations in reflection intensity and wavelength. Consequently, the swift, reversible movement of water through the extensively folded iridocyte membrane directly regulates the optical characteristics of this adaptable, biological multilayer reflector (Fig. 10(b)).[149]

Woo *et al.* recently developed methods to carry out detailed studies needed to comprehend this extraordinary system at a mechanistic level. Study showed that the process involves aligning the animal's visual characteristics with those of its surroundings, but actually, it does not faithfully replicate the substrate's appearance; instead, it involves visually triggered statistical estimation and generation of that appearance. The routes followed during a camouflage change are winding, sporadic – comprising alternating pattern movement and relative steadiness – and not stereotyped. In consequence, it is the high dimensional, non-stereotyped, diverse skin patterns that enable cephalopods to possess incomparable camouflage ability (Fig. 10(c) and (d)).[153] These discoveries can potentially aid in the creation of distinct categories of adjustable photonic materials.

4.2 Chameleons

Numerous chameleons, especially panther chameleons, possess the extraordinary capacity to display intricate and swift alterations in coloration during social engagements such as male competitions or mating rituals.[155] Upon encountering a rival male or a potentially receptive female, an adult male panther chameleon is capable of changing the base color of its skin from green to yellow or orange, while blue patches become paler and red intensifies with subtle changes in hue (Fig. 10(e)). This transformation takes place within a few minutes and is completely reversible.

Panther chameleons' skin comprises two overlapping dense layers of iridophore cells that contain guanine crystals with varying sizes, shapes, and arrangements. The configuration of materials with high and low refractive indices ($n_{guanine}$ = 1.83, $n_{cytoplasm}$ = 1.33) is accountable for the creation of a PhC. TEM micrographs reveal that guanine crystals are arranged in face-centered cubic lattices within the skin of a mature male chameleon (Fig. 10(f)). When subjected to an external stimulus, a shift towards longer wavelengths in the reflected light occurs as a result of the expansion of the nanocrystal spacing, leading to a change in color. Furthermore, research indicates that a denser distribution of iridophores containing larger crystals reflects a significant portion of sunlight, particularly in the near-infrared spectrum. Measurements demonstrate a notably high level of reflectivity in the near-infrared region, resulting in

This journal is © The Royal Society of Chemistry 2025

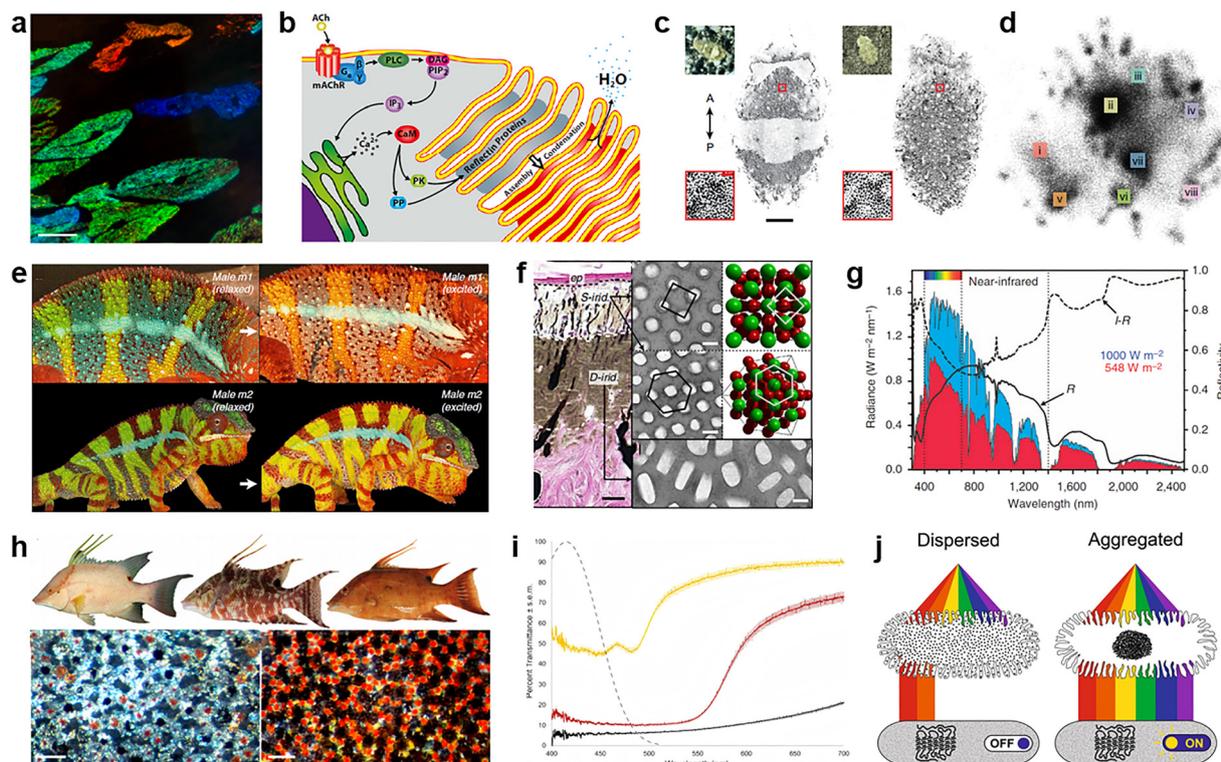*Chem. Soc. Rev.*, 2025, **54**, 10690–10723 | **10705**

Fig. 10   Structures and mechanisms of biological dynamic systems. (a)–(d) Tunable iridescence of squids. (a) Iridocyte cells in the dermis under dark-field illumination. Scale bar: 50 μm. (b) The mechanism by which the iridocytes of squids produce iridescent colors. Reproduced with permission from ref. 149. Copyright (2013) National Academy of Sciences. (c) Two examples of camouflage skin patterns classified as disruptive (left) and mottled (right). Scale bar: 10 mm. (d) Based on a large image set of one representative cuttlefish of ten analyzed, the skin-pattern space was visualized using a 2D uniform manifold approximation and projection embedding. Reproduced with permission from ref. 153. Copyright (2023) Springer Nature. (e)–(g) Color change of chameleons. (e) The mechanism diagram illustrates the reversible color change in two male chameleons: when stimulated, the skin undergoes a transition from green to yellow/orange, while the mid-body stripes shift from blue to white. (f) TEM image of avian guanine nanocrystals in the excited state and a 3D model of the face-centered cubic lattice. (g) The reflectivity of a white skin sample from a panther chameleon (black solid curve) and the solar radiation spectrum (blue-shaded area) at the sea level, which together determine the amount of solar radiation absorbed by deep tissues (red shaded area). Reproduced with permission from ref. 156. Copyright (2015) CC BY. (h)–(j) Dynamic color change of hogfish (*Lachnolaimus maximus*). (h) By aggregating and dispersing pigment granules within chromatophore units, a bright or dark appearance can be generated, thereby achieving color change. Scale bar: 100 μm. (i) The percentage of light transmission for different types of chromatophore units in the pigmented skin of hogfish. (j) The mechanism diagram showing the functional relationship between the chromatophore pigment and photoreceptors in the skin of hogfish. Reproduced with permission from ref. 159. Copyright (2023) CC BY.

a substantial reduction in sunlight absorption. Panther chameleons screen 45% of the radiation energy in that spectral range through dermal reflection (Fig. 10(g)).[156] Therefore, through the regulation of excitation and retraction, panther chameleons demonstrate the distinctive capacity to adjust the skin color reversibly, serving purposes such as camouflage, communication, or thermoregulation.[157]

4.3 Color-changing fish

The phenomenon of dynamic color alteration represents a swift, adaptable, and context-specific response, characterized by similar physiological traits across a wide range of animal species. Despite their varied evolutionary backgrounds, a shared trait among color-changing animals is the inherent light sensitivity of their skin and the anticipated correlation of this sensory capability with their capacity for change.[158]

Take hogfish for example, following the settlement phase, individuals of both genders exhibit the ability to undergo

dynamic color transformation, transitioning between a minimum of three chromatic variations: consistent white, consistent reddish-brown, and a variegated hue (Fig. 10(h)).[159] Through an analysis of the structure, function, and optical properties of dermal photoreception in hogfish, Schweikert *et al.* demonstrated that this system suggests that the dispersion of pigments in chromatophores inhibits the reception of short wavelength light by SWS1 (short-wavelength-sensitive-1) photoreceptors, while the aggregation of pigments enhances the reception of light by the SWS1 photoreceptors, rendering them responsive to alterations in chromatophore coloration. Consequently, the anticipated role of dermal photoreception in hogfish is to discern these changes in chromatophore pigments, thereby providing sensory input regarding the performance of color transformation (Fig. 10(i) and (j)).[159] This model of sensory response offers understanding into the importance of dermal photoreception in color-changing organisms.

10706 | *Chem. Soc. Rev.*, 2025, **54**, 10690–10723

This journal is © The Royal Society of Chemistry 2025

5. Bioinspired materials for thermal management

The great success in understanding the diverse strategies and mechanisms of thermal management that many natural creatures employ has at least two direct outcomes. On the one hand, it stimulates continuing interests and efforts to keep investigating unstudied species, identifying new structures from them, and revealing unprecedented mechanisms "smartly" developed through evolution.[160] On the other hand, and in a more practical perspective, the findings of aforementioned activities have inspired the rapid development of photonic materials and devices with novel functions and/or largely improved performance.[161–163] In this section, we review the progress in bioinspired materials for thermal management, focusing specifically on radiative cooling, thermal radiation harvesting, and dynamic responses.

5.1 Bioinspired materials for radiative cooling

Efficient passive radiative cooling requires reduced solar absorption and enhanced radiative heat dissipation simultaneously (Fig. 1(a)).[6,24,25] The reflective property in the vis-NIR region and antireflective property in the MIR region, as discussed in Section 2, are usually associated with specialized hierarchical structures and each with certain mechanisms.[164–166] Therefore, the design of materials for radiative cooling can be eased by first looking up the biological solutions known for having these properties and then replicating the structures with appropriate engineering and adaptions.[37,53,138] We start by exemplifying this process with a demonstration of flexible photonic films inspired by the longicorn beetle *Neocerambyx gigas*.[53] This type of beetles is known to be very adaptable to regions of a hot climate all year round, such as Thailand and Indonesia. On investigating the optical and thermodynamic properties of *N. gigas*, Zhang and coworkers first discovered how these beetles' thermoregulatory function stems from the fluffs on their forewings, and, subsequently, applied the principle to device design. Fig. 11(a) depicts a simplified flow chart of the conceptualization. After knowing the mechanism of the fluffs being responsible for body temperature reduction, the key to making an artificial version is to realize the critical structural features with commonly accessible materials, preferentially in a way compatible with mass production. In this case, the dual-scale triangular-shaped structure is replicated by simply spin-coating a precursor solution of PDMS containing randomly distributed Al_2O_3 microspheres onto a wafer-scale template with inverted pyramid (or alternatively, cone) arrays, followed by thermal curing in a vacuum. A subsequent, secondary spin-coating process can be performed to obtain films on a larger scale (Fig. 11(b), left panel). Note that no metal back plane is needed in this device. Compared with the natural prototype, the fabricated bio-RC film (Fig. 11(b), right panel) shows an even enhanced performance. Not only does the pyramid array resembles the pleats on the corrugated facet of fluffs to produce high vis-NIR reflectivity from Mie scattering and total internal reflection, as well as high MIR emissivity due to the gradual refractive index change along the surface normal, but the use of the PDMS

matrix and ceramic microspheres further helps to increase MIR absorption thanks to their respective dielectric properties. Fig. 11(c) compares the measured optical responses of the bio-RC film and of a flat PDMS film with embedded Al_2O_3 nanoparticles. The drastically enhanced vis-NIR reflectance proves the beneficial role of the interfacial microstructures. In a representative daytime radiative cooling performance measurement, the bio-RC film shows an average temperature drop of ~5.1 °C relative to the ambient air (Fig. 11(d), upper and central panels), corresponding to a cooling power around 90.8 W m^{-2} (Fig. 11(d), lower panel).

An alternative route to achieving scalable manufacture, which, strictly speaking, is not a biomimetic solution, is to process natural materials directly. A promising product of "cooling wood" from practicing this strategy is reported in ref. 167. Wood has been widely used as a building material for thousands of years. In modern times, it still stands out owing to superior sustainability and economic efficiency, among other advantages. By complete delignification and mechanical pressing of natural wood, an engineered radiative cooling structural material is obtained, exhibiting bright whiteness in the visible and blackness in the MIR region. The mechanism behind these optical properties can be readily told by examining the wood's microstructures shown in Fig. 11(e): the partially aligned multiscale cellulose fibers behave as disordered low-loss scattering elements at all visible wavelengths, resulting in broadband, strong, and diffusive reflection. Meanwhile, high and wide-angle infrared emissivity is generated by the molecular vibrational and stretching modes of cellulose. As shown in Fig. 11(f), across the atmospheric window, the average emissivity exceeds 0.9 for a wide range of emission angles between ±60°. Combining the desirable visible and MIR responses, the fabricated cooling wood can produce an average radiative cooling power of 53 W m^{-2} over the 24-hour period, potentially contributing to cooling energy savings between 20 and 60%. It is also worth mentioning that besides the cooling function, the engineered wood receives an 8-fold enhancement in mechanical strength, while further treatments can improve its weatherability and resistance to other environment factors. For example, by bonding TiO_2 and mica particles to the cellulose nanofibers of delignified wood, the wood receives significantly better UV stability,[168] a highly desirable property for outdoor and longtime use (Fig. 11(g)).

The effectiveness of disordered microscopic scatterers in rendering macroscopic whiteness has reflected in many other photonic materials for radiative cooling. Inspired by the interconnected random network of chitin filaments in the scales of *Cyphochilus*, the whitest known insect in the world, a hierarchically structured radiative cooling ceramic was developed by Lin *et al.*[169] Through phase inversion and sintering, a three-component precursor can be made into a ceramic composed of porous α-alumina structurally similar to the *Cyphochilus* scales (Fig. 11(h)), resulting in intense whiteness under natural light. Meanwhile, the vibrational modes of alumina's Al–O bond lead simultaneously to a high emissivity within the atmospheric window. In a continuous 84-hour outdoor measurement,
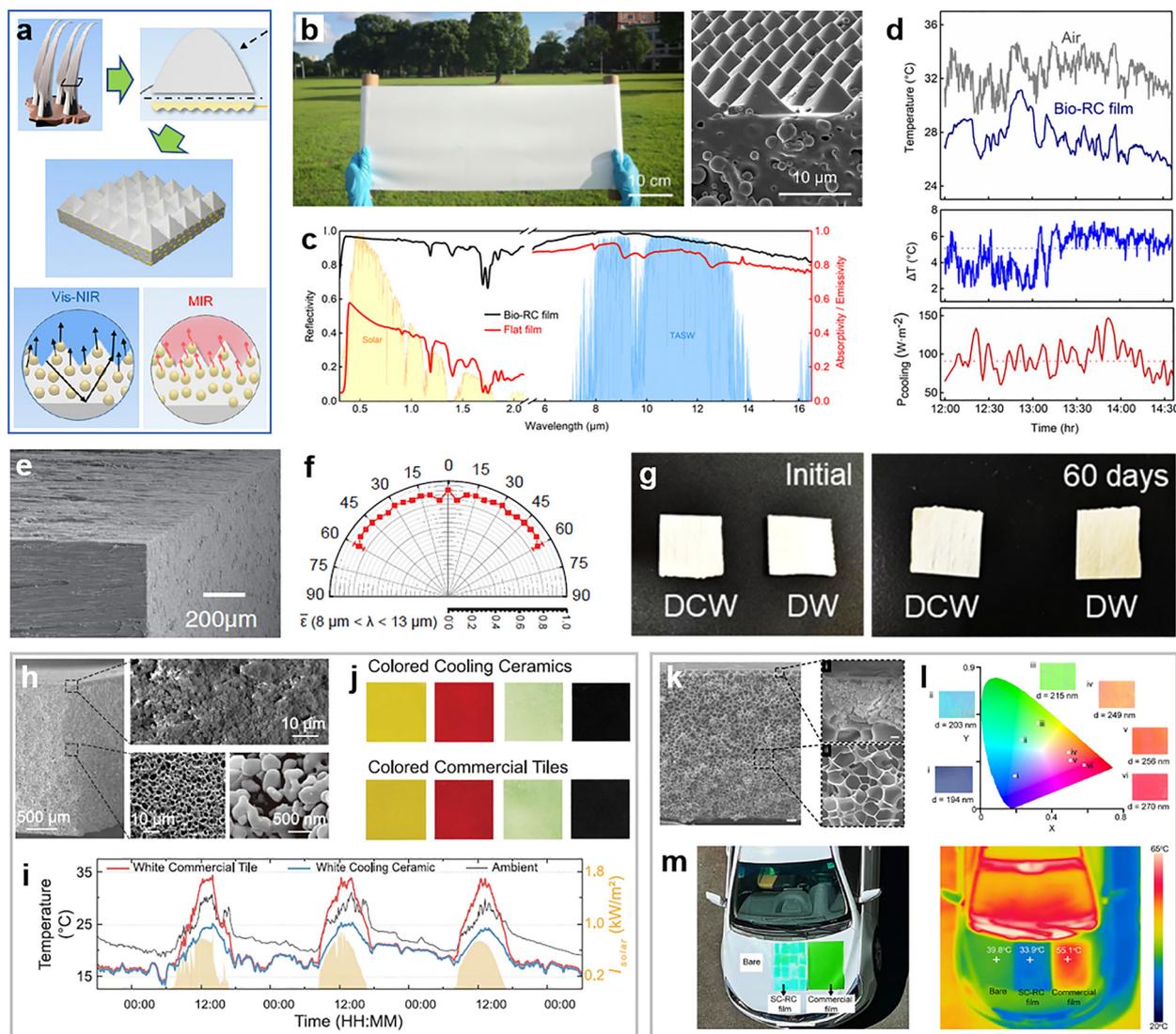
This journal is © The Royal Society of Chemistry 2025

Chem. Soc. Rev., 2025, **54**, 10690–10723 | **10707**

Fig. 11 Bioinspired materials for radiative cooling. (a)–(d) A photonic film inspired by the longicorn beetle *Neocerambyx gigas*. (a) Schematic showing the conceptual flow from the fluffs on the forewings of *N. gigas* (upper left) to the bio-RC film with dual-scale nanostructures (center), through modeling the fluffs' triangular cross section with a corrugated facet (upper right). The vis-NIR component of solar irradiation is reflected through Mie scattering and total internal reflection (lower left), whereas the MIR emissivity is enhanced by the gradual refractive index change and phonon polariton resonances (lower right). (b) Photograph of a fabricated film (left panel) and the SEM image of its section (right panel). (c) Measured optical properties of the bio-RC film (black curves) in comparison to those of a flat PDMS film with randomly embedded Al_2O_3 nanoparticles (red curves). Shaded areas in the background are the normalized ASTM G173 global solar spectrum (in yellow) and atmospheric transparency window (in light blue). (d) Temperatures of the ambient air and of the bio-RC film under direct sunlight (upper panel) measured in Shanghai in late May 2019, resulting in a subambient temperature drop around 5.1 °C (middle panel) and a radiative cooling power around 90.8 W m^{-2} (lower panel). Reproduced with permission from ref. 53. Copyright (2020) National Academy of Sciences. (e), (f) Engineered wood for radiative cooling. (e) SEM image of the cooling wood. (f) Polar plot of the cooling wood's emissivity averaged across the atmospheric window. Reproduced with permission from ref. 167. Copyright (2019) AAAS. (g) Optical images of the durable cooling wood (DCW) and delignified wood (DW) before (left panel) and after (right panel) long-time exposure to UV light. The color change of DW signifies degrading caused by oxidation, whereas DCW shows superior UV stability. Reproduced with permission from ref. 168. Copyright (2025) American Chemical Society. (h)–(j) A cooling ceramic inspired by the beetle *Cyphochilus*. (h) SEM image of a fabricated sample. (i) Comparison of the temperatures of the ambient air, a commercial white tile and the white cooling ceramic, measured in Hong Kong in mid-November 2021. Shaded areas indicate the solar intensity. (j) Photographs of colored cooling ceramics and commercial tiles in the same color. Reproduced with permission from ref. 169. Copyright (2023) AAAS. (k)–(m) Structurally colored radiative cooling films inspired by the scarab beetle. (k) Cross-sectional SEM image of a green film showing colloidal PhCs embedded in ordered micropits near the surface (panel i) and disordered pores inside the film (panel ii). (l) Photographs of selected colored films and their coordinates on the CIE chromaticity diagram. (m) Photograph and an infrared image of a car with the hood covered with structurally colored cooling films and a commercial film of a similar color. Reproduced with permission from ref. 173. Copyright (2025) Elsevier.

the cooling ceramic consistently yielded a temperature well below that of the ambient air and outperformed the white commercial

tiles during the daytime (Fig. 11(i)). Furthermore, introducing colors to the cooler (as conceptualized by the dashed line in

10708 | *Chem. Soc. Rev.*, 2025, **54**, 10690–10723

This journal is © The Royal Society of Chemistry 2025

Fig. 1(b)) for aesthetic considerations becomes convenient with this ceramic platform, which can be done by simply sintering a thin layer of colored glaze on top of the white substrate. In contrast, rational design employing optimization or parameter sweep would be necessary to find suitable structural parameters for devices not using pigments or photoluminescence.[33,170–172] The fabricated colored ceramics have nearly identical visual appearance to commercial tiles (Fig. 11(j)) but offer better performance in reducing the thermal load, primarily due to the higher NIR reflectance. In another design of colorful coolers proposed by Hou *et al.*, the thermal management function is obtained with a polymer-rich film, of which the hierarchically porous structure mimics that of the elytra of scarab beetles,[173] and the coloration results also from a structural origin, *i.e.*, PhCs composed of close-packed colloidal polystyrene nanoparticles (Fig. 11(k)). The resulting color spans from purple to red (Fig. 11(l)), determined by the size of the particles. Because the PhCs are blade-coated on the surface of the cooling film with densely distributed micropits, the structural color is mechanically durable against abrasion. In a daytime outdoor test, the films showed superior cooling performance, reducing the temperature of a car hood by ~ 5.9 °C, while a commercial film caused drastic heating (Fig. 11(m)).

5.2 Bioinspired materials for solar energy harvesting and photothermal conversion

Many scenarios of thermal management do not have simultaneous requirements on appearance (vis-NIR response) and thermoregulation (MIR response) as passive radiative cooling does. For example, in pursuit of renewable energy, development of new materials for harvesting solar light has attracted tremendous efforts from academia and industry. Various applications, such as photovoltaics, desalination, and sterilization, de-icing, can be derived once solar energy is efficiently captured (Fig. 1(c)). In the ideal case, a material that absorbs all the solar light impinging on it appears black. Being the ultimate opposite of whiteness, interestingly, blackness can also arise from structural disorder on the micro- and nanoscale, when some critical dimensions fall into the proper range for trapping light. Representative examples found in birds' feathers and butterfly wings have been discussed earlier in Section 3.2. If we use blackness and broadband high absorption in an interchangeable manner, the favorable MIR response for passive radiative cooling can also be considered as "MIR blackness". But unlike in most radiative cooling devices that rely more strongly on the vibrational modes or phonon resonances of materials to absorb MIR light, the black appearance of living organisms can have an origin from materials (*e.g.*, light absorbing pigments), structures, or both. Here, we focus on solar energy harvesting inspired by disordered structures in biomaterials, followed by a brief discussion on other applications of photothermal conversion.

Going forward from the previous studies on black butterfly wings, Siddique *et al.* analyzed the scales of *Pachliopta aristolochiae* locally and managed to relate structural variations, particularly the air-filling fraction, to the wings' optical properties.[117] It is then revealed that the most important component enabling the broadband absorption in the UV-vis-NIR regime is the 2D disordered network of nanoholes in chitin, while the contributions of ridges and bottom laminae are secondary. Inspired by this discovery, thin photovoltaic absorbers are designed and fabricated by introducing disordered air holes to a-Si:H thin films (Fig. 12(a)). The seemingly simple strategy is proved surprisingly effective. Compared to an unpatterned a-Si:H film of the same thickness, the absorber with patterned through-holes exhibits a darker appearance over a wide range of viewing angles, which is consistent with measured absorption spectra (Fig. 12(b)). A noticeable improvement by the bioinspired nanostructures is the remarkable absorption for wavelengths above 550 nm. A plain a-Si:H film poorly absorbs light in this regime because of its low extinction coefficient. In contrast, the disordered nanohole distribution with optimized air-filling fractions not only enhances the absorption through light in-coupling and trapping, but also improves angular and polarization robustness with good mechanical stability, suggesting a promising solution for thin-film-based solar cells. Further increase of solar absorption towards perfect absorbers can be accomplished with more sophisticated interfacial engineering. Fig. 12(c) presents an example that takes inspiration from the compound eyes of Chinese mitten crabs (*Eriocheir sinensis*).[174] By mimicking the cornea layer of crystalline cones with multilayered reduced graphene oxide coated on a gold film of honeycomb apertures, the fabricated device exhibits a broadband solar absorption up to 0.95 over the entire visible regime (Fig. 12(d)), enabling very efficient photothermal conversion without sacrificing the mechanical stability.

One direct application of solar light harvesting at an interface is de-icing. In a freezing environment, converting solar irradiation efficiently into heat can delay ice formation or melt the ice accumulated on a surface.[175–178] Superhydrophobicity is also favored for de-icing, in order to quickly remove the melted water.[179,180] Biological materials provide solutions to fulfilling both requirements.[181] Inspired by the cactus thorns, a photothermal icephobic surface was realized in ref. 182 by laser patterning the copper substrate into arrays of microspines (Fig. 12(e)), followed by proper surface treatments.[183] The fabricated device shows excellent photothermal as well as hydrophobic properties and is abrasion-resistant due to the honeycomb boundaries (Fig. 12(f)). When fabricated on a copper alloy transmission line, the surface successfully removes the freezing rain at −10 °C under 1 sun illumination. Other bionic structures for photothermal de-icing have also proved quite effective.[184] In a similar vein and inspired by fish scales, photothermal fabrics with modified surface wettability were reported in ref. 185. The fabrics are coated with black polypyrrole nanoparticles to mimic the ridge arrays of the scales and then modified with cellulose nanocrystals playing the role of hydrophilic proteins in mucus.[186,187] This results in anti-fouling membranes with a high solar-absorbing efficiency (Fig. 12(g)), specifically suitable for applications in oil-polluted water.

Alternatively, biological structures can be used as a template or precursor for materials synthesis.[188] Ref. 189 reports such an attempt by applying solutions containing carbon nanotubes (CNTs) to the wings of *Morpho sulkowskyi* butterflies to form a
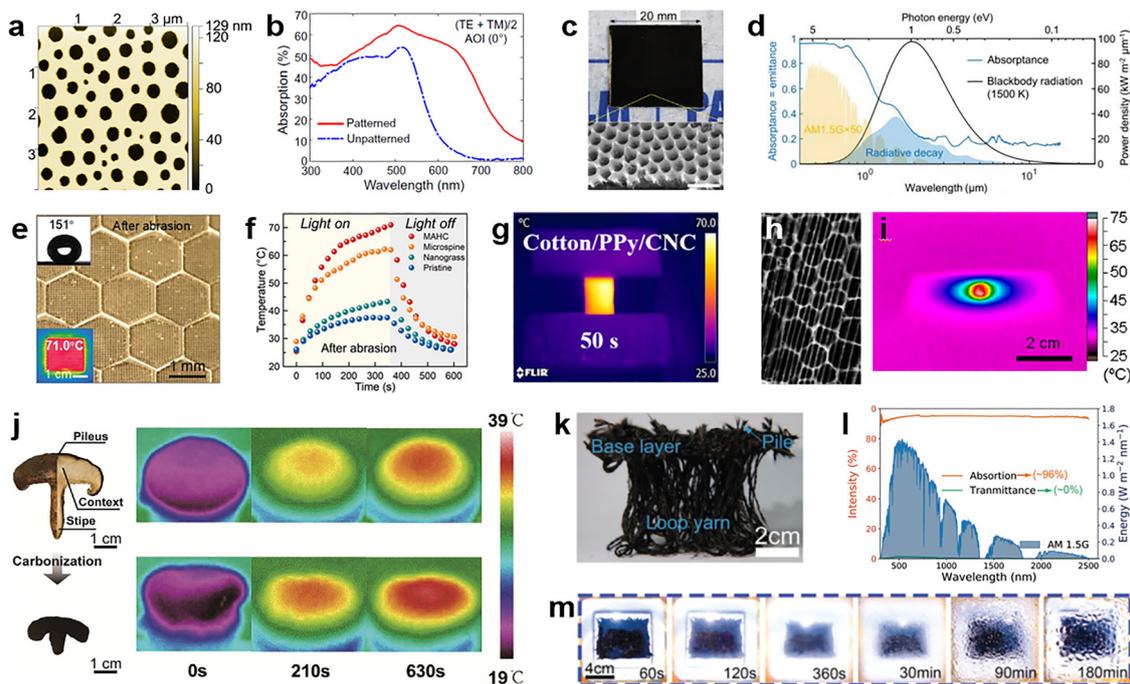
This journal is © The Royal Society of Chemistry 2025

Chem. Soc. Rev., 2025, **54**, 10690–10723 | **10709**

Fig. 12 Bioinspired photonic materials for solar energy harvesting. (a), (b) A bioinspired patterned thin absorber. (a) Atomic force microscopy image of the a-Si:H thin film showing a short-range ordered hole distribution within the plane parallel to the surface. (b) Comparison of absorption spectra of thin-film photovoltaic absorbers with (red curve) and without (blue curve) disordered nanoholes. Reproduced with permission from ref. 117. Copyright (2017) CC BY-NC. (c), (d) A perfect absorber inspired by crab-eye. (c) Optical (upper panel) and SEM (lower panel) images of a fabricated prefect absorber. Scale bar: 1 μm. (d) Absorption spectrum (light blue curve) of the device in (c) showing broadband high absorption over the visible wavelengths. Reproduced with permission from ref. 174. Copyright (2024) Wiley-VCH. (e), (f) A photothermal icephobic surface inspired by cactus thorns for de-icing. (e) Optical image of the surface consisting of microspine arrays surrounded by honeycomb walls, along with the image of water droplet showing a large contact angle (upper left inset) and the infrared optical image of the device under 1 sun illumination (lower left inset) (f) Comparison of temperature variations of surfaces with different micro- and nano-structures. Reproduced with permission from ref. 182. Copyright (2023) Wiley-VCH. (g) Infrared optical image of dry photothermal fabrics under simulated sunlight. Reproduced with permission from ref. 185. Copyright (2025) Elsevier. (h), (i) CNT-butterfly wing composites for laser-induced remote heating. (h) SEM image of the CNT-butterfly wing composite. (i) Thermographic image of the surface of the composite under the irradiation of a 785 nm laser at ∼80 mW mm^{-2}. Reproduced with permission from ref. 189. Copyright (2013) American Chemical Society. (j) Efficient solar steam generation can be achieved with natural (upper row) and carbonized (lower row) mushrooms by taking advantage of their unique heat behaviors under solar illumination. Reproduced with permission from ref. 190. Copyright (2017) Wiley-VCH. (k)–(m) Pistia-inspired photothermal fabric for low-cost vapor generation. (k) Image of the loop-pile fabric consisting of a base layer, piles, and loop yarns. (l) Absorption (orange curve) and transmittance (green curve) spectra of the fabric. (m) The vapor condensation behavior of a loop-pile fabric-based device in an outdoor experiment. Reproduced with permission from ref. 191. Copyright (2022) Wiley-VCH.

multifunctional biohybrid. Although the modified wings change little in color, a honeycomb-shaped CNT network is self-assembled following the pattern of the wing scales (Fig. 12(h)). Thanks to the superior photothermal properties of CNTs and the light-trapping capability of honeycomb structures, the CNT-butterfly wing composite converts NIR laser irradiation to heat very efficiently (Fig. 12(i)), far surpassing the performance of control samples without CNTs or modified with other carbon materials. The demonstrated remote heating, along with other functions such as high electrical conductivity and repetitive DNA amplification, showcases another interesting case of biomaterials.

Discrete applications of solar energy harvesting usually require considerations more than light absorption. In desalination and sterilization, for instance, the overall energy conversion efficiency is dictated by several factors including solar absorption, heat localization, water supply, vapor transportation, *etc.* Fulfilling all these requirements simultaneously is

challenging in design, but evolution-driven optimization may provide natural shortcuts. In ref. 190, it is found that shiitake mushrooms can function as efficient solar steam-generation devices. In standard characterization, a natural mushroom with an umbrella-shaped black pileus already gives an ∼79% absorption of solar energy. A simple carbonization treatment, which increases the surface roughness, thereby further reducing reflection, yields a higher absorption of 96%. Assisted by the porous context and the fibrous stipe facilitating water supply and vapor escape, the curved surface of the pileus about twice the size of its projected area enables stronger evaporation and thus greater temperature reduction. These properties are also beneficial for suppressing heat loss of all types. As shown in Fig. 12(j), under 1 sun illumination, the temperature of a natural (carbonized) mushroom increases quickly and reaches the quasi-steady state around 37.5 °C (38 °C) in about 10 minutes. The result leads to theoretically a 2.2 (2.9) times higher evaporation rate than that of pure water. To make low-cost industrial

10710 | *Chem. Soc. Rev.*, 2025, **54**, 10690–10723

This journal is © The Royal Society of Chemistry 2025

production of solar steaming devices possible, textile material is a better choice. Inspired by the morphology of the root system and resulting differential transpiration of the aquatic plant Pistia, Wang *et al.* developed a loop-pile fabric using waste short carbon fibers.[191] The fabricated fabrics resemble Pistia in structure (Fig. 12(k)), with a base layer and piles mimicking layered leaves as a photothermal body and loop yarns mimicking the roots. Because of the dielectric properties of carbon as well as the porous structure and rough surfaces of each component, the fabric exhibits a high solar absorption of about 96% (Fig. 12(l)). When put in place, the base layer and piles are set above the water surface, while the yarns go deep into water and pump water to the upper layer through the capillary effect. In an outdoor experiment, the bioinspired fabric generates water vapor quickly: the glass cover becomes foggy in just 2 min, and visible water droplets are formed after $\sim$30 min (Fig. 12(m)). The measured evaporation rate approaches 1.5 kg m^{-2} h^{-1}, about 3 times that of a control setup without the fabric. As the fabrication process is compatible with industrial textile equipment and the waste carbon fiber is much cheaper than many commonly used raw materials, the prototyped device provides a new possibility for manufacturing low-cost solar evaporators. More recently, various bioinspired materials for solar-driven interfacial water evaporation have been reported, primarily derived from plants.[192–195] Other functions critical to the development of renewable energy, such as solar-thermal energy storage, have made progress as well by taking a cue from the *Cyprinus carpio* fish.[196]

Besides solar energy harvesting, bioinspired materials also find applications in other subjects of thermal regulation where the photothermal conversion property is specialized. In dealing with the challenges in thermal imaging, an innovative uncooled detecting approach is derived from the iridescent wing scales of tropical *Morpho* butterflies.[197] Its working principle is based on the thermal expansion of the air-filled hierarchical scale structures,[198] which is caused by absorbing IR photons and induces visible iridescence changes as readout signals. In particular, the submicrometer dimensions of the functional elements hold great promise for improving the spatial resolution of thermal imaging. Different designs have been proposed and evaluated to engineer the device performance or extend their function.[199–201] For instance, by decorating the wing scales with CNTs, high-speed mid-wave IR detection with 18–62 mK temperature sensitivity is demonstrated in ref. 197. Fig. 13(a) illustrates a revised scheme where the decoration is made locally with thin gold patches near the edges of horizontal lamellae, resulting in a cantilever-like structure.[202] Compared with the original version of global doping with CNTs, the selective modification leads to a non-uniform expansion of each lamella due to the difference in the thermal expansion coefficients of gold and chitin. Under the irradiation of a broadband IR lamp, the fabricated sample shows a change of 0.11 in relative reflectance for a temperature increase of 5 °C (Fig. 13(b)). These values correspond to a temperature sensitivity of 32 mK, improved by about two times in comparison to that of the CNT-doped device. In a follow-up study, the same team explored an alternative detection scheme that did not rely on temperature-induced

structural changes. Instead, the optical readout signal, *i.e.*, the change of reflectance at visible wavelengths, is a consequence of the IR-stimulated desorption of vapor molecules from the wing scales (Fig. 13(c)).[203,204] Without the need to decorate structures, this scheme further improves the temperature sensitivity of the detection to a few mK, while the response speed remains decent.

Functionally opposite to passive radiative cooling, passive heating represents another aspect of thermal regulation. In simple words, an ideal passive heating device needs to have a cladding layer that is transparent to solar light but thermally insulative to minimize heat loss, an efficient photothermal conversion layer to convert sunlight to heat, and a third component for energy storage and heat release. In ref. 205, a biomimetic multilayered material is devised inspired by the skin structure of polar bear. Three functional layers are stacked from top to bottom following the above order (Fig. 13(d)): the silica aerogel has a near unity transmittance across the UV-vis-NIR regime and an ultralow thermal conductivity, playing the role of thermal insulation hair. The middle layer for photothermal conversion consists of a glass plate coated with black paint, mimicking the black skin of solar bear. Lastly, a bottom layer of phase-change material (PCM) composed of *n*-octadecane microcapsules is introduced, which can provide high latent heat *via* solid–solid phase transition, allowing the storage and release of heat for maintaining a relatively comfortable temperature against cold environments. Fig. 13(e) shows the performance of this material in an outdoor experiment conducted on a sunny day in winter. While the roof of the model houses coated by the aerogel and black paint reaches 90 °C at noon, the inside of the control house without PCM is substantially colder (green curve). In contrast, the use of PCM can produce a maximum indoor temperature difference of 28 °C over the daytime (red curve). For each component of the passive heating device, improvements can be made with biomimetic strategies as well. An interesting example of PCM is presented in Fig. 13(f), where a MXene aerogel-based film is designed and fabricated, inspired by the thermal management system of antifreeze beetles.[206]

5.3 Bioinspired dynamic materials

Materials for radiative cooling and heating have attracted great attention owing to their exceptional optical and optothermal properties. Nonetheless, for most applications, maintaining a relatively stable temperature is of more interest, primarily because humans can only live and work within a narrow temperature range, necessitating the use of thermostats and other thermal regulation systems. There has been extensive research into dynamic thermoregulatory materials.[207] The appearance-changing skins of animals such as cephalopods, chameleons, and hummingbirds provide rich inspiration for the development of visible and IR regulation systems, and their distinctive structures and functions have fueled considerable advances in adaptive optics and photonics for various applications, including biomimetic flexible active surfaces, light-emitting displays, intelligent radiation devices, adaptable IR camouflage,
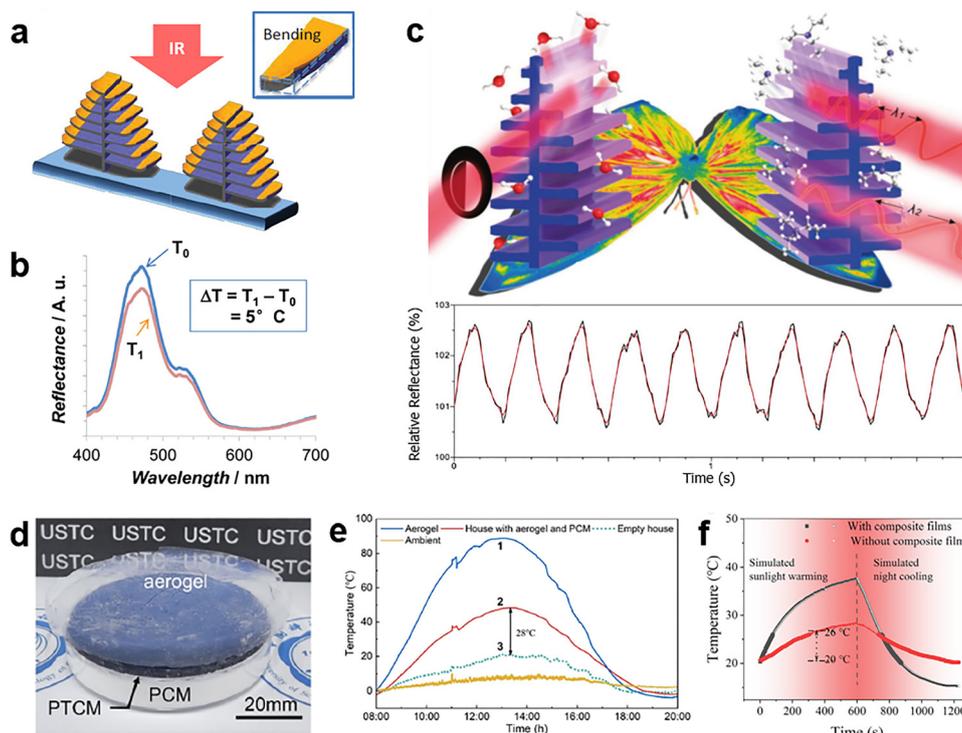
This journal is © The Royal Society of Chemistry 2025

Chem. Soc. Rev., 2025, **54**, 10690–10723 | **10711**

Fig. 13 Bioinspired photonic materials for various thermal management applications. (a)–(c) *Morpho* butterfly wings for IR detection. (a) Under IR light illumination, the non-uniform thermal expansion of the Au-modified lamellae induces a local deformation at the edge of each lamella layer, resulting in (b) a change of reflection in the visible region. Reproduced with permission from ref. 202. Copyright (2014) Wiley-VCH. (c) The desorption of vapor molecules stimulated by IR light illumination is also sufficient to cause changes in optical reflection (upper panel), showing dynamic responses when the incident IR light is modulated (lower panel). Reproduced with permission from ref. 203. Copyright (2020) Wiley-VCH. (d) A multilayered device inspired by the physiological skin structure of polar bear and (e) its performance for passive heating. Curves 1–3 are measured at the photothermal layer on the roof of the model house, inside the model houses equipped with and without PCM, respectively. Reproduced with permission from ref. 205. Copyright (2022) American Chemical Society. (f) MXene aerogel-based phase change film for thermal management. Reproduced with permission from ref. 206. Copyright (2022) Elsevier.

and intelligent thermal control technologies.[145,208–211] The main inspiration for developing IR regulation materials comes from the ability of the skin to dynamically modulate its radiation energy in the IR region in response to an external stimulus. According to the Stefan–Boltzmann law, the radiated IR energy is proportional to ε, the emissivity of the emitting surface, and the fourth power of the object's temperature T. Thus, the dynamic manipulation of materials' ε at IR wavelengths enables the implementation of adaptive IR camouflage and smart thermoregulation.[23]

5.3.1 Bioinspired materials for smart thermal control. The implementation of efficient intelligent thermal regulation is of paramount importance for the functionality of numerous contemporary technologies, including electronic circuits, smart thermal management textiles, zero-energy sustainable building and urban infrastructure. The captivating dynamic color-shifting dermal adaptation observed in coleoid cephalopods serves as a powerful source of inspiration for the development of next-generation adaptive thermal control systems. Similarly, chameleons possess the ability to swiftly alter their body colors for communication purposes, demonstrating adaptive thermal management by actively adjusting the lattice of guanine nano-crystals within their dermal iridophores.[10,149]

The proportion of energy consumption attributed to buildings globally stands at a staggering 30%, with their greenhouse gas emissions accounting for 10% of the total global emissions.[212] This presents significant environmental and economic challenges for the future of sustainable development. Within this substantial energy consumption, approximately 48% is solely dedicated to space heating and cooling, necessitating innovative approaches to sustainably manage building temperatures and create net-zero energy buildings.[213–215] While the development of radiative cooling and solar thermal materials has successfully aided buildings in cooling during summer and harvesting heat during winter, these static materials (solely for cooling or heating) are incapable of adjusting to the dynamic climate changes throughout the year. Consequently, this greatly limits the energy-saving performance of air conditioning systems over the entire year.[216] Therefore, adapting the response to solar and infrared spectra in real-time of building fronts to help them adapt to seasonal temperature changes has emerged as a fresh chance to enhance energy efficiency in buildings.

Taking inspiration from the temperature-responsive skin color of chameleons, Dong *et al.* have effectively integrated temperature-responsive solar absorption and passive daytime radiative cooling technology to achieve a "warm in winter

and cool in summer" effect. They designed and produced a temperature-responsive radiative cooling coating with color variability, which has the capability to regulate 41% of visible light.[216] Inspired by the Himalayan rabbit's hair and Mimosa pudica's leaves, Zhang *et al.* introduced a dynamic radiative heat management device that operates at zero energy, utilizing visible light and infrared thermochromism. The combination of these two spectral control mechanisms enables the device to independently control a wide spectral range from visible light to MIR, thereby allowing the device to autonomously adjust its heat management mode with zero energy consumption in response to temperature changes.[217] A building facade with the ability to directly achieve various climate control functions through independent and multifunctional optical reconfigurations could significantly reduce energy consumption. Kay *et al.* showcased a comprehensive "optofluidic" platform designed for buildings, enabling independent and combined control of total light transmission (95% modulation), NIR-selective absorption (70% modulation), and dispersion (Fig. 14(a)). The combinational optical adjustability allows for the customizable

maximization of the amount, wavelength, and location of solar radiation transmitted within buildings, leading to annual simulated energy savings of over 43% compared to current technologies (Fig. 14(b) and (c)).[218]

The intelligent thermal control windows are also a highly representative technology in energy-efficient buildings (Fig. 1(d) and (e)).[219–222] A perfect smart window should offer transparency across the visible spectrum under varying temperature conditions.[221] The solar transmittance is influenced by both the visible and NIR spectra, leading to the warming of a room. Transitioning the NIR state from opaqueness in the summer to transparency in the winter is thus highly sought-after. Furthermore, an optimal smart window should exhibit a high emissivity in the long-wave infrared spectrum (ε_{LWIR}) at elevated temperatures to facilitate radiant cooling during hot weather, and a low ε_{LWIR} at lower temperatures to inhibit radiant cooling under cold conditions. In ref. 222, a layer-by-layer assembly method inspired by the structural coloration and color-changing mechanisms observed in living organisms was employed for the large-area fabrication of mechanically
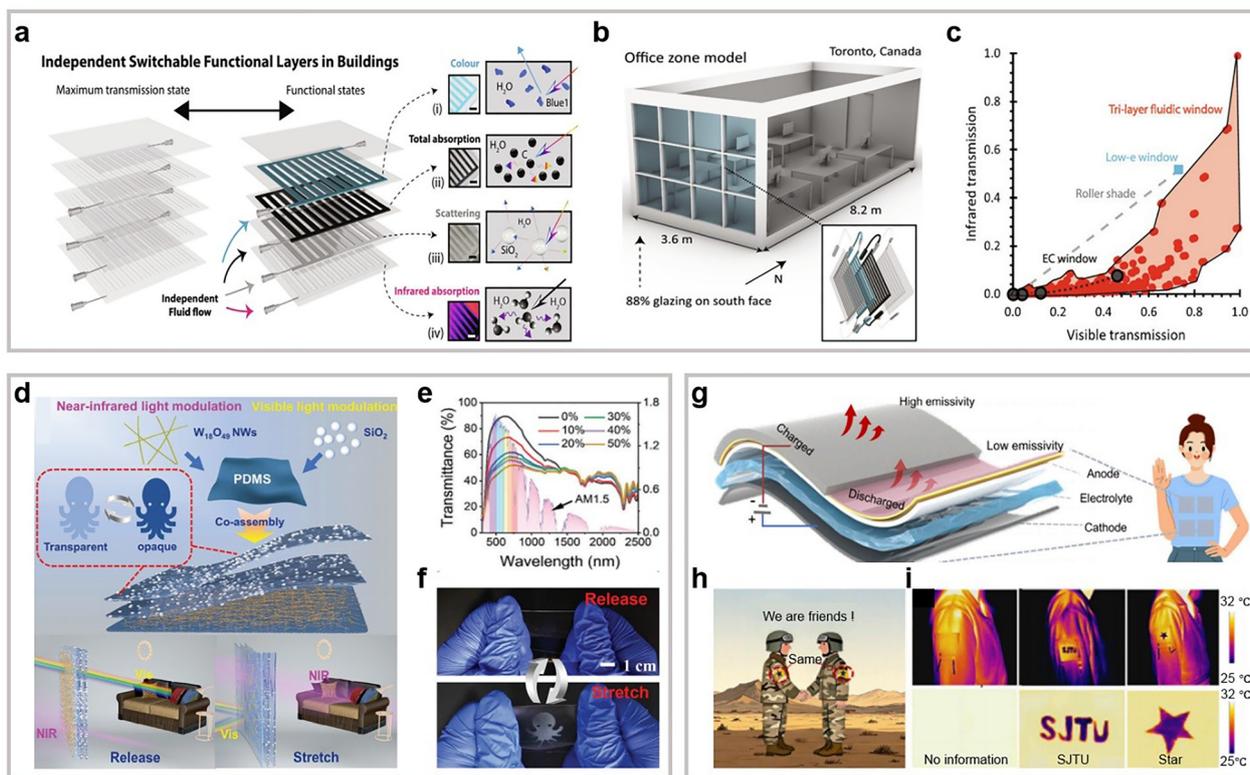

Fig. 14 Bioinspired materials for smart thermal control. (a)–(c) Multilayered optofluidics for sustainable buildings. (a) A schematic diagram of independent multilayer switchable responsive elements within the building facade, where fluid flow within different layers enables a variety of optical responses. (b) Utilizing the office model for energy simulation. (c) The parameter space encompasses all fluid combinations with specular visible, specular NIR, and diffuse visible optical properties. Reproduced with permission from ref. 218. Copyright (2023) National Academy of Sciences. (d)–(f) Bioinspired mechanically responsive smart windows. (d) Schematic illustration of the production process and mechanochromic mechanism for smart windows. (e) Changes in spectral transmittance of fabricated films under various stretching conditions. (f) A digital image illustrating the reversible formation and vanishing of octopus-like patterns within a sample film when it was subjected to mechanical stretching and subsequent releasing, highlighting its potential for anti-counterfeiting purposes. Reproduced with permission from ref. 222. Copyright (2024) Wiley-VCH. (g)–(i) Flexible electro-driven nanophotonic devices for dynamic radiative thermoregulation. (g) Illustration of the architectural configuration and working principle of the devices for thermal management and electric power supply. (h) Visualization and (i) thermal imaging of the devices utilized for cryptographic applications. Reproduced with permission from ref. 227. Copyright (2025) American Chemical Society.

This journal is © The Royal Society of Chemistry 2025

Chem. Soc. Rev., 2025, 54, 10690–10723 | 10713

responsive films. These films were designed for multiwavelength spectral modulation in the visible and NIR regions, with potential applications in smart windows (Fig. 14(d)). The incorporation of SiO_2 nanoparticles and $W_{18}O_{49}$ nanowires into the film structure enabled an optical modulation rate of up to 42.4% at a wavelength of 550 nm and 18.4% in the NIR region (Fig. 14(e) and (f)).[222] With advantages of low costs, easy preparation, and simple construction, these research findings hold promise for advancing energy-saving and zero-energy technology, and potentially bringing about new breakthroughs in intelligent thermal management for buildings.

In recent times, several technologies have displayed significant potential for use in challenging real-world thermal management situations. The advancement of new localized or wearable thermoregulatory platforms presents an exciting prospect and has the capacity to greatly diminish global energy consumption.[223,224] Drawing inspiration from the dynamic color-changing ability of squid skin, Leung et al. developed a composite material with adjustable thermoregulatory properties. The composite material is capable of regulating a quarter of the anticipated metabolic heat flux for a sedentary individual, and it can also adjust localized changes in a wearer's body temperature by almost tenfold.[225] Along this line, the same team further demonstrated how another squid skin-inspired heat-managing composite material could fulfill the critical requirements in the food and beverage industry for sustainable packaging.[226] However, integrating multifunctionalities into flexible thermal management systems remains challenging. Inspired by cephalopod skin, Xie et al. showcased a flexible electro-driven nanophotonic device with dual functions: dynamic radiative thermoregulation and continuous energy supply (Fig. 14(g)).[227] It achieves high IR emissivity tuning from 0.19 in the heating mode to 0.85 in the cooling mode for a 13 °C temperature modulation, meeting the needs of personal thermal comfort. The dynamic IR emissivity modulation further enables information encryption. By controlling the lithiation process, distinct patterns (e.g., letters, numbers, and stars) are clearly visible using IR imaging (Fig. 14(h) and (i)), showing great potential for information recognition and secure encryption applications. Zeng et al. have introduced a groundbreaking concept of versatile and adaptable multifunctional devices, employing a sophisticated hierarchical structural design. As a result, they demonstrated correlated alterations in optical signals, such as transparency, reflectance, and coloration. This remarkable adaptability allows for diverse applications, including encryption devices responsive to multiple stimuli, dynamic optics responsive to moisture and photothermal stimuli, and pressure-mapping sensors assisted by smartphone apps.[228]

5.3.2 Bioinspired materials for adaptive camouflage. The development of camouflage technology, aimed at concealing or obscuring an object within its surroundings, has been a subject of considerable interest for a variety of significant applications. In general, camouflage technology is typically divided into two primary classifications, namely color camouflage and IR camouflage. Depending on the specific scenarios, the spectral requirements could vary a lot, and the curve in Fig. 1(f) outlines a representative profile not yet found to have a natural solution.[229] Bioinspiration for stealth has so far mainly been seen in the study of adaptive camouflage.[10] Numerous organisms in the natural world have developed the remarkable capability to change color and dynamically blend into their surroundings visually, serving as a means of protection, signaling potential threats, and concealing themselves from predators.[142] The epidermis of cephalopods, including octopus, cuttlefish, and squids, provides a compelling demonstration of on-demand active cloaking by selectively reflecting visible and infrared wavelengths as required, thereby facilitating their adaptation to the environment through the swift modulation of chromatophore arrangements within the dermal layer in response to rapid neural and muscle signals.[144,230] Researchers have announced the creation of infrared camouflage materials inspired by cephalopods, achieved through the development of adaptable crumpled textures for infrared reflection coatings.[150] Additionally, a camouflage system inspired by cephalopods has been developed, allowing for color changes in both the visible and infrared spectra by injecting colored or temperature-controlled fluids into highly flexible elastomer microchannels. Furthermore, they have successfully demonstrated visible color-changing materials inspired by chameleons, which can be easily activated by various external stimuli such as mechanical force, electric stimulation, humidity control, and thermal effects.

Xu et al. drew inspiration from the extraordinary abilities of a cephalopod to create and produce unparalleled, electrically powered IR-reflecting adaptive materials and devices.[231] Intriguingly, when electrically activated, the device transformed into a substantial level surface and displayed a noticeable temperature contrast with its surroundings, rendering it distinguishable from the background.

However, conventional single-band stealth is difficult to align with the growing demand for multiband compatibility and intelligent adaptation. Here, Lee and colleagues showcased an active, imperceptible artificial skin that transitions seamlessly from visible to infrared, offering on-demand camouflage in both daytime and nighttime using a single controlling factor: temperature. The dual-functionality (with the ability to actively cool and heat) of the thermoelectric component allows for precise temperature control of each pixel, thus enabling thermal camouflage in the infrared spectrum through synchronization with the surrounding temperature.[232] Inspired by cephalopods, a visible-IR-radar multi-band camouflage MXene nanocomposite cholesteric liquid crystal elastomer (MXene-CLCE) was reported (Fig. 15(a)). Large-area CLCE flexible films were fabricated via in situ Michael addition and free radical photopolymerization of liquid crystal precursors, and further functionalized by introducing an isocyanate interfacial layer to achieve covalent chemical bonding between the MXene nanocoating and the CLCE film. The resulting MXene-CLCE exhibited dynamic structural color changes, tunable IR radiation, and switchable microwave shielding properties (Fig. 15(b)–(d)).[143] This research provides a novel approach for the development and application of multi-band camouflage smart materials, holding great potential

10714 | Chem. Soc. Rev., 2025, 54, 10690–10723

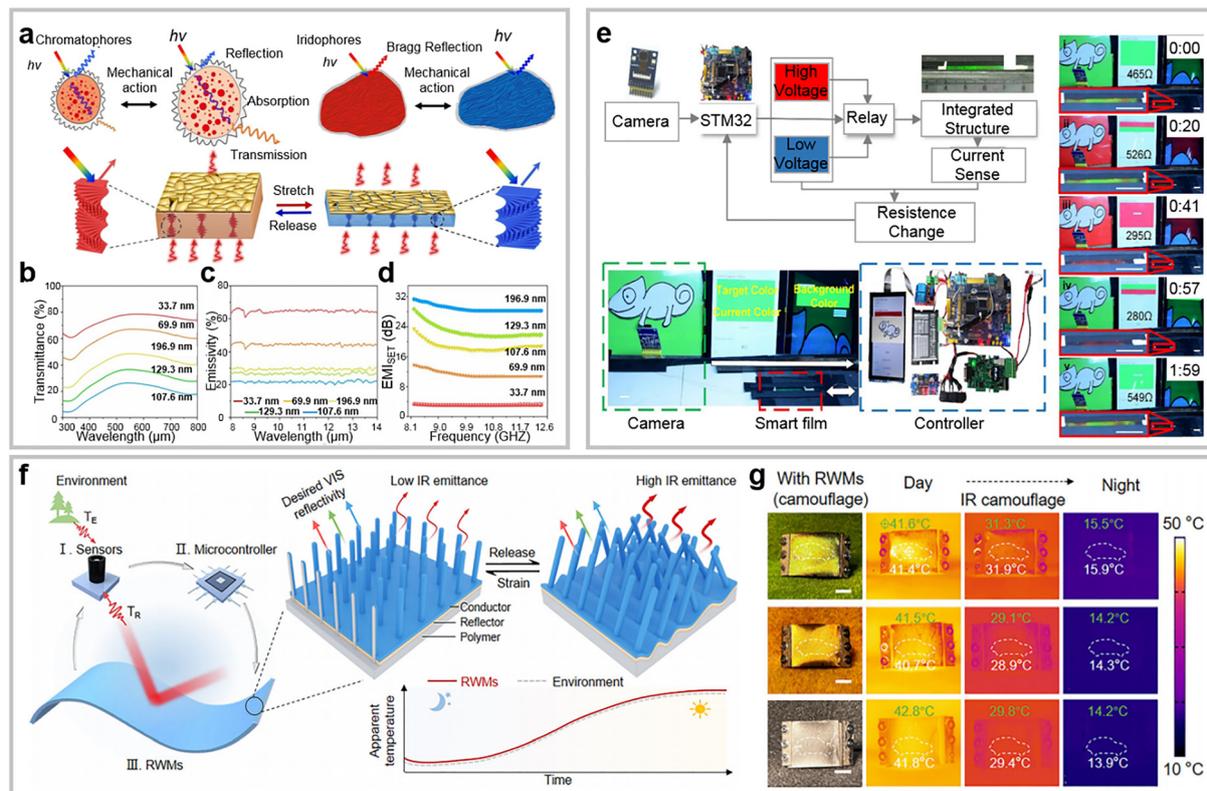This journal is © The Royal Society of Chemistry 2025

Fig. 15 Bioinspired materials for adaptive IR camouflage. (a)–(d) Cephalopod-inspired MXene-integrated mechanochromic cholesteric liquid crystal elastomers for multispectral camouflage. (a) Schematic illustration of the designed dynamic multispectral camouflage cephalopod-inspired MXene-CLCE before and after actuation. (b) Reflection spectra, (c) infrared emissivity spectra, and (d) electromagnetic interference shielding effectiveness of the red-reflecting MXene-CLCE at various strains (from 0% to 120%). Reproduced with permission from ref. 143. Copyright (2025) Wiley-VCH. (e) The active tunable color system with integrated smart skin. Reproduced with permission from ref. 233. Copyright (2023) The Royal Society. (f), (g) Reconfigurable wire metamaterials for visible and self-adaptive IR camouflage. (f) Design concept and working principle of the metamaterial. (g) Visible and thermal images of a vehicle model with metamaterial-covered roof under jungle, desert, and road backgrounds during day/night. Green digits denote the background apparent temperature, and white digits show the vehicle/metamaterial temperature. Scale bar: 1 cm. Reproduced with permission from ref. 235. Copyright (2025) Wiley-VCH.

for applications in military stealth, intelligent optical camouflage, and dynamic thermal management.

Driven by the progress in artificial intelligence (AI) and sensor technologies, bionic adaptive camouflage systems are poised to exhibit enhanced capabilities in intelligence and adaptability. Future developments in this domain are anticipated to transcend the limitations of singular functionalities, such as color variation or thermal concealment. Instead, a convergence of multiple features, encompassing optical camouflage, thermal camouflage, electromagnetic camouflage, and environmental perception, is expected to be realized. This multifunctional integration is projected to significantly augment the system's capacity to adapt and maintain concealment in environments characterized by complexity and dynamism. A novel 2D material, $Ti_3C_2T_x$ MXene, along with an interfacial engineering approach, is utilized in the creation of a flexible robotic skin that exhibits multifunctionality inspired by cephalopod skin. Electrically controlled arrays were constructed using MXene-coated dielectric elastomer actuators to achieve dynamic thermal camouflage. Through the utilization of interfacial instability, the MXene robotic skin with adaptable

microtextures showcases adjustable infrared emission (0.30–0.80), allowing for dynamic thermal camouflage in soft robots.[141] Inspired by chameleon adaptive coloration, Zhang et al. developed a multifunctional smart skin comprising PhC nanohole arrays, CNT coatings, and liquid crystal elastomers. It integrates tunable structural coloration, sensing, and actuation in a single structure, coupled with an image acquisition unit (mimicking eyes) and a controller (mimicking a brain) to form an active tunable system emulating the dynamic color change of chameleons (Fig. 15(e)).[233] Kim et al. developed a chameleon-inspired soft robot with an artificial camouflage skin, integrating thermochromic liquid crystals and vertically aligned silver nanowire heaters in a multi-tiered structure. This design overcomes the traditional lateral pixel limitations by overlaying heater-induced temperature profiles for dynamic coloration.[234] Other than chameleon and cephalopod camouflages, inspirations have also been drawn from other biological models. For example, motivated by animal skin/hair thermal adaptation, Wang and coworkers developed a programmable, self-adaptive IR camouflage system with autonomous IR regulation via temperature feedback for all-day programmable camouflage.[235] The system

This journal is © The Royal Society of Chemistry 2025

Chem. Soc. Rev., 2025, **54**, 10690–10723 | **10715**

combines flexible reconfigurable wire metamaterials, IR sensors, a microcontroller, and a motor driver into a self-adaptive closed-loop (Fig. 15(f)), eliminating manual operation. Using simulated backgrounds (jungle/desert/road) and cloaks of the corresponding colors (green/yellow/grey), the device's dual capabilities in visible and IR camouflage were validated, matching adaptively the background apparent temperature from about 41 to 14 °C from day to night with unrecognizable temperature differences (Fig. 15(g)). Overall, these discoveries constitute notable progress in the ongoing exploration of bioinspired light and heat manipulation, potentially catalyzing advancements in the development of electronic gadgets, solar cells, soft robotics, and techniques for thermal detection and regulation.

6. Summary and outlook

Throughout human history, the natural world has been a vital source of inspiration and innovation for technological advancements. Organisms that have evolved over billions of years possess sophisticated microstructures that enable them to effectively manipulate light and heat radiation, thereby adapting to environmental changes and ensuring their survival and evolution. The optical structures and their underlying mechanisms are crucial for the survival and reproduction of these organisms. Understanding the optical structures and systems in biology can enhance our comprehension of the ecological adaptability and evolutionary mechanisms of organisms, offering new insights into the field of life sciences. Moreover, research on bioinspired optical materials and systems provides essential perspectives for elucidating the fundamental structure–function relationships in optical and photonic systems. In recent decades, significant efforts have been devoted to uncovering the intricate structures of these biological models, elucidating the mechanisms behind their exceptional optical and thermal properties, and advancing fabrication techniques. These bioinspired materials and structures can effectively control the conduction, radiation, and absorption of heat, thereby playing a significant role in various engineering and scientific applications, including energy-efficient buildings, wearable thermal management, camouflage, invisibility, and other fields. Consequently, a fundamental understanding of biophotonics has propelled remarkable progress in the development of biomimetic and bioinspired photonic devices.

In this comprehensive review, we examined the typical photonic structures and principles employed by biological organisms for thermal regulation, alongside the latest advancements in thermal management and heat utilization technologies inspired by biomimetic materials. We overviewed the typical optical responses available from nature, and how their combinations fit different thermal management scenarios. In these investigations, the diverse microstructures found in living organisms are categorized into three primary classes based on their distinctive optical characteristics: bioinspired antireflective microstructures, reflective microstructures, and dynamic radiative microstructures. We have comprehensively reviewed

the optical phenomena and their underlying physical mechanisms of microstructures for thermal regulation from diverse research endeavors. The intricate structures and remarkable thermal regulation abilities found in biological systems have not only advanced the fabrication of materials and systems for radiative cooling and heating, but also sparked interest in the investigation of adaptive IR camouflage and thermal control technologies. It is clear that drawing inspiration from biology can provide an appealing pathway for innovating the design and operational fundamentals of thermal controlled materials and systems, leading to enhanced performance and additional functionalities compared to those achieved through traditional engineering approaches.

Bioinspired photonic materials have enormous potential for thermal management applications. Accelerating the maturation of this exciting field presents numerous challenges as well as opportunities (Fig. 16). First, the biological models that have been discovered and studied by researchers as well as that possess thermal management and thermal radiation functionalities represent merely the tip of the iceberg. The intricate mechanisms governing the detailed thermal regulation and utilization, especially the interplay between their dynamically evolving complex structures and thermal behaviors, have yet to be fully elucidated. Nature offers a wide array of prototypes for the design and fabrication of new photonic materials. Future research may focus on polar and deep-sea organisms. The insulation mechanism of polar bear fur has been confirmed,[236,237] while the insulation and heat conduction mechanisms of other polar organisms, such as penguins, remain to be verified. In addition, deep-sea organisms, including tube worms, krill, deep-sea fish, jellyfish, sponges, and corals, inhabit unique environments characterized by high pressure, darkness, and low/high temperature. Organisms in these environments may possess special heat management strategies. New mechanisms and photonic structures,[238] such as non-reciprocal thermal radiation,[239] also need further investigation. The close association of numerous remarkable optical properties with their evolutionary functions and environmental conditions, including those found in extreme environments, underscores the importance of uncovering new phenomena, structures, and the underlying physical mechanisms as the foundation for biomimetics.

Second, the performance disparity between artificial biomimetic structures and biological microstructures largely stems from the intricate complexity of the latter, which poses a significant challenge for achieving a high degree of precision in artificial fabrication. The functionality arises from the capacity to manipulate these systems across hierarchical length scales, ranging from the molecular level to the macroscale. In the future, it is our aspiration to develop more refined manufacturing processes, such as digital fabrication. Furthermore, the majority of materials are still in the laboratory stage, and there is a hope to develop large-scale, low-cost, and scalable manufacturing processes to promote their practical application in various fields.

Third, by establishing performance testing standards and improving existing materials, the comprehensive performance
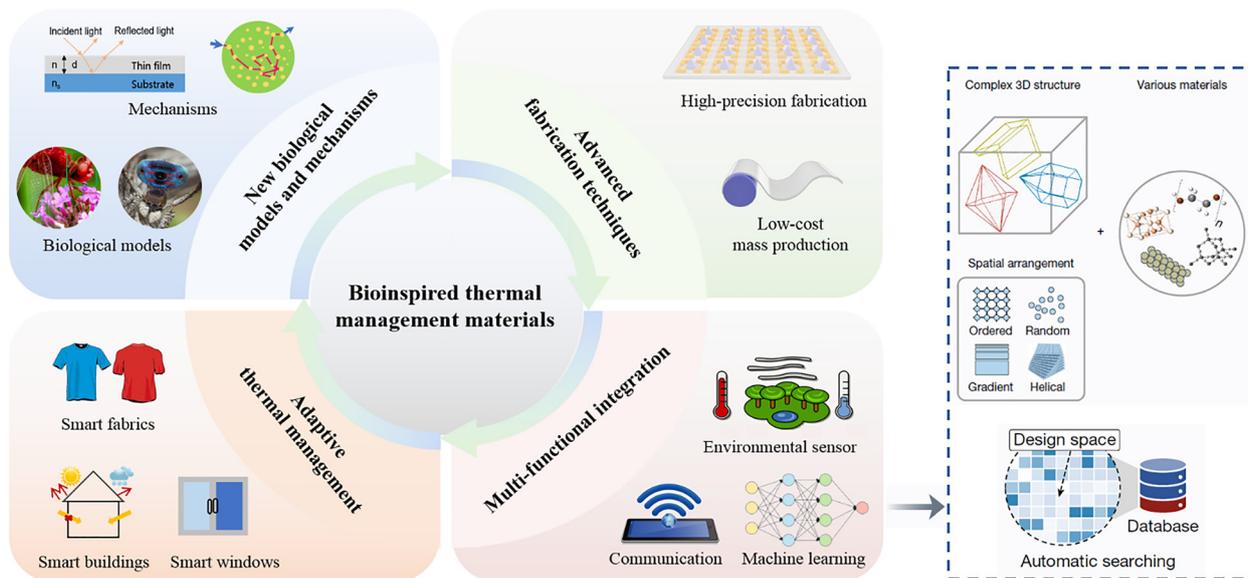
10716 | Chem. Soc. Rev., 2025, 54, 10690–10723

This journal is © The Royal Society of Chemistry 2025

Fig. 16 Summary and outlook of bioinspired materials for thermal management. Photographs of the red dragonfly (*Crocothemis servilia*) and peacock spider (*Maratus, Salticidae*) are reproduced, respectively, with permissions from ref. 93. Copyright (2022) Elsevier and from ref. 104. Copyright (2019) CC BY. Schematic in the box on the right is reproduced with permission from ref. 259. Copyright (2025) Springer Nature.

of bioinspired photonic materials can be enhanced to meet various application demands. Currently, some bioinspired materials need improvements in strength and toughness. For example, certain bionic composites with high hardness may experience performance degradation over long-term use. Their optical properties in specific bands are also suboptimal, leading to low photothermal conversion efficiencies. The same issue occurs at extreme temperatures, affecting long-term stability. Future research should focus on evaluating the thermal properties of these materials, with key indicators such as thermal conductivity, stability, and temperature dependence. Mechanical properties, *e.g.*, flexural strength and modulus, are also crucial. Environmental adaptability, including the humidity influence coefficient, needs assessments as well. For further improvement of performance, combining different materials is a viable way to integrate their strengths and functionalities, and there is still a lot of space to enhance the optical and thermal properties by optimizing micro-/nanostructures and refining the fabrication processes.

Fourth, most existing approaches to thermal control and camouflage are inherently static. For camouflage, the ability to conceal is typically limited to a specific ambient temperature or background color, making it difficult to achieve genuinely adaptive concealment in complex and unfamiliar environments. Likewise, current strategies of thermal management lack or are short in the capacity to respond dynamically to environmental changes. Future development could prioritize the creation of advanced adaptive thermal management systems that can tune their properties and functions autonomously, and ideally in real time, to react to the changing external conditions.[141,234,240–243]

Last but not the least, in light of emerging research on internet of things and AI technologies, we propose an intelligent thermal management system for future thermoregulation. The biological regulation of thermal energy can be integrated with additional functionalities to attain enhanced overall efficiencies and performance. For example, thermal management can be combined with computation, environmental sensors, energy harvesting, displays and other functions to form an intelligent interactive integrated system.[244–246] The formidable task of creating advanced thermal energy control systems with integrated elements and features persists a significant challenge. Meanwhile, AI has the potential to change the current landscape of materials design.[247] As discussed in Section 2, unlike in most common applications, materials for thermal management usually feature simultaneous ultrabroad bandwidths and band-selective functionalities. In the past, a main reason that we turned to biological models for inspiration is the difficulty in designing complex hierarchical structures from scratch with traditional computational tools by trial and error. This pain may be greatly relieved by employing AI-based or AI-assisted design frameworks.[248–254] For a specific application, although there is an ideal spectrum (Fig. 1), practical devices do not need to meet exactly that line shape to reach high performance, because local discrepancies have limited influences on the overall optothermal properties after averaging over the entire wavelength range. With relaxed requirements on spectral accuracy, AI-based design methods are particularly strong in searching the enormous combinations of materials and structures for desirable functions,[255–258] and this search can be reinforced by training the model with knowledge extracted from biological materials. In a recent demonstration, Zhou's team and collaborators showcased a machine learning-based inverse design framework for efficient discovery of high-performance thermal meta-emitters.[259] Through introducing a robust descriptor capable of translating 3D

This journal is © The Royal Society of Chemistry 2025

Chem. Soc. Rev., 2025, **54**, 10690–10723 | **10717**

structural and materials data into parameters that neural networks can process, the accessible design space is greatly extended (Fig. 16, right panel). One limitation with biomimicry is that biological models resulting from evolution, which essentially is a multi-objective optimization process, may compromise on maximizing the performance in a selected function to meet the requirements of other functions. With AI-empowered search tools, it is reasonable to assume that the performance of bioinspired materials can be further improved by lifting this constraint or by tackling the multiple objectives in a more efficient way.

In summary, bioinspiration is a means, not a goal. The overarching objective is to surpass the constraints inherent in nature and engineer sophisticated bionic artificial systems that can effectively address human needs, rather than to merely replicate biological mechanisms. As research in bioinspired and biomimetic engineering continues to progress, the exceptional structures and features identified in biological models are expected to drive the development of increasingly sophisticated functional materials for a wider range of applications. Despite the challenges ahead, the field of bioinspired photonic and thermal microstructured materials is poised for rapid growth, promising significant advancements in biophotonics and thermal management.

Author contributions

K. Y. wrote Sections 1, 2, 3.1.2, 3.3, 5.1 and 5.2; G. K. wrote Sections 3.1.1, 3.1.3, 3.2, 3.4, 4, 5.3 and 6; C. X., S. C., Y. Zhang, X. L. and J. L. also contributed to the writing of Sections 3–5. All authors participated in revising the manuscript.

Conflicts of interest

There are no conflicts to declare.

Data availability

No primary research results, software or code have been included and no new data were generated or analysed as part of this review.

Acknowledgements

References

1 E. A. Tansey and C. D. Johnson, *Adv. Physiol. Educ.*, 2015, **39**, 139–148.

2 M. Taleghani, M. Tenpierik, S. Kurvers and A. van den Dobbelsteen, *Renewable Sustainable Energy Rev.*, 2013, **26**, 201–215.

3 R. Hu, Y. Liu, S. Shin, S. Huang, X. Ren, W. Shu, J. Cheng, G. Tao, W. Xu, R. Chen and X. Luo, *Adv. Energy Mater.*, 2020, **10**, 1903921.

4 A. L. Moore and L. Shi, *Mater. Today*, 2014, **17**, 163–174.

5 J. Lin, X. Liu, S. Li, C. Zhang and S. Yang, *Int. J. Heat Mass Transfer*, 2021, **167**, 120834.

6 X. Yin, R. Yang, G. Tan and S. Fan, *Science*, 2020, **370**, 786–791.

7 S. Tadepalli, J. M. Slocik, M. K. Gupta, R. R. Naik and S. Singamaneni, *Chem. Rev.*, 2017, **117**, 12705–12763.

8 P. Vukusic and J. R. Sambles, *Nature*, 2003, **424**, 852–855.

9 W.-G. Bae, H. N. Kim, D. Kim, S.-H. Park, H. E. Jeong and K.-Y. Suh, *Adv. Mater.*, 2014, **26**, 675–700.

10 J. Yang, X. Zhang, X. Zhang, L. Wang, W. Feng and Q. Li, *Adv. Mater.*, 2021, **33**, 2004754.

11 Q. Sun, G. Zhi, S. Zhou, X. Dong, Q. Shen, R. Tao and J. Qi, *Adv. Mater. Technol.*, 2024, **9**, 2400263.

12 Y. Peng and Y. Cui, *Joule*, 2020, **4**, 724–742.

13 A. E. Seago, P. Brady, J.-P. Vigneron and T. D. Schultz, *J. R. Soc., Interface*, 2009, **6**, S165–S184.

14 S. Kinoshita and S. Yoshioka, *ChemPhysChem*, 2005, **6**, 1442–1459.

15 A. G. Dumanli and T. Savin, *Chem. Soc. Rev.*, 2016, **45**, 6698–6724.

16 Q. Shen, Z. Luo, S. Ma, P. Tao, C. Song, J. Wu, W. Shang and T. Deng, *Adv. Mater.*, 2018, **30**, 1707632.

17 P. Wu, J. Wang and L. Jiang, *Mater. Horiz.*, 2020, **7**, 338–365.

18 S. Dou, H. Xu, J. Zhao, K. Zhang, N. Li, Y. Lin, L. Pan and Y. Li, *Adv. Mater.*, 2021, **33**, 2000697.

19 D. Nepal, S. Kang, K. M. Adstedt, K. Kanhaiya, M. R. Bockstaller, L. C. Brinson, M. J. Buehler, P. V. Coveney, K. Dayal, J. A. El-Awady, L. C. Henderson, D. L. Kaplan, S. Keten, N. A. Kotov, G. C. Schatz, S. Vignolini, F. Vollrath, Y. Wang, B. I. Yakobson, V. V. Tsukruk and H. Heinz, *Nat. Mater.*, 2023, **22**, 18–35.

20 Y. Wang, T. Guo, Z. Tian, K. Bibi, Y.-Z. Zhang and H. N. Alshareef, *Adv. Mater.*, 2022, **34**, 2108560.

21 G. Liu, J. Xu and K. Wang, *Nano Energy*, 2017, **41**, 269–284.

22 S. Kundu and A. Patra, *Chem. Rev.*, 2017, **117**, 712–757.

23 L. Zhu, L. Tian, S. Jiang, L. Han, Y. Liang, Q. Li and S. Chen, *Chem. Soc. Rev.*, 2023, **52**, 7389–7460.

24 S. Fan and W. Li, *Nat. Photonics*, 2022, **16**, 182–190.

25 D. Zhao, A. Aili, Y. Zhai, S. Xu, G. Tan, X. Yin and R. Yang, *Appl. Phys. Rev.*, 2019, **6**, 021306.

26 Z. Yan, H. Zhai, D. Fan and Q. Li, *Prog. Mater. Sci.*, 2024, **144**, 101291.

27 S. Wu, H. Sun, M. Duan, H. Mao, Y. Wu, H. Zhao and B. Lin, *Cell Rep. Phys. Sci.*, 2023, **4**, 101370.

10718 | *Chem. Soc. Rev.*, 2025, **54**, 10690–10723

This journal is © The Royal Society of Chemistry 2025

28 Y. Ke, J. Chen, G. Lin, S. Wang, Y. Zhou, J. Yin, P. S. Lee and Y. Long, *Adv. Energy Mater.*, 2019, **9**, 1902066.

29 S. C. Fu, X. L. Zhong, Y. Zhang, T. W. Lai, K. C. Chan, K. Y. Lee and C. Y. H. Chao, *Energy Build.*, 2020, **225**, 110313.

30 L. Zhu, A. Raman, K. X. Wang, M. A. Anoma and S. Fan, *Optica*, 2014, **1**, 32–38.

31 P. N. Dyachenko, S. Molesky, A. Y. Petrov, M. Störmer, T. Krekeler, S. Lang, M. Ritter, Z. Jacob and M. Eich, *Nat. Commun.*, 2016, **7**, 11809.

32 Z. A. Kudyshev, A. V. Kildishev, V. M. Shalaev and A. Boltasseva, *Appl. Phys. Rev.*, 2020, **7**, 021407.

33 W. Li, Y. Shi, Z. Chen and S. Fan, *Nat. Commun.*, 2018, **9**, 4240.

34 S. Wang, T. Jiang, Y. Meng, R. Yang, G. Tan and Y. Long, *Science*, 2021, **374**, 1501–1504.

35 X. Liu, Z. Yan, H. Wang, Q. Zhao, H. Zhou and T. Fan, *Laser Photonics Rev.*, 2023, **17**, 2200635.

36 T. Kim, J.-Y. Bae, N. Lee and H. H. Cho, *Adv. Funct. Mater.*, 2019, **29**, 1807319.

37 N. N. Shi, C.-C. Tsai, F. Camino, G. D. Bernard, N. Yu and R. Wehner, *Science*, 2015, **349**, 298–301.

38 H. Zhou, J. Xu, X. Liu, H. Zhang, D. Wang, Z. Chen, D. Zhang and T. Fan, *Adv. Funct. Mater.*, 2018, **28**, 1705309.

39 G. Jacucci, L. Schertel, Y. Zhang, H. Yang and S. Vignolini, *Adv. Mater.*, 2021, **33**, 2001215.

40 N. Funt, B. A. Palmer, S. Weiner and L. Addadi, *ChemPlusChem*, 2017, **82**, 914–923.

41 A. L. Holt, A. M. Sweeney, S. Johnsen and D. E. Morse, *J. R. Soc., Interface*, 2011, **8**, 1386–1399.

42 S. Zhao, P. C. Brady, M. Gao, R. I. Etheredge, G. W. Kattawar and M. E. Cummings, *J. R. Soc., Interface*, 2015, **12**, 20141390.

43 S. Kinoshita, S. Yoshioka and J. Miyazaki, *Rep. Prog. Phys.*, 2008, **71**, 076401.

44 A. R. Parker, D. R. Mckenzie and M. C. J. Large, *J. Exp. Biol.*, 1998, **201**, 1307–1313.

45 T. M. Jordan, J. C. Partridge and N. W. Roberts, *Nat. Photonics*, 2012, **6**, 759–763.

46 G. R. R. Bell, L. M. Mäthger, M. Gao, S. L. Senft, A. M. Kuzirian, G. W. Kattawar and R. T. Hanlon, *Adv. Mater.*, 2014, **26**, 4352–4356.

47 D. Gur, B. Leshem, D. Oron, S. Weiner and L. Addadi, *J. Am. Chem. Soc.*, 2014, **136**, 17236–17242.

48 P. C. Brady, A. A. Gilerson, G. W. Kattawar, J. M. Sullivan, M. S. Twardowski, H. M. Dierssen, M. Gao, K. Travis, R. I. Etheredge, A. Tonizzo, A. Ibrahim, C. Carrizo, Y. Gu, B. J. Russell, K. Mislinski, S. Zhao and M. E. Cummings, *Science*, 2015, **350**, 965–969.

49 G. Guidetti, H. Sun, B. Marelli and F. G. Omenetto, *Sci. Adv.*, 2020, **6**, eaba8966.

50 L. Whitehead, M. Mossman and A. Kushnir, *Phys Canada*, 2008, **64**, 7–12.

51 Q. Willot, P. Simonis, J.-P. Vigneron and S. Aron, *PLoS One*, 2016, **11**, e0152325.

52 A. Bay, P. Cloetens, H. Suhonen and J. P. Vigneron, *Opt. Express*, 2013, **21**, 764–780.

53 H. Zhang, K. C. S. Ly, X. Liu, Z. Chen, M. Yan, Z. Wu, X. Wang, Y. Zheng, H. Zhou and T. Fan, *Proc. Natl. Acad. Sci. U. S. A.*, 2020, **117**, 14657–14666.

54 D. S. Wiersma, *Nat. Photonics*, 2013, **7**, 188–196.

55 P. D. García, R. Sapienza and C. López, *Adv. Mater.*, 2010, **22**, 12–19.

56 T. Lemcoff, L. Alus, J. S. Haataja, A. Wagner, G. Zhang, M. J. Pavan, V. J. Yallapragada, S. Vignolini, D. Oron, L. Schertel and B. A. Palmer, *Nat. Photonics*, 2023, **17**, 485–493.

57 L. M. Beck, V. J. Yallapragada, A. Upcher, B. A. Palmer, L. Addadi and D. Oron, *Opt. Express*, 2021, **29**, 20863–20871.

58 P. Vukusic, B. Hallam and J. Noyes, *Science*, 2007, **315**, 348.

59 S. M. Luke, B. T. Hallam and P. Vukusic, *Appl. Opt.*, 2010, **49**, 4246–4254.

60 M. Burresi, L. Cortese, L. Pattelli, M. Kolle, P. Vukusic, D. S. Wiersma, U. Steiner and S. Vignolini, *Sci. Rep.*, 2014, **4**, 6075.

61 G. Jacucci, O. D. Onelli, A. De Luca, J. Bertolotti, R. Sapienza and S. Vignolini, *Interface Focus*, 2019, **9**, 20180050.

62 S. H. Lee, S. M. Han and S. E. Han, *APL Photonics*, 2020, **5**, 056103.

63 F. Utel, L. Cortese, D. S. Wiersma and L. Pattelli, *Adv. Opt. Mater.*, 2019, **7**, 1900043.

64 B. D. Wilts, X. Sheng, M. Holler, A. Diaz, M. Guizar-Sicairos, J. Raabe, R. Hoppe, S.-H. Liu, R. Langford, O. D. Onelli, D. Chen, S. Torquato, U. Steiner, C. G. Schroer, S. Vignolini and A. Sepe, *Adv. Mater.*, 2018, **30**, 1702057.

65 D. G. Stavenga, S. Stowe, K. Siebke, J. Zeil and K. Arikawa, *Proc. R. Soc. London, Ser. B*, 2004, **271**, 1577–1584.

66 S. H. Choi, S.-W. Kim, Z. Ku, M. A. Visbal-Onufrak, S.-R. Kim, K.-H. Choi, H. Ko, W. Choi, A. M. Urbas, T.-W. Goo and Y. L. Kim, *Nat. Commun.*, 2018, **9**, 452.

67 P. W. Anderson, *Phys. Rev.*, 1958, **109**, 1492–1505.

68 T. Schwartz, G. Bartal, S. Fishman and M. Segev, *Nature*, 2007, **446**, 52–55.

69 B. Zhu, W. Li, Q. Zhang, D. Li, X. Liu, Y. Wang, N. Xu, Z. Wu, J. Li, X. Li, P. B. Catrysse, W. Xu, S. Fan and J. Zhu, *Nat. Nanotechnol.*, 2021, **16**, 1342–1348.

70 X.-E. Wu, Y. Wang, X. Liang, Y. Zhang, P. Bi, M. Zhang, S. Li, H. Liang, S. Wang, H. Wang, H. Lu and Y. Zhang, *Adv. Funct. Mater.*, 2024, **34**, 2313539.

71 J. J. Allen, G. R. R. Bell, A. M. Kuzirian, S. S. Velankar and R. T. Hanlon, *J. Morphol.*, 2014, **275**, 371–390.

72 E. Van Hooijdonk, C. Barthou, J. P. Vigneron and S. Berthier, *J. Opt. Soc. Am. B*, 2012, **29**, 1104–1111.

73 S. Mouchet, J.-F. Colomer, C. Vandenbem, O. Deparis and J.-P. Vigneron, *Opt. Express*, 2013, **21**, 13228–13240.

74 Y.-Y. Diao and X.-Y. Liu, *Opt. Express*, 2011, **19**, 9232–9241.

75 X. Liu, D. Wang, Z. Yang, H. Zhou, Q. Zhao and T. Fan, *Adv. Opt. Mater.*, 2019, **7**, 1900687.

76 P. Vukusic, R. Kelly and I. Hooper, *J. R. Soc., Interface*, 2009, **6**, S193–S201.

77 D. Ge, G. Wu, L. Yang, H.-N. Kim, W. Hallwachs, J. M. Burns, D. H. Janzen and S. Yang, *Proc. Natl. Acad. Sci. U. S. A.*, 2017, **114**, 7379–7384.

This journal is © The Royal Society of Chemistry 2025

Chem. Soc. Rev., 2025, **54**, 10690–10723 | **10719**

78 A. Ghoshal, E. Eck, M. Gordon and D. E. Morse, *J. R. Soc., Interface*, 2016, **13**, 20160285.

79 A. Ghoshal, E. Eck and D. E. Morse, *Optica*, 2016, **3**, 108–111.

80 S. Chattopadhyay, Y. F. Huang, Y. J. Jen, A. Ganguly, K. H. Chen and L. C. Chen, *Mater. Sci. Eng., R*, 2010, **69**, 1–35.

81 S. An, B. Shi, M. Jiang, B. Fu, C. Song, P. Tao, W. Shang and T. Deng, *Chem. Rev.*, 2023, **123**, 7081–7118.

82 J. Cai and L. Qi, *Mater. Horiz.*, 2015, **2**, 37–53.

83 F. L. Gonzalez and M. J. Gordon, *Opt. Express*, 2014, **22**, 12808–12816.

84 A. Blagodatski, M. Kryuchkov, A. Sergeev, A. A. Klimov, M. R. Shcherbakov, G. A. Enin and V. L. Katanaev, *Sci. Rep.*, 2014, **4**, 6004.

85 H. Ding, D. Liu, B. Li, W. Ze, S. Niu, C. Xu, Z. Han and L. Ren, *ACS Appl. Mater. Interfaces*, 2021, **13**, 19450–19459.

86 A. Blagodatski, A. Sergeev, M. Kryuchkov, Y. Lopatina and V. L. Katanaev, *Proc. Natl. Acad. Sci. U. S. A.*, 2015, **112**, 10750–10755.

87 X. Gao, X. Yan, X. Yao, L. Xu, K. Zhang, J. Zhang, B. Yang and L. Jiang, *Adv. Mater.*, 2007, **19**, 2213–2217.

88 M. Kryuchkov, J. Lehmann, J. Schaab, V. Cherepanov, A. Blagodatski, M. Fiebig and V. L. Katanaev, *J. Nanobiotechnol.*, 2017, **15**, 61.

89 S. Lou, X. Guo, T. Fan and D. Zhang, *Energy Environ. Sci.*, 2012, **5**, 9195–9216.

90 D. G. Stavenga, S. Foletti, G. Palasantzas and K. Arikawa, *Proc. R. Soc. B*, 2006, **273**, 661–667.

91 D. Wu, J.-N. Wang, L.-G. Niu, X. L. Zhang, S. Z. Wu, Q.-D. Chen, L. P. Lee and H. B. Sun, *Adv. Opt. Mater.*, 2014, **2**, 751–758.

92 J. Sun, X. Wang, J. Wu, C. Jiang, J. Shen, M. A. Cooper, X. Zheng, Y. Liu, Z. Yang and D. Wu, *Sci. Rep.*, 2018, **8**, 5438.

93 H. Ding, B. Li, Z. Wang, S. Niu, Z. Han and L. Ren, *Matter*, 2022, **5**, 2990–3008.

94 H.-J. Choi, H. Daihong, J. Junho and H. Lee, *Appl. Spectrosc. Rev.*, 2019, **54**, 719–735.

95 Z. Han, Z. Wang, B. Li, X. Feng, Z. Jiao, J. Zhang, J. Zhao, S. Niu and L. Ren, *ACS Appl. Mater. Interfaces*, 2019, **11**, 17019–17027.

96 A. Papadopoulos, E. Skoulas, A. Mimidis, G. Perrakis, G. Kenanakis, G. D. Tsibidis and E. Stratakis, *Adv. Mater.*, 2019, **31**, 1901123.

97 A. Yoshida, M. Motoyama, A. Kosaku and K. Miyamoto, *Zool. Sci.*, 1997, **14**, 737–741, 735.

98 G. Zhang, J. Zhang, G. Xie, Z. Liu and H. Shao, *Small*, 2006, **2**, 1440–1443.

99 M. Spinner, A. Kovalev, S. N. Gorb and G. Westhoff, *Sci. Rep.*, 2013, **3**, 1846.

100 V. R. Binetti, J. D. Schiffman, O. D. Leaffer, J. E. Spanier and C. L. Schauer, *Integr. Biol.*, 2009, **1**, 324–329.

101 R. H. Siddique, G. Gomard and H. Hölscher, *Nat. Commun.*, 2015, **6**, 6909.

102 V. Narasimhan, R. H. Siddique, J. O. Lee, S. Kumar, B. Ndjamen, J. Du, N. Hong, D. Sretavan and H. Choo, *Nat. Nanotechnol.*, 2018, **13**, 512–519.

103 I. R. Hooper, P. Vukusic and R. J. Wootton, *Opt. Express*, 2006, **14**, 4891–4897.

104 D. E. McCoy, V. E. McCoy, N. K. Mandsberg, A. V. Shneidman, J. Aizenberg, R. O. Prum and D. Haig, *Proc. R. Soc. B*, 2019, **286**, 20190589.

105 D. E. McCoy and R. O. Prum, *J. Exp. Biol.*, 2019, **222**, jeb208140.

106 D. E. McCoy, T. Feo, T. A. Harvey and R. O. Prum, *Nat. Commun.*, 2018, **9**, 1.

107 P. Vukusic, J. R. Sambles and C. R. Lawrence, *Proc. R. Soc. B*, 2004, **271**, S237–S239.

108 W. Wang, W. Zhang, X. Fang, Y. Huang, Q. Liu, M. Bai and D. Zhang, *Opt. Lett.*, 2014, **39**, 4208–4211.

109 W. Zhang, J. Gu, Q. Liu, H. Su, T. Fan and D. Zhang, *Phys. Chem. Chem. Phys.*, 2014, **16**, 19767–19780.

110 A. L. Davis, H. F. Nijhout and S. Johnsen, *Nat. Commun.*, 2020, **11**, 1294.

111 Z. Han, S. Niu, C. Shang, Z. Liu and L. Ren, *Nanoscale*, 2012, **4**, 2879–2883.

112 Q. Zhao, T. Fan, J. Ding, D. Zhang, Q. Guo and M. Kamada, *Carbon*, 2011, **49**, 877–883.

113 Q. Zhao, X. Guo, T. Fan, J. Ding, D. Zhang and Q. Guo, *Soft Matter*, 2011, **7**, 11433–11439.

114 J. Tian, W. Zhang, X. Fang, Q. Liu, J. Gu, T. Deng, Y. Wang and D. Zhang, *J. Mater. Chem. C*, 2015, **3**, 1672–1679.

115 J. Tian, W. Zhang, J. Gu, T. Deng and D. Zhang, *Nano Energy*, 2015, **17**, 52–62.

116 R. Yan, M. Chen, H. Zhou, T. Liu, X. Tang, K. Zhang, H. Zhu, J. Ye, D. Zhang and T. Fan, *Sci. Rep.*, 2016, **6**, 20001.

117 R. H. Siddique, Y. J. Donie, G. Gomard, S. Yalamanchili, T. Merdzhanova, U. Lemmer and H. Hölscher, *Sci. Adv.*, 2017, **3**, e1700232.

118 A. Krishna, X. Nie, A. D. Warren, J. E. Llorente-Bousquets, A. D. Briscoe and J. Lee, *Proc. Natl. Acad. Sci. U. S. A.*, 2020, **117**, 1566–1572.

119 J. D. Joannopoulos, S. G. Johnson, J. N. Winn and R. D. Meade, *Photonic Crystals: Molding the Flow of Light*, Princeton University Press, 2nd edn, 2011.

120 J. Zi, X. Yu, Y. Li, X. Hu, C. Xu, X. Wang, X. Liu and R. Fu, *Proc. Natl. Acad. Sci. U. S. A.*, 2003, **100**, 12576–12578.

121 B. D. Wilts, K. Michielsen, J. Kuipers, H. De Raedt and D. G. Stavenga, *Proc. R. Soc. B*, 2012, **279**, 2524–2530.

122 K. Michielsen and D. G. Stavenga, *J. R. Soc., Interface*, 2008, **5**, 85–94.

123 J. P. Vigneron and P. Simonis, *Phys. B*, 2012, **407**, 4032–4036.

124 S. Kinoshita, *Structural colors in the realm of nature*, World Scientific, 2008.

125 A. R. Parker, V. L. Welch, D. Driver and N. Martini, *Nature*, 2003, **426**, 786–787.

126 L. Han and S. Che, *Adv. Mater.*, 2018, **30**, 1705708.

127 O. Deparis and J. P. Vigneron, *Mater. Sci. Eng., B*, 2010, **169**, 12–15.

128 X. Wu, A. Erbe, D. Raabe and H.-O. Fabritius, *Adv. Funct. Mater.*, 2013, **23**, 3615–3620.

10720 | *Chem. Soc. Rev.*, 2025, **54**, 10690–10723

This journal is © The Royal Society of Chemistry 2025

129 V. Saranathan, C. O. Osuji, S. G. J. Mochrie, H. Noh, S. Narayanan, A. Sandy, E. R. Dufresne and R. O. Prum, *Proc. Natl. Acad. Sci. U. S. A.*, 2010, **107**, 11676–11681.

130 A. Haché and G.-G. Allogho, *Opt. Commun.*, 2011, **284**, 1656–1660.

131 S. Johnsen, *Ann. Rev. Ma.r Sci.*, 2014, **6**, 369–392.

132 K. Shavit, A. Wagner, L. Schertel, V. Farstey, D. Akkaynak, G. Zhang, A. Upcher, A. Sagi, V. J. Yallapragada, J. Haataja and B. A. Palmer, *Science*, 2023, **379**, 695–700.

133 H. Yin, B. Dong, X. Liu, T. Zhan, L. Shi, J. Zi and E. Yablonovitch, *Proc. Natl. Acad. Sci. U. S. A.*, 2012, **109**, 10798–10801.

134 M. D. Shawkey and G. E. Hill, *J. Exp. Biol.*, 2006, **209**, 1245–1250.

135 S. R. Mouchet, S. Luke, L. T. McDonald and P. Vukusic, *Faraday Discuss.*, 2020, **223**, 9–48.

136 P. O. Prum, in *Bird Coloration. Mechanisms and Measurements*, ed. G. E. Hill and K. J. McGraw, Harvard University Press, Cambridge, 2006, vol. I, pp. 295–353.

137 H. Q. Nguyen, H. Serret, Y. Bae, S. Ji, S. Chae, Y. I. Kim, J. Ha and Y. Jang, *Sci. Rep.*, 2020, **10**, 1343.

138 X. Liu, C. Xiao, P. Wang, M. Yan, H. Wang, P. Xie, G. Liu, H. Zhou, D. Zhang and T. Fan, *Adv. Opt. Mater.*, 2021, **9**, 2101151.

139 A. Krishna, X. Nie, A. D. Briscoe and J. Lee, *Sci. Rep.*, 2021, **11**, 24143.

140 C.-C. Tsai, R. A. Childers, N. Nan Shi, C. Ren, J. N. Pelaez, G. D. Bernard, N. E. Pierce and N. Yu, *Nat. Commun.*, 2020, **11**, 551.

141 K. Li, Z. Li, Z. Xiong, Y. Wang, H. Yang, W. Xu, L. Jing, M. Ding, J. Zhu, J. S. Ho and P.-Y. Chen, *Adv. Funct. Mater.*, 2022, **32**, 2110534.

142 X. Zhang, Y. Yang, P. Xue, C. Valenzuela, Y. Chen, X. Yang, L. Wang and W. Feng, *Angew. Chem., Int. Ed.*, 2022, **61**, e202211030.

143 Y. Liu, R. Bi, X. Zhang, Y. Chen, C. Valenzuela, Y. Yang, H. Liu, L. Yang, L. Wang and W. Feng, *Angew. Chem., Int. Ed.*, 2025, **64**, e202422636.

144 J. Zhang, P. Wang, W. Xie, H. Wang, Y. Zhang and H. Zhou, *ACS Nano*, 2024, **18**, 24741–24769.

145 H. Shi, S. Wu, M. Si, S. Wei, G. Lin, H. Liu, W. Xie, W. Lu and T. Chen, *Adv. Mater.*, 2022, **34**, 2107452.

146 G. Bogdanov, A. A. Strzelecka, N. Kaimal, S. L. Senft, S. Lee, R. T. Hanlon and A. A. Gorodetsky, *Science*, 2025, **388**, 1389–1395.

147 E. N. Shook, G. T. Barlow, D. Garcia-Rosales, C. J. Gibbons and T. G. Montague, *Curr. Opin. Neurobiol.*, 2024, **86**, 102876.

148 P. Liu, C. Xu and A. A. Gorodetsky, *J. Mater. Chem. C*, 2025, **13**, 11040–11051.

149 D. G. DeMartini, D. V. Krogstad and D. E. Morse, *Proc. Natl. Acad. Sci. U. S. A.*, 2013, **110**, 2552–2556.

150 C. Xu, M. Colorado Escobar and A. A. Gorodetsky, *Adv. Mater.*, 2020, **32**, 1905717.

151 Y. Liu, Z. Feng, C. Xu, A. Chatterjee and A. A. Gorodetsky, *ACS Nano*, 2021, **15**, 17299–17309.

152 Y. Bao, Y. Han, L. Yang, N. Li, J. Luo, W. Qu, R. Chen, A. K.-Y. Jen, T. Li, H. Chen, W.-L. Song and D. Fang, *Adv. Funct. Mater.*, 2019, **29**, 1806383.

153 T. Woo, X. Liang, D. A. Evans, O. Fernandez, F. Kretschmer, S. Reiter and G. Laurent, *Nature*, 2023, **619**, 122–128.

154 L. M. Mäthger, S. L. Senft, M. Gao, S. Karaveli, G. R. R. Bell, R. Zia, A. M. Kuzirian, P. B. Dennis, W. J. Crookes-Goodson, R. R. Naik, G. W. Kattawar and R. T. Hanlon, *Adv. Funct. Mater.*, 2013, **23**, 3980–3989.

155 K. Chen and L. Li, *Adv. Mater.*, 2019, **31**, 1901115.

156 J. Teyssier, S. V. Saenko, D. van der Marel and M. C. Milinkovitch, *Nat. Commun.*, 2015, **6**, 6368.

157 M. Q. R. Pembury Smith and G. D. Ruxton, *Biol. Rev.*, 2020, **95**, 1325–1340.

158 J. L. Kelley and W. I. L. Davies, *Front. Ecol. Evol.*, 2016, **4**, 106.

159 L. E. Schweikert, L. E. Bagge, L. F. Naughton, J. R. Bolin, B. R. Wheeler, M. S. Grace, H. D. Bracken-Grissom and S. Johnsen, *Nat. Commun.*, 2023, **14**, 4642.

160 O. Deparis and S. R. Mouchet, *Natural Photonics and Bioinspiration*, Artech House, 2021.

161 M. I. Osotsi, W. Zhang, I. Zada, J. Gu, Q. Liu and D. Zhang, *Natl. Sci. Rev.*, 2020, **8**, nwaa107.

162 D. Zhang, W. Zhang, J. Gu, T. Fan, Q. Liu, H. Su and S. Zhu, *Prog. Mater. Sci.*, 2015, **68**, 67–96.

163 S. R. Mouchet, *J. R. Soc., Interface*, 2025, **22**, 20240284.

164 A. P. Raman, M. A. Anoma, L. Zhu, E. Rephaeli and S. Fan, *Nature*, 2014, **515**, 540–544.

165 Y. Zhai, Y. Ma, S. N. David, D. Zhao, R. Lou, G. Tan, R. Yang and X. Yin, *Science*, 2017, **355**, 1062–1066.

166 F. Xie, W. Jin, J. R. Nolen, H. Pan, N. Yi, Y. An, Z. Zhang, X. Kong, F. Zhu, K. Jiang, S. Tian, T. Liu, X. Sun, L. Li, D. Li, Y.-F. Xiao, A. Alu, S. Fan and W. Li, *Science*, 2024, **386**, 788–794.

167 T. Li, Y. Zhai, S. He, W. Gan, Z. Wei, M. Heidarinejad, D. Dalgo, R. Mi, X. Zhao, J. Song, J. Dai, C. Chen, A. Aili, A. Vellore, A. Martini, R. Yang, J. Srebric, X. Yin and L. Hu, *Science*, 2019, **364**, 760–763.

168 C. Cai, X. Zhao, C. Miao, X. Tian, F. Xie, F. Luo, M. Zhang, X. Wu, J. Liu, B. Jiang and Y. Fu, *Nano Lett.*, 2025, **25**, 4369–4378.

169 K. Lin, S. Chen, Y. Zeng, T. C. Ho, Y. Zhu, X. Wang, F. Liu, B. Huang, C. Y.-H. Chao, Z. Wang and C. Y. Tso, *Science*, 2023, **382**, 691–697.

170 G. J. Lee, Y. J. Kim, H. M. Kim, Y. J. Yoo and Y. M. Song, *Adv. Opt. Mater.*, 2018, **6**, 1800707.

171 W. Wang, H. Xing, X. Shu, X. Zhao, X. Yan, B. Hong, L. Sun, W. Zhang and G. P. Wang, *Optica*, 2023, **10**, 1059–1066.

172 Z. Ding, L. Pattelli, H. Xu, W. Sun, X. Li, L. Pan, J. Zhao, C. Wang, X. Zhang, Y. Song, J. Qiu, Y. Li and R. Yang, *Small*, 2022, **18**, 2202400.

173 X. Hou, K. Zhang, X. Lai, L. Hu, F. Vogelbacher, Y. Song, L. Jiang and M. Li, *Matter*, 2025, **8**, 101898.

174 Q. Liao, K. Zhu, X. Hao, C. Wu, J. Li, H. Cheng, J. Yan, L. Jiang and L. Qu, *Adv. Mater.*, 2024, **36**, 2313366.

This journal is © The Royal Society of Chemistry 2025

Chem. Soc. Rev., 2025, **54**, 10690–10723 | 10721

175 X. Yin, Y. Zhang, D. Wang, Z. Liu, Y. Liu, X. Pei, B. Yu and F. Zhou, *Adv. Funct. Mater.*, 2015, **25**, 4237–4245.

176 T. Cheng, R. He, Q. Zhang, X. Zhan and F. Chen, *J. Mater. Chem. A*, 2015, **3**, 21637–21646.

177 S. Dash, J. de Ruiter and K. K. Varanasi, *Sci. Adv.*, 2018, **4**, eaat0127.

178 E. Mitridis, T. M. Schutzius, A. Sicher, C. U. Hail, H. Eghlidi and D. Poulikakos, *ACS Nano*, 2018, **12**, 7009–7017.

179 S. Wu, Y. Du, Y. Alsaid, D. Wu, M. Hua, Y. Yan, B. Yao, Y. Ma, X. Zhu and X. He, *Proc. Natl. Acad. Sci. U. S. A.*, 2020, **117**, 11240–11246.

180 W. Ma, Y. Li, C. Y. H. Chao, C. Y. Tso, B. Huang, W. Li and S. Yao, *Cell Rep. Phys. Sci.*, 2021, **2**, 100384.

181 W. Cui, Y. Jiang, K. Mielonen and T. A. Pakkanen, *Appl. Surf. Sci.*, 2019, **466**, 503–514.

182 M. Zhou, L. Zhang, L. Zhong, M. Chen, L. Zhu, T. Zhang, X. Han, Y. Hou and Y. Zheng, *Adv. Mater.*, 2024, **36**, 2305322.

183 R. Pan, H. Zhang and M. Zhong, *ACS Appl. Mater. Interfaces*, 2021, **13**, 1743–1753.

184 S. Xuan, H. Yin, G. Li, Y. Yang, Y. Wang, J. Liu, S. Liu, X. Li, Y. Song, T. Wu and K. Yin, *Mater. Horiz.*, 2024, **11**, 3561–3572.

185 M. Wang, J. Hu, M. Li, L. Zhang, M. Salimi, M. Amidpour and Z. Chen, *Nano Energy*, 2025, **136**, 110726.

186 J. Yong, F. Chen, Q. Yang, J. Huo and X. Hou, *Chem. Soc. Rev.*, 2017, **46**, 4168–4217.

187 J. Yong, F. Chen, Q. Yang, G. Du, C. Shan, H. Bian, U. Farooq and X. Hou, *J. Mater. Chem. A*, 2015, **3**, 9379–9384.

188 W. Zhang, D. Zhang, T. Fan, J. Gu, J. Ding, H. Wang, Q. Guo and H. Ogawa, *Chem. Mater.*, 2009, **21**, 33–40.

189 E. Miyako, T. Sugino, T. Okazaki, A. Bianco, M. Yudasaka and S. Iijima, *ACS Nano*, 2013, **7**, 8736–8742.

190 N. Xu, X. Hu, W. Xu, X. Li, L. Zhou, S. Zhu and J. Zhu, *Adv. Mater.*, 2017, **29**, 1606762.

191 J. Wang, Q. Shi, C. Li, Y. Zhang, S. Du, J. Mao and J. Wang, *Adv. Funct. Mater.*, 2022, **32**, 2201922.

192 J. Wang, Z. Chen, L. Feng, F. Yu, C. Ran, N. Xu, Z. Jia, C. Li, Y. Zheng, W. Shi and M. Li, *Nano Energy*, 2023, **114**, 108631.

193 C. Gao, Y. Li, L. Lan, Q. Wang, B. Zhou, Y. Chen, J. Li, J. Guo and J. Mao, *Adv. Sci.*, 2024, **11**, 2306833.

194 L. Zeng, D. Deng, E. H. Soad, X. Fang and Y. Bai, *ACS Appl. Mater. Interfaces*, 2025, **17**, 4913–4924.

195 J. Hu, M.-M. Pazuki, R. Li, M. Salimi, H. Cai, Y. Peng, Z. Liu, T. Zhao, M. Amidpour, Y. Wei and Z. Chen, *Adv. Mater.*, 2025, **37**, 2420482.

196 X. Li, J. Zhang, Y. Liu, Y. Xu, Y. Xie, T. Hu, B. Fu, C. Song, W. Shang, P. Tao and T. Deng, *Sci. Adv.*, 2024, **10**, eadr8445.

197 A. D. Pris, Y. Utturkar, C. Surman, W. G. Morris, A. Vert, S. Zalyubovskiy, T. Deng, H. T. Ghiradella and R. A. Potyrailo, *Nat. Photonics*, 2012, **6**, 195–200.

198 G. S. Smith, *Am. J. Phys.*, 2009, **77**, 1010–1019.

199 X. Qing, Y. Liu, J. Wei, R. Zheng, C. Zhu and Y. Yu, *Adv. Opt. Mater.*, 2019, **7**, 1801494.

200 D. Grujić, D. Vasiljević, D. Pantelić, L. Tomić, Z. Stamenković and B. Jelenković, *Opt. Express*, 2018, **26**, 14143–14158.

201 H. Xue, D. Liu, D. Chi, C. Xu, S. Niu, Z. Han and L. Ren, *Adv. Mater. Interfaces*, 2021, **8**, 2100142.

202 F. Zhang, Q. Shen, X. Shi, S. Li, W. Wang, Z. Luo, G. He, P. Zhang, P. Tao, C. Song, W. Zhang, D. Zhang, T. Deng and W. Shang, *Adv. Mater.*, 2015, **27**, 1077–1082.

203 Q. Shen, S. Ma, Z. Luo, S. An, J. He, R. Zhang, P. Tao, C. Song, J. Wu, R. A. Potyrailo, T. Deng and W. Shang, *Adv. Opt. Mater.*, 2020, **8**, 1901647.

204 R. A. Potyrailo, T. A. Starkey, P. Vukusic, H. Ghiradella, M. Vasudev, T. Bunning, R. R. Naik, Z. Tang, M. Larsen, T. Deng, S. Zhong, M. Palacios, J. C. Grande, G. Zorn, G. Goddard and S. Zalubovsky, *Proc. Natl. Acad. Sci. U. S. A.*, 2013, **110**, 15567–15572.

205 J. Wang, X. Shan, P. Hu, C. Zhang, D. Yuan, X. Hu and J. Wang, *ACS Appl. Mater. Interfaces*, 2022, **14**, 46569–46580.

206 X. Ji, Y. Jiang, T. Liu, S. Lin and A. Du, *Cell Rep. Phys. Sci.*, 2022, **3**, 100815.

207 H. Wei, J. Gu, F. Ren, L. Zhang, G. Xu, B. Wang, S. Song, J. Zhao, S. Dou and Y. Li, *Small*, 2021, **17**, 2100446.

208 J. K. Choe, J. Yi, H. Jang, H. Won, S. Lee, H. Lee, Y. Jang, H. Song and J. Kim, *Adv. Mater.*, 2024, **36**, 2304302.

209 X. Qiu, J. Liu, B. Zhou and X. Zhang, *Adv. Funct. Mater.*, 2023, **33**, 2300321.

210 D. Ürge-Vorsatz, L. F. Cabeza, S. Serrano, C. Barreneche and K. Petrichenko, *Renewable Sustainable Energy Rev.*, 2015, **41**, 85–98.

211 Y. Wang, X. Cao, J. Cheng, B. Yao, Y. Zhao, S. Wu, B. Ju, S. Zhang, X. He and W. Niu, *ACS Nano*, 2021, **15**, 3509–3521.

212 S. Li, E. Yang, Y. Li, X. Mo, Z. Chen, Z. Zhou, G. Tao, Y. Long and B. Hu, *Nano Energy*, 2024, **129**, 110023.

213 R. Kay, C. Katrycz, K. Nitièma, J. A. Jakubiec and B. D. Hatton, *Nat. Commun.*, 2022, **13**, 4120.

214 Z. Zhou, Y. Fang, X. Wang, E. Yang, R. Liu, X. Zhou, Z. Huang, H. Yin, J. Zhou and B. Hu, *Nano Energy*, 2022, **93**, 106865.

215 Z. Shao, A. Huang, C. Cao, X. Ji, W. Hu, H. Luo, J. Bell, P. Jin, R. Yang and X. Cao, *Nat. Sustain.*, 2024, **7**, 796–803.

216 Y. Dong, W. Meng, F. Wang, H. Han, H. Liang, X. Li, Y. Zou, C. Yang, Z. Xu, Y. Yan and Z. Cheng, *Nano Lett.*, 2023, **23**, 9034–9041.

217 Q. Zhang, Y. Wang, Y. Lv, S. Yu and R. Ma, *Proc. Natl. Acad. Sci. U. S. A.*, 2022, **119**, e2207353119.

218 R. Kay, J. A. Jakubiec, C. Katrycz and B. D. Hatton, *Proc. Natl. Acad. Sci. U. S. A.*, 2023, **120**, e2210351120.

219 Y. Ke, Q. Zhang, T. Wang, S. Wang, N. Li, G. Lin, X. Liu, Z. Dai, J. Yan, J. Yin, S. Magdassi, D. Zhao and Y. Long, *Nano Energy*, 2020, **73**, 104785.

220 X.-H. Li, C. Liu, S.-P. Feng and N. X. Fang, *Joule*, 2019, **3**, 290–302.

221 Y. Jia, D. Liu, D. Chen, Y. Jin, C. Chen, J. Tao, H. Cheng, S. Zhou, B. Cheng, X. Wang, Z. Meng and T. Liu, *Nat. Commun.*, 2023, **14**, 5087.

10722 | *Chem. Soc. Rev.*, 2025, **54**, 10690–10723

This journal is © The Royal Society of Chemistry 2025

222 F.-X. Zhao, M.-H. Wang, Z.-Y. Huang, M.-H. Zhu, C. Chen, Q.-H. Pan, B. Yu, Y.-T. Wang, X. Guo, Y.-J. Qian, L.-W. Zhang, X.-J. Qiu, S.-Z. Sheng, Z. He, J.-L. Wang and S.-H. Yu, *Adv. Mater.*, 2024, **36**, 2408192.

223 T.-H. Chen, Y. Hong, C.-T. Fu, A. Nandi, W. Xie, J. Yin and P.-C. Hsu, *PNAS Nexus*, 2023, **2**, 1–10.

224 Y. Zhang, H. Zhu, S. An, W. Xing, B. Fu, P. Tao, W. Shang, J. Wu, M. D. Dickey, C. Song and T. Deng, *Nat. Commun.*, 2024, **15**, 5395.

225 E. M. Leung, M. Colorado Escobar, G. T. Stiubianu, S. R. Jim, A. L. Vyatskikh, Z. Feng, N. Garner, P. Patel, K. L. Naughton, M. Follador, E. Karshalev, M. D. Trexler and A. A. Gorodetsky, *Nat. Commun.*, 2019, **10**, 1947.

226 M. A. Badshah, E. M. Leung, P. Liu, A. A. Strzelecka and A. A. Gorodetsky, *Nat. Sustain.*, 2022, **5**, 434–443.

227 W. Xie, J. Zhang, P. Wang, Y. Sun, J. Li, J. Xu, D. Zhang and H. Zhou, *Nano Lett.*, 2025, **25**, 10193–10201.

228 S. Zeng, Z. Yang, Z. Hou, C. Park, M. D. Jones, H. Ding, K. Shen, A. T. Smith, H. X. Jin, B. Wang, H. Jiang and L. Sun, *Proc. Natl. Acad. Sci. U. S. A.*, 2022, **119**, e2118991119.

229 X. Liu, P. Wang, C. Xiao, L. Fu, J. Xu, D. Zhang, H. Zhou and T. Fan, *Adv. Funct. Mater.*, 2023, **33**, 2212068.

230 T. Ma, J. Bai, T. Li, S. Chen, X. Ma, J. Yin and X. Jiang, *Proc. Natl. Acad. Sci. U. S. A.*, 2021, **118**, e2114345118.

231 C. Xu, G. T. Stiubianu and A. A. Gorodetsky, *Science*, 2018, **359**, 1495–1500.

232 J. Lee, H. Sul, Y. Jung, H. Kim, S. Han, J. Choi, J. Shin, D. Kim, J. Jung, S. Hong and S. H. Ko, *Adv. Funct. Mater.*, 2020, **30**, 2003328.

233 W. Zhang, H. Tian, T. Liu, H. Liu, F. Zhao, X. Li, C. Wang, X. Chen and J. Shao, *Mater. Horiz.*, 2023, **10**, 2024–2034.

234 H. Kim, J. Choi, K. K. Kim, P. Won, S. Hong and S. H. Ko, *Nat. Commun.*, 2021, **12**, 4658.

235 P. Wang, Y. Sun, Y. Zhang, H. Wang, Y. Zhang, C. Xiao, S. Chen, G. Kong, Z. Zhou, D. Zhang, C.-W. Qiu and H. Zhou, *Adv. Mater.*, 2025, **37**, 2503587.

236 M. Wu, Z. Shao, N. Zhao, R. Zhang, G. Yuan, L. Tian, Z. Zhang, W. Gao and H. Bai, *Science*, 2023, **382**, 1379–1383.

237 Y. Cui, H. Gong, Y. Wang, D. Li and H. Bai, *Adv. Mater.*, 2018, **30**, 1706807.

238 D. G. Baranov, Y. Xiao, I. A. Nechepurenko, A. Krasnok, A. Alù and M. A. Kats, *Nat. Mater.*, 2019, **18**, 920–930.

239 S. Yang, M. Liu, C. Zhao, S. Fan and C.-W. Qiu, *Nat. Photonics*, 2024, **18**, 412–424.

240 P. Du, Z. Guo, Y. Li, J. Zhang, J. Muhammad, Z. Cai and F. Ge, *J. Appl. Polym. Sci.*, 2022, **139**, 52021.

241 G. Ye, Y. Wan, J. Wu, W. Zhuang, Z. Zhou, T. Jin, J. Zi, D. Zhang, X. Geng and P. Yang, *Nano Energy*, 2022, **97**, 107148.

242 Z. Wang, Y. Bo, P. Bai, S. Zhang, G. Li, X. Wan, Y. Liu, R. Ma and Y. Chen, *Science*, 2023, **382**, 1291–1296.

243 X. Li, C. Cao, C. Liu, W. He, K. Wu, Y. Wang, B. Xu, Z. Tian, E. Song, J. Cui, G. Huang, C. Zheng, Z. Di, X. Cao and Y. Mei, *Nat. Commun.*, 2022, **13**, 7819.

244 X. Shi, Y. Zuo, P. Zhai, J. Shen, Y. Yang, Z. Gao, M. Liao, J. Wu, J. Wang, X. Xu, Q. Tong, B. Zhang, B. Wang, X. Sun, L. Zhang, Q. Pei, D. Jin, P. Chen and H. Peng, *Nature*, 2021, **591**, 240–245.

245 M. Park, J.-Y. Yoo, T. Yang, Y. H. Jung, A. Vázquez-Guardado, S. Li, J.-H. Kim, J. Shin, W.-Y. Maeng, G. Lee, S. Yoo, H. Luan, J.-T. Kim, H.-S. Shin, M. T. Flavin, H.-J. Yoon, N. Miljkovic, Y. Huang, W. P. King and J. A. Rogers, *Proc. Natl. Acad. Sci. U. S. A.*, 2023, **120**, e2217828120.

246 J. He, C. Lu, H. Jiang, F. Han, X. Shi, J. Wu, L. Wang, T. Chen, J. Wang, Y. Zhang, H. Yang, G. Zhang, X. Sun, B. Wang, P. Chen, Y. Wang, Y. Xia and H. Peng, *Nature*, 2021, **597**, 57–63.

247 K. Yao and Y. Zheng, *Nanophotonics and Machine Learning*, Springer, Cham, 2023.

248 Q. Guan, A. Raza, S. S. Mao, L. F. Vega and T. Zhang, *ACS Photonics*, 2023, **10**, 715–726.

249 M. J. Kim, J. T. Kim, M. J. Hong, S. W. Park and G. J. Lee, *Opt. Express*, 2024, **32**, 16235–16247.

250 H. Keawmuang, T. Badloe, C. Lee, J. Park and J. Rho, *Sol. Energy Mater. Sol. Cells*, 2024, **271**, 112848.

251 R. Unni, K. Yao and Y. Zheng, *Adv. Photonics*, 2024, **6**, 056006.

252 S. Yu, P. Zhou, W. Xi, Z. Chen, Y. Deng, X. Luo, W. Li, J. Shiomi and R. Hu, *Light: Sci. Appl.*, 2023, **12**, 291.

253 J. J. García-Esteban, J. Bravo-Abad and J. C. Cuevas, *Phys. Rev. Appl.*, 2021, **16**, 064006.

254 Z. Ding, X. Li, Q. Ji, Y. Zhang, H. Li, H. Zhang, L. Pattelli, Y. Li, H. Xu and J. Zhao, *ACS Mater. Lett.*, 2024, **6**, 2416–2424.

255 W. Ma, Z. Liu, Z. A. Kudyshev, A. Boltasseva, W. Cai and Y. Liu, *Nat. Photonics*, 2021, **15**, 77–90.

256 J. Jiang, M. Chen and J. A. Fan, *Nat. Rev. Mater.*, 2021, **6**, 679–700.

257 P. R. Wiecha, A. Arbouet, C. Girard and O. L. Muskens, *Photon. Res.*, 2021, **9**, B182–B200.

258 P. R. Wiecha, *Curr. Opin. Solid State Mater. Sci.*, 2024, **28**, 101129.

259 C. Xiao, M. Liu, K. Yao, Y. Zhang, M. Zhang, M. Yan, Y. Sun, X. Liu, X. Cui, T. Fan, C. Zhao, W. Hua, Y. Ying, Y. Zheng, D. Zhang, C.-W. Qiu and H. Zhou, *Nature*, 2025, **643**, 80–88.

This journal is © The Royal Society of Chemistry 2025

Chem. Soc. Rev., 2025, **54**, 10690–10723 | **10723**